# Numerical renormalization group method for quantum impurity systems

Ralf Bulla*

*Theoretische Physik III, Elektronische Korrelationen und Magnetismus, Institut für Physik, Universität Augsburg, 86135 Augsburg, Germany and Institut für Theoretische Physik, Universität zu Köln, 50937 Köln, Germany*

Theo A. Costi†

*Institut für Festkörperforschung, Forschungszentrum Jülich, 52425 Jülich, Germany*

Thomas Pruschke‡

*Institut für Theoretische Physik, Universität Göttingen, 37077 Göttingen, Germany*

(Published 2 April 2008)

In the early 1970s, Wilson developed the concept of a fully nonperturbative renormalization group transformation. When applied to the Kondo problem, this numerical renormalization group (NRG) method gave for the first time the full crossover from the high-temperature phase of a free spin to the low-temperature phase of a completely screened spin. The NRG method was later generalized to a variety of quantum impurity problems. The purpose of this review is to give a brief introduction to the NRG method, including some guidelines for calculating physical quantities, and to survey the development of the NRG method and its various applications over the last 30 years. These applications include variants of the original Kondo problem such as the non-Fermi-liquid behavior in the two-channel Kondo model, dissipative quantum systems such as the spin-boson model, and lattice systems in the framework of the dynamical mean-field theory.

DOI: 10.1103/RevModPhys.80.395 PACS number(s): 75.20.Hr, 71.27.+a, 71.30.+h

## CONTENTS



*bulla@thp.uni-koeln.de
†t.costi@fz-juelich.de
‡pruschke@theorie.physik.uni-goettingen.de

## I. INTRODUCTION

The last decades have seen steadily increasing interest in a wide range of physical systems involving quantum impurities. The expression "quantum impurity system" is used in a very general sense here, namely, a small

 

system (the impurity) with only a few degrees of freedom coupled to a large system (the environment or bath) with very many degrees of freedom, where both subsystems have to be treated quantum mechanically.

The use of the terminology "impurity" is historical. In the Kondo problem, the small system is a magnetic impurity, such as an iron ion, interacting with the conduction electrons of a nonmagnetic metal such as gold (Hewson, 1993a). Other realizations are, for example, artificial impurities such as quantum dots hosting only a small number of electrons. Here the environment is formed by electrons in the leads. The term "quantum impurity systems" can also be used for what are traditionally called dissipative systems. As an example, let the impurity correspond to a spin degree of freedom and the environment be composed of a bosonic bath; this describes the well-known spin-boson model experimentally relevant, for example, for dissipative two-level systems like tunneling centers in glasses (Leggett *et al.*, 1987).

Any theoretical method for the investigation of quantum impurity systems has to face a number of serious obstacles. First of all, because the environment typically consists of a (quasi)continuum of quantum-mechanical degrees of freedom, one has to consider a wide range of energies—from a high-energy cutoff (which can be of the order of several eV) down to arbitrarily small excitation energies. On the other hand, because the impurity degrees of freedom usually form an interacting quantum-mechanical system, their coupling to a continuum of excitations with arbitrarily small energies can result in infrared divergences in perturbational treatments. A well-known example of this difficulty is the Kondo problem: Its physics is governed by an energy scale, the Kondo temperature $T_K$, which depends nonanalytically on the spin-exchange coupling $J$ between the impurity and the conduction band of the host, $\ln T_K \propto -1/J$ [see Hewson (1993a) for a detailed description of the limitations of the perturbational approach for the Kondo model and the single-impurity Anderson model]. One is thus faced with the task of performing nonperturbative calculations for an interacting quantum-mechanical many-body system with a continuum of excitations covering a broad spectrum of energies.

An efficient way to treat systems with such a broad and continuous spectrum of energies is the renormalization group approach. It allows one, in general, to go in a certain sequence of renormalization group steps from high energies, such as the bandwidth, to low energies, such as the Kondo temperature. General introductions to the renormalization group concepts have been given by Ma (1976), Goldenfeld (1992), and Salmhofer (1999) [see also Wilson and Kogut (1974) and Wilson (1975b)]. Here we focus on a specific implementation of the renormalization group idea: Wilson's numerical renormalization group (NRG) method (Wilson, 1975a). This approach is different from most renormalization group methods as it is nonperturbative in all system parameters; however, the price one has to pay is that the renormalization group steps have to be performed numerically.

The general strategy of the NRG method is the following (more details are given in Sec. II). As a specific example, consider the Kondo model, which describes a magnetic impurity with spin $\vec{S}$ coupled to the electrons of a conduction band, assumed to be noninteracting, via an interaction of the form $J\vec{S}\cdot\vec{s}$, with $\vec{s}$ the spin density of electrons at the impurity site. The NRG method starts with a logarithmic discretization of the conduction band in intervals $[\Lambda^{-(n+1)}\omega_c, \Lambda^{-n}\omega_c]$ and $[-\Lambda^{-n}\omega_c, -\Lambda^{-(n+1)}\omega_c]$ $(n=0,1,2,\ldots)$. We call $\Lambda>1$ the NRG discretization parameter. After a sequence of transformations, the discretized model is mapped onto a semi-infinite chain with the impurity spin representing the first site of the chain. The Kondo model in the semi-infinite chain form is diagonalized iteratively, starting from the impurity site and successively adding degrees of freedom to the chain. The exponentially growing Hilbert space in this iterative process is truncated by keeping a certain fraction of the lowest-lying many-particle states. Because of the logarithmic discretization, the hopping parameters between neighboring sites fall off exponentially, i.e., going along the chain corresponds to accessing decreasing energy scales in the calculation.

In this way, Wilson achieved a nonperturbative description of the full crossover from a free impurity spin at high temperatures to a screened spin at low temperatures (Wilson, 1975a), thus solving the so-called Kondo problem as discussed by Hewson (1993a). After this first application more than 30 years ago, the NRG method has been successfully generalized and applied to a much wider range of quantum impurity problems. The first extension was the investigation of the single-impurity Anderson model (Anderson, 1961), which extends the Kondo model by including charge fluctuations at the impurity site. Krishna-murthy *et al.* (1980a, 1980b) described all the technical details, the analysis of fixed points, and the calculation of static quantities for this model.

Subsequently, the development of the NRG method concentrated on the analysis of more complicated impurity models, involving either more environment or more impurity degrees of freedom. For example, in the two-channel Kondo model the impurity spin couples to two conduction bands. This model, which has a non-Fermi-liquid fixed point with associated non-Fermi-liquid properties, was first investigated with the NRG method by Cragg *et al.* (1980). The numerical calculations for such a two-channel model are, however, much more cumbersome because the Hilbert space grows by a factor of 16 in each step of the iterative diagonalization, instead of the factor of 4 in the single-channel case. Pang and Cox (1991) and Affleck *et al.* (1992) later analyzed the stability of the non-Fermi-liquid fixed point with respect to various perturbations such as channel anisotropy.

The two-impurity Kondo model as a paradigm for the competition of local Kondo screening and nonlocal magnetic correlations was studied with the NRG method by

Jones and Varma (1987); Jones *et al.* (1988); Sakai *et al.* (1990); Sakai and Shimizu (1992a, 1992b); and Silva *et al.* (1996). Here the focus was on whether the two regimes are connected by a quantum phase transition or rather by a smooth crossover. Later on, such studies were extended to the two-channel situation (Ingersent *et al.*, 1992).

Originally, the NRG method was used to determine thermodynamic properties of quantum impurity systems. The calculation of dynamic quantities with the NRG method started with the $T=0$ absorption and photoemission spectra of the x-ray Hamiltonian (Oliveira and Wilkins, 1981, 1985), followed by the $T=0$ single-particle spectral function for the orbitally nondegenerate and degenerate Anderson model (Frota and Oliveira, 1986; Sakai *et al.*, 1989; Brito and Frota, 1990; Costi and Hewson, 1990, 1992b). The resulting spectral functions are obtained on all energy scales, with a resolution proportional to the frequency, as discussed in Sec. III.B. The calculation of finite-temperature spectral functions $A(\omega,T)$ is more problematic since in principle all excitations can contribute. Nevertheless, the NRG method has been shown to give accurate results for $A(\omega,T)$ too, which also allows one to calculate transport properties (Costi and Hewson, 1992b; Costi *et al.*, 1994a; Suzuki *et al.*, 1996). A subsequent development was the introduction of the reduced density matrix, which allows one to calculate dynamic quantities in equilibrium in the presence of external fields (Hofstetter, 2000). The calculation of nonequilibrium transient dynamics requires a multiple-shell NRG procedure (Costi, 1997a) and has been accomplished with the aid of a complete basis set and the reduced density matrix (Anders and Schiller, 2005). The first applications of this approach show promising results, for both fermionic and bosonic systems (Anders and Schiller, 2005, 2006; Anders *et al.*, 2007). Another recent generalization of the NRG approach is to quantum impurities coupled to a bosonic bath [bosonic NRG method, see Bulla *et al.* (2005); for early related approaches see Evangelou and Hewson (1982)]. The bosonic NRG method has already been successfully applied to the sub-Ohmic spin-boson model, which shows a line of quantum critical points separating localized and delocalized phases (Bulla *et al.*, 2003).

Additional motivation to further improve the NRG method came from the development of the dynamical mean-field theory (DMFT) (Metzner and Vollhardt, 1989; Georges *et al.*, 1996) in which a lattice model of correlated electrons, such as the Hubbard model, is mapped onto a single-impurity Anderson model with the impurity coupled to a bath whose structure has to be determined self-consistently. This requires the NRG method to handle impurity models with an arbitrary density of states of conduction electrons and to calculate directly the impurity self-energy (Bulla *et al.*, 1998). The first applications of the NRG method within the DMFT framework concentrated on the Mott transition in the Hubbard model, and accurate results could be obtained for both $T=0$ (Sakai and Kuramoto, 1994; Bulla, 1999) and finite temperatures (Bulla *et al.*, 2001). Within DMFT, the NRG method has been applied to the periodic Anderson model (Pruschke *et al.*, 2000), the Kondo lattice model (Costi and Manini, 2002), multiband Hubbard models (Pruschke and Bulla, 2005), the ferromagnetic Kondo lattice model with interactions in the band (Liebsch and Costi, 2006), and lattice models with a coupling to local phonon modes such as the Holstein model (Meyer *et al.*, 2002) and the Hubbard-Holstein model (Koller, Meyer, *et al.*, 2004).

The observation that the coupling between electronic degrees of freedom in quantum dots and the surrounding leads can give rise to Kondo-like features in the transport characteristics has also led to a resurgence of interest in quantum impurity systems, both experimentally and theoretically. An important feature of quantum dot systems is their flexibility, and a number of different setups have been realized so far, and investigated theoretically by various methods including the NRG. Applications of the NRG method in this field include the standard Kondo effect (Izumida *et al.*, 1998; Gerland *et al.*, 2000; Costi, 2001; Borda *et al.*, 2005), coupled quantum dots (Hofstetter and Schoeller, 2002; Borda *et al.*, 2003; Hofstetter and Zaránd, 2004; Cornaglia and Grempel, 2005b; Galpin *et al.*, 2006b), quantum dots in a superconductor (Choi, Lee, *et al.*, 2004), and quantum dots coupled to ferromagnetic leads (Martinek *et al.*, 2003; Choi, Sánchez, and López, 2004).

From this brief overview one can see that the range of applicability of the NRG method has widened considerably since Wilson's original paper, covering physical phenomena such as the Mott transition, quantum dot physics, local criticality, quantum dissipative systems, etc. Further applications still lie ahead and various optimizations of the technique itself are yet being developed—we return to this point in the summary section.

This paper is the first review of the NRG method (since Wilson's original paper on the Kondo problem) that attempts to cover both the technical details and the various applications. In this way, the reader should get an overview of the field, learn about the current status of the individual applications, and come up with ideas for further calculations. This review can only be a start for a deeper understanding of the NRG method. The following shorter reviews on selected topics are also helpful: Sec. IV in Hewson (1993a) contains a pedagogical introduction to the NRG method as applied to the Kondo problem, Gonzalez-Buxton and Ingersent (1998) discussed the soft-gap Anderson and Kondo models, Costi (1999) gives a general overview of the key concepts, including the application to the anisotropic Kondo model, Bulla *et al.* (2005) presented a detailed introduction to the bosonic NRG method, and, finally, the first calculations for the single-impurity Anderson model by Krishna-murthy *et al.* (1980a, 1980b) are still valuable as an overview of the method and details of the analysis of fixed points.

The review is organized as follows. In Sec. II we start with an introduction to the basic concepts of the NRG approach. The single-impurity Anderson model serves

as an example here, but the strategy applies to quantum impurity systems quite generally. At the end of this section, we discuss the flow of the many-particle eigenvalues and the appearance of fixed points in this flow. This analysis already gives important insights into the physics of a given model, but the calculation of physical quantities needs some extra care, as described in Sec. III. This section is divided into Sec. III.A (thermodynamic and static quantities, such as entropy, specific heat, and susceptibilities) and Sec. III.B (dynamic quantities, both in and out of equilibrium).

The following two sections deal with the various applications of the NRG method and we distinguish here between quantum impurity systems (Sec. IV) and lattice models within DMFT (Sec. V). Section IV covers most work using the NRG method that has been published so far. We present results for systems which show the standard Kondo effect (Sec. IV.A; this also includes most of the NRG results on quantum dots), the two-channel Kondo problem (Sec. IV.B), models displaying impurity quantum phase transitions (Sec. IV.C), quantum impurity systems with orbital degrees of freedom (Sec. IV.D), and, finally, impurities coupled to bosonic degrees of freedom (Sec. IV.E). The section on lattice models within DMFT (Sec. V) covers calculations for the Hubbard model (Sec. V.A), the periodic Anderson and Kondo lattice models (Sec. V.B), and lattice models with coupling to phonons (Sec. V.C). In the summary we discuss open problems as well as possible directions for future developments of the NRG approach.

We finish the Introduction with a few remarks on the selection of the material presented and the references: Due to the flexibility of the NRG method, the review covers a broad range of physical phenomena, in particular in Secs. IV and V. We, however, give only brief introductions to these phenomena and refer the reader to the references in particular reviews or seminal books. Furthermore, due to lack of space, we shall not usually review results from other theoretical approaches that have been applied to quantum impurity systems, such as Bethe ansatz, quantum Monte Carlo, resolvent perturbation theory, local-moment approach, etc., unless these appear crucial for an understanding of relevant NRG results. Comparisons between the results from the NRG method and these approaches are, in most cases, included in the papers cited here [see also Hewson (1993a)]. This means that we focus, almost completely, on references that use the NRG method.

## II. INTRODUCTION TO THE NUMERICAL RENORMALIZATION GROUP METHOD

The NRG method can be applied to systems of the following form: a quantum mechanical impurity with a small number of degrees of freedom (so that it can be diagonalized exactly) coupled to a bath of fermions or bosons, usually with a continuous excitation spectrum. There is no restriction on the structure of the impurity part of the Hamiltonian; it might contain, for example, a Coulomb repulsion of arbitrarily large strength. The bath, however, is required to consist of noninteracting fermions or bosons, otherwise the various mappings described below cannot be performed.

In this review, whenever we discuss models of a different kind, such as the Hubbard model, they will be mapped onto impurity models of the above type. For the Hubbard model and other lattice models of correlated electrons, this is achieved via the dynamical mean-field theory (see Sec. V).

A few remarks about the dimensionality of quantum impurity systems are in order. The impurity itself forms a zero-dimensional object, whereas the environment exists in $d=1$, 2, or 3 dimensions; for a magnetic impurity in a conduction band one usually considers a three-dimensional host. To study impurity properties of such a model, however, it is not necessary to treat the model in its original dimension. For a noninteracting bath, the bath degrees of freedom can be integrated out, with the effect that all information about the environment (from the perspective of the impurity) can be encoded in the bath spectral function $\Delta(\omega)$. Information about the dimensionality of the environment has been lost at this stage, but the knowledge of $\Delta(\omega)$ is sufficient to calculate the impurity properties. Such a representation is used as the starting point for the NRG procedure, as shown in Fig. 1(a).

Before we start with the technical details of the NRG approach, we give a brief overview of the general strategy. For basically all NRG applications, one proceeds as follows.

(a) Division of the energy support of the bath spectral function into a set of logarithmic intervals.

(b) Reduction of the continuous spectrum to a discrete set of states (logarithmic discretization).

(c) Mapping of the discretized model onto a semi-infinite chain.

(d) Iterative diagonalization of this chain.

(e) Further analysis of the many-particle energies, matrix elements, etc., calculated during the iterative diagonalization. This yields information on fixed points and static and dynamic properties of the quantum impurity model.

Parts (a)–(c) of this strategy are sketched in Fig. 1, where we consider a constant bath spectral function within the interval $[-1,1]$. The NRG discretization parameter $\Lambda$ defines a set of discretization points $\pm\Lambda^{-n}$, $n=0,1,2,\ldots$, and a corresponding set of intervals. The continuous spectrum in each of these intervals [Fig. 1(a)] is approximated by a single state [Fig. 1(b)]. The resulting discretized model is mapped onto a semi-infinite chain with the impurity (filled circle) corresponding to the first site of this chain. Due to the logarithmic discretization, the hopping matrix elements turn out to decrease exponentially with increasing distance from the impurity, $t_n \propto \Lambda^{-n/2}$.

While the various steps leading to the semi-infinite chain are fairly straightforward from a mathematical

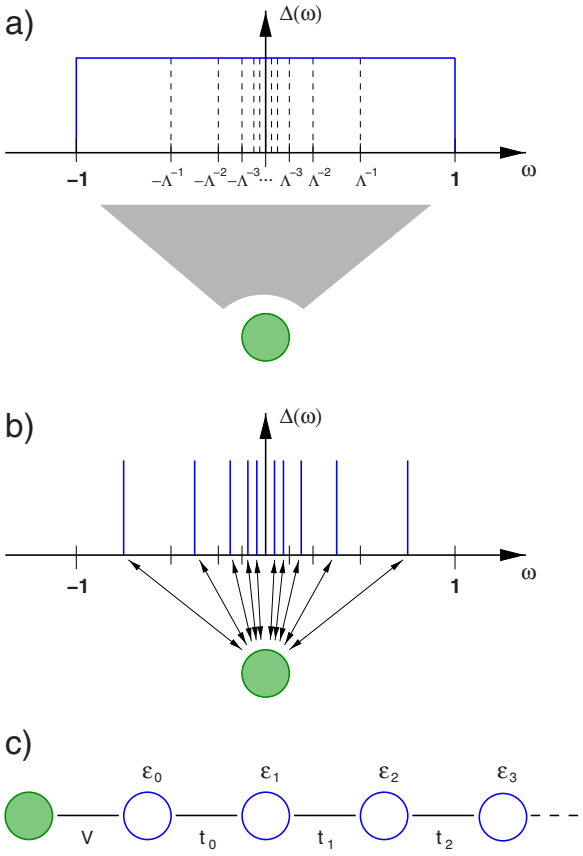


FIG. 1. (Color online) Initial steps of the NRG method illustrated for the single-impurity Anderson model in which an impurity (filled circle) couples to a continuous conduction band via the hybridization function $\Delta(\omega)$. (a) A logarithmic set of intervals is introduced through the NRG discretization parameter $\Lambda$. (b) The continuous spectrum within each of these intervals is approximated by a single state. (c) The resulting discretized model is mapped onto a semi-infinite chain where the impurity couples to the first conduction electron site via the hybridization $V$; the parameters of the tight-binding model [see Eq. (26)] are $\varepsilon_n$ and $t_n$.

point of view, the philosophy behind this strategy is not so obvious. Quite generally, numerical diagonalization of Hamiltonian matrices allows one to take into account the various impurity-related terms in the Hamiltonian, such as a local Coulomb repulsion, in a nonperturbative way. The actual implementation of such a numerical diagonalization scheme requires some sort of discretization of the original model, which has a continuum of bath states. There are, however, many ways to discretize such a system, so we will try and explain why the logarithmic discretization is the most suitable one here. As it turns out, quantum impurity models are often characterized by energy scales orders of magnitudes smaller than the bare energy scales of the model Hamiltonian. If the ratio of these energy scales is, for example, of the order of $10^5$, a linear discretization would require energy intervals of size at most $10^{-6}$ to properly resolve the lowest scale in the system. Since for a finite system the splitting of energies is roughly inversely proportional to the system size, one would need of the order of $10^6$ sites, which renders an exact diagonalization impossible.

The logarithmic discretization reduces this problem in that the low-energy resolution now depends exponentially on the number of sites in the discretized model. Of course, the accuracy of such an approach has to be checked by suitable extrapolations of the discretization parameters, in particular a $\Lambda \to 1$ extrapolation, which recovers the original continuum model. Often it turns out that for $\Lambda$ of the order of 2 the results are already accurate to within a few percent and a $\Lambda \to 1$ extrapolation indeed reproduces exact results, if these are available.

However, this argument in favor of the logarithmic discretization neither explains the need for a mapping to a chain Hamiltonian, as in Fig. 1(c), nor resolves the problem of an exponentially growing Hilbert space with increasing chain length. As far as the first point is concerned, an iterative diagonalization of the discretized model as shown in Fig. 1(b) has been implemented for the spin-boson model (Bulla *et al.*, 2005). For reasons that are not yet completely clear, such an approach is only partly successful. We mention here that, for a fermionic model such as the single-impurity Anderson model, iterative diagonalization of the model in the semi-infinite chain form is more convenient, since one site of the chain can be added in each step without violating particle-hole symmetry [for a detailed discussion of this point, see Bulla *et al.* (2005)].

The quantum impurity model in the semi-infinite chain form is solved by iterative diagonalization, which means that in each step of the iterative scheme one site of the chain is added to the system and the Hamiltonian matrices of the enlarged cluster are diagonalized numerically. As already pointed out, without taking further steps to reduce the size of the Hilbert space, this procedure would have to end for chain sizes of $\approx 10$. Here the renormalization group concept enters the procedure through the dependence of the hopping matrix elements on the chain length, $t_n \propto \Lambda^{-n/2}$. Adding one site to the chain corresponds to decreasing the relevant energy scale by a factor $\sqrt{\Lambda}$. Furthermore, because the coupling $t_n$ to the newly added site falls off exponentially, only states of the shorter chain within a comparatively small energy window will actually contribute to the states of the chain with the additional site. This observation allows one to introduce a simple truncation scheme: after each step only the lowest-lying $N_s$ many-particle states are retained and used to build up the Hamiltonian matrices of the next iteration step, thus keeping the size of the Hilbert space fixed as one goes along the chain.

All these technical steps will be discussed in detail in the following. We briefly remark on the general setup of this section. We keep this section as general as possible because it should serve as an introduction to the NRG technique, whose application to a variety of problems is then the subject of the remainder of this review. This quest for generality is, however, contrasted by the large variety of possible impurity-bath interactions. In-

stead of presenting explicit formulas for all possible quantum impurity models, we restrict ourselves to the single-impurity Anderson model as a specific—and most important—example here. The original introductions to the technique for the Kondo model (Wilson, 1975a) and the single-impurity Anderson model (Krishna-murthy *et al.*, 1980a, 1980b) were restricted to a constant bath density of states [or better, a constant hybridization function $\Delta(\omega)$ as defined below]. Here, we consider a general frequency-dependent $\Delta(\omega)$ from the outset. This generalization is essential for various applications of the NRG method [the soft-gap models (see Sec. IV.C.2) and lattice models within DMFT (see Sec. V)] where the physics is largely determined by the frequency dependence of $\Delta(\omega)$. If the hybridization function is nonzero for positive frequencies only, manipulations of the bath degrees of freedom equally hold for a bosonic bath [see Bulla *et al.* (2005)].

In this section we cover the steps (a)–(d) of the list given above. Concerning the analysis of the data [step (e) in the list], we discuss the flow of the many-particle spectra and all related issues here. The calculation of static and dynamic quantities will be described in Sec. III.

### A. Structure of the Hamiltonian

The Hamiltonian of a general quantum impurity model consists of three parts, the impurity $H_{\text{imp}}$, the bath $H_{\text{bath}}$, and the impurity-bath interaction $H_{\text{imp-bath}}$:

$$H = H_{\text{imp}} + H_{\text{bath}} + H_{\text{imp-bath}}. \tag{1}$$

For the single-impurity Anderson model (SIAM) (Anderson, 1961) with the Hamiltonian $H = H_{\text{SIAM}}$, these three terms are given by

$$H_{\text{imp}} = \sum_{\sigma} \varepsilon_f f_\sigma^\dagger f_\sigma + U f_\uparrow^\dagger f_\uparrow f_\downarrow^\dagger f_\downarrow,$$

$$H_{\text{bath}} = \sum_{k\sigma} \varepsilon_k c_{k\sigma}^\dagger c_{k\sigma},$$

$$H_{\text{imp-bath}} = \sum_{k\sigma} V_k (f_\sigma^\dagger c_{k\sigma} + c_{k\sigma}^\dagger f_\sigma). \tag{2}$$

In this Hamiltonian, the fermionic operators $c_{k\sigma}^{(\dagger)}$ correspond to band states with spin $\sigma$ and energy $\varepsilon_k$, and $f_\sigma^{(\dagger)}$ to impurity states with energy $\varepsilon_f$. The Coulomb interaction between two electrons occupying the impurity site is parametrized by $U$, and the two subsystems are coupled via a $k$-dependent hybridization $V_k$.

The influence of the bath on the impurity is completely determined by the so-called hybridization function $\Delta(\omega)$:

$$\Delta(\omega) = \pi \sum_k V_k^2 \delta(\omega - \varepsilon_k). \tag{3}$$

Thus, if we are interested only in the impurity contributions to the physics of the SIAM, we can rewrite the Hamiltonian in a variety of ways, provided the manipulations involved do not change the form of $\Delta(\omega)$. Without loss of generality, we assume that the support of $\Delta(\omega)$ completely lies within the interval $[-D, D]$, with $D > 0$ chosen suitably. Henceforth, we use $D = 1$ as the energy unit.

One such possible reformulation is given by the following Hamiltonian:

$$H = H_{\text{imp}} + \sum_{\sigma} \int_{-1}^{1} d\varepsilon\, g(\varepsilon) a_{\varepsilon\sigma}^\dagger a_{\varepsilon\sigma} + \sum_{\sigma} \int_{-1}^{1} d\varepsilon\, h(\varepsilon)(f_\sigma^\dagger a_{\varepsilon\sigma} + a_{\varepsilon\sigma}^\dagger f_\sigma). \tag{4}$$

Here we introduced a one-dimensional energy representation for the conduction band with band cutoffs at energies $\pm 1$, a dispersion $g(\varepsilon)$, and a hybridization $h(\varepsilon)$. The band operators satisfy the standard fermionic commutation relations: $[a_{\varepsilon\sigma}^\dagger, a_{\varepsilon'\sigma'}]_+ = \delta(\varepsilon - \varepsilon')\delta_{\sigma\sigma'}$. It has been shown by Bulla, Pruschke, and Hewson (1997) that the two functions $g(\varepsilon)$ and $h(\varepsilon)$ are related to the hybridization function $\Delta(\omega)$ via

$$\Delta(\omega) = \pi \frac{d\varepsilon(\omega)}{d\omega} h[\varepsilon(\omega)]^2, \tag{5}$$

where $\varepsilon(\omega)$ is the inverse function to $g(\varepsilon)$, $g[\varepsilon(\omega)] = \omega$. For a given $\Delta(\omega)$ there are many possibilities to divide the $\omega$ dependence between $\varepsilon(\omega)$ and $h[\varepsilon(\omega)]$. This feature will turn out to be useful later.

For a constant $\Delta(\omega) = \Delta_0$ within the interval $[-1, 1]$, Eq. (5) can be satisfied by choosing $\varepsilon(\omega) = \omega$ [this corresponds to $g(\varepsilon) = \varepsilon$] and $h^2(\varepsilon) = \Delta_0/\pi$.

An alternative strategy to arrive at the one-dimensional energy representation Eq. (4) was used by Krishna-murthy *et al.* (1980a), with the impurity in the original model in a three-dimensional metallic host, with dispersion $\varepsilon_{\vec{k}}$ and hybridization $V_{\vec{k}}$. Here the conduction band states are expressed as a set of spherical waves around the impurity and the impurity couples only to the $s$-wave states. Labeling the $s$-wave states by energy rather than by momentum directly gives a representation analogous to Eq. (4).

### B. Logarithmic discretization

The Hamiltonian in the integral representation Eq. (4) is a convenient starting point for the logarithmic discretization of the conduction band. As shown in Fig. 1(a), the parameter $\Lambda > 1$ defines a set of intervals with discretization points

$$x_n = \pm \Lambda^{-n}, \quad n = 0, 1, 2, \ldots. \tag{6}$$

The width of the intervals is given by

$$d_n = \Lambda^{-n}(1 - \Lambda^{-1}). \tag{7}$$

Within each interval we now introduce a complete set of orthonormal functions

$$\psi_{np}^{\pm}(\varepsilon)=\begin{cases}\dfrac{1}{\sqrt{d_n}}e^{\pm i\omega_n p\varepsilon} & \text{for } x_{n+1}<\pm\varepsilon<x_n,\\ 0 & \text{outside this interval.}\end{cases} \tag{8}$$

The index $p$ takes all integer values between $-\infty$ and $+\infty$, and the fundamental frequencies for each interval are given by $\omega_n=2\pi/d_n$. The next step is to expand the conduction electron operators $a_{\varepsilon\sigma}$ in this basis, i.e.,

$$a_{\varepsilon\sigma}=\sum_{np}\left[a_{np\sigma}\psi_{np}^{+}(\varepsilon)+b_{np\sigma}\psi_{np}^{-}(\varepsilon)\right], \tag{9}$$

which corresponds to a Fourier expansion in each of the intervals. The inverse transformation reads

$$a_{np\sigma}=\int_{-1}^{1}d\varepsilon[\psi_{np}^{+}(\varepsilon)]^{*}a_{\varepsilon\sigma},$$

$$b_{np\sigma}=\int_{-1}^{1}d\varepsilon[\psi_{np}^{-}(\varepsilon)]^{*}a_{\varepsilon\sigma}. \tag{10}$$

The operators $a_{np\sigma}^{(\dagger)}$ and $b_{np\sigma}^{(\dagger)}$ defined in this way fulfill the usual fermionic commutation relations. The Hamiltonian Eq. (4) is now expressed in terms of these discrete operators.

In particular, the transformed hybridization term (first part only) is

$$\int_{-1}^{1}d\varepsilon h(\varepsilon)f_{\sigma}^{\dagger}a_{\varepsilon\sigma}=f_{\sigma}^{\dagger}\sum_{np}\left[a_{np\sigma}\int^{+,n}d\varepsilon h(\varepsilon)\psi_{np}^{+}(\varepsilon)+b_{np\sigma}\int^{-,n}d\varepsilon h(\varepsilon)\psi_{np}^{-}(\varepsilon)\right], \tag{11}$$

where we have defined

$$\int^{+,n}d\varepsilon\equiv\int_{x_{n+1}}^{x_n}d\varepsilon,\quad \int^{-,n}d\varepsilon\equiv\int_{-x_n}^{-x_{n+1}}d\varepsilon. \tag{12}$$

For a constant $h(\varepsilon)=h$, the integrals in Eq. (11) filter out the $p=0$ component only

$$\int^{\pm,n}d\varepsilon h\psi_{np}^{\pm}(\varepsilon)=\sqrt{d_n}h\delta_{p,0}. \tag{13}$$

In other words, the impurity couples only to the $p=0$ components of the conduction band states. It will become clear soon that this point was essential in Wilson's original line of arguments, so we maintain this feature [$h(\varepsilon)$ being constant in each interval of the logarithmic discretization] also for a general, nonconstant $\Delta(\omega)$. Note that this restriction for the function $h(\varepsilon)$ does not lead to additional approximations for a nonconstant $\Delta(\omega)$ as one can shift all the remaining $\varepsilon$ dependence to the dispersion $g(\varepsilon)$, see Eq. (5).

As discussed by Chen and Jayaprakash (1995a) in the context of the soft-gap model [see also Chen and Jayaprakash (1995b)], one can even set $h(\varepsilon)=h$ for all $\varepsilon$. Here we follow the proposal by Bulla, Pruschke, and Hewson (1997), that is, we introduce a step function for $h(\varepsilon)$

$$h(\varepsilon)=h_n^{\pm},\quad x_{n+1}<\pm\varepsilon<x_n, \tag{14}$$

with $h_n^{\pm}$ given by the average of the hybridization function $\Delta(\omega)$ within the respective intervals,

$$h_n^{\pm 2}=\frac{1}{d_n}\int^{\pm,n}d\varepsilon\frac{1}{\pi}\Delta(\varepsilon). \tag{15}$$

This leads to the following form of the hybridization term:

$$\int_{-1}^{1}d\varepsilon\, h(\varepsilon)f_{\sigma}^{\dagger}a_{\varepsilon\sigma}=\frac{1}{\sqrt{\pi}}f_{\sigma}^{\dagger}\sum_{n}\left(\gamma_n^{+}a_{n0\sigma}+\gamma_n^{-}b_{n0\sigma}\right), \tag{16}$$

with $\gamma_n^{\pm 2}=\int^{\pm,n}d\varepsilon\,\Delta(\varepsilon)$.

Next, we turn to the conduction electron term, which transforms into

$$\int_{-1}^{1}d\varepsilon\, g(\varepsilon)a_{\varepsilon\sigma}^{\dagger}a_{\varepsilon\sigma}=\sum_{np}\left(\xi_n^{+}a_{np\sigma}^{\dagger}a_{np\sigma}+\xi_n^{-}b_{np\sigma}^{\dagger}b_{np\sigma}\right)+\sum_{n,p\neq p'}\left[\alpha_n^{+}(p,p')a_{np\sigma}^{\dagger}a_{np'\sigma}-\alpha_n^{-}(p,p')b_{np\sigma}^{\dagger}b_{np'\sigma}\right]. \tag{17}$$

The first term on the right-hand side of Eq. (17) is diagonal in the index $p$. The discrete set of energies $\xi_n^{\pm}$ can be expressed as (Bulla, Pruschke, and Hewson, 1997)

$$\xi_n^{\pm}=\frac{\int^{\pm,n}d\varepsilon\,\Delta(\varepsilon)\varepsilon}{\int^{\pm,n}d\varepsilon\,\Delta(\varepsilon)}\quad\left(=\frac{1}{2}\Lambda^{-n}(1+\Lambda^{-1})\right), \tag{18}$$

where we added the result for a constant $\Delta(\varepsilon)$ in parentheses. The coupling of the conduction band states with different $p,p'$ (the second term) recovers the continuum [no approximation has been made so far; Eq. (17) is still exact]. For the case of a linear dispersion $g(\varepsilon)=\varepsilon$, the prefactors $\alpha_n^{\pm}(p,p')$ are the same for both positive and negative $\varepsilon$ and take the following form:

$$\alpha_n^{\pm}(p,p')=\frac{1-\Lambda^{-1}}{2\pi i}\frac{\Lambda^{-n}}{p'-p}\exp\left(\frac{2\pi i(p'-p)}{1-\Lambda^{-1}}\right). \tag{19}$$

The actual discretization of the Hamiltonian is now achieved by dropping the terms with $p\neq 0$ in the expression for the conduction band, Eq. (17). This is, of course, an approximation, the quality of which is not clear from the outset. To motivate this step we can argue that (i) the $p\neq 0$ states couple only indirectly to the impurity [via their coupling to the $p=0$ states in Eq. (17)] and (ii) the coupling between the $p=0$ and $p\neq 0$ states has a prefactor $(1-\Lambda^{-1})$ which vanishes in the limit $\Lambda\to 1$. In this sense one can view the couplings to the states with $p\neq 0$ as small parameters and consider the restriction to $p=0$ as the zeroth-order step in a perturbation expansion with respect to the coefficients $a_n^{\pm}(p,p')$ (Wilson, 1975a). As it turns out, the accuracy of the results obtained from the $p=0$ states only is surprisingly good even for values of $\Lambda$ as large as $\Lambda=2$, so that in all NRG

calculations the $p \neq 0$ states have not been considered so far.

Finally, after dropping the $p \neq 0$ terms and relabeling the operators $a_{n0\sigma} \equiv a_{n\sigma}$, etc., we arrive at the discretized Hamiltonian as depicted by Fig. 1(b),

$$H = H_{\rm imp} + \sum_{n\sigma} (\xi_n^+ a_{n\sigma}^\dagger a_{n\sigma} + \xi_n^- b_{n\sigma}^\dagger b_{n\sigma}) + \frac{1}{\sqrt{\pi}} \sum_\sigma f_\sigma^\dagger \sum_n (\gamma_n^+ a_{n\sigma} + \gamma_n^- b_{n\sigma}) + \frac{1}{\sqrt{\pi}} \sum_\sigma \left( \sum_n (\gamma_n^+ a_{n\sigma}^\dagger + \gamma_n^- b_{n\sigma}^\dagger) \right) f_\sigma. \tag{20}$$

Before we continue with the mapping of the Hamiltonian Eq. (20) onto a semi-infinite chain, Fig. 1(c), we make a few remarks on alternative discretizations of the continuous bath spectral function.

The above procedure applies for general $\Delta(\omega)$, and also for different upper and lower cutoffs $D_u$ and $D_l$. A special case is $D_l = 0$, which occurs for a bosonic bath [see Bulla *et al.* (2005)]; here the logarithmic discretization is performed for positive frequencies only, and the operators $b_{n\sigma}^{(\dagger)}$ in Eq. (20) are no longer present.

In Sec. III we discuss the problems that the discreteness of the model Eq. (20) can (in some cases) cause for the calculation of physical quantities. As it is not possible in the actual calculations to recover the continuum by taking the limit $\Lambda \to 1$ (or by including the $p \neq 0$ terms), averaging over various discretizations for fixed $\Lambda$ has been suggested (Frota and Oliveira, 1986; Yoshida *et al.*, 1990; Oliveira and Oliveira, 1994). The discretization points are then modified as

$$x_n = \begin{cases} 1, & n = 0, \\ \Lambda^{-n+z}, & n \geq 1, \end{cases} \tag{21}$$

where $z$ covers the interval $[0,1)$. This $z$ averaging is, indeed, successful, as it removes certain artificial oscillations (see Sec. III.A.4), but it should be stressed here that the continuum limit introduced by integrating over $z$ is not the same as the true continuum limit $\Lambda \to 1$.

Another shortcoming of the discretized model is that the hybridization function $\Delta(\omega)$ is systematically underestimated. It is therefore convenient to multiply $\Delta(\omega)$ by a correction factor $A_\Lambda$ which accelerates the convergence to the continuum limit. For a constant hybridization the correction factor takes the value

$$A_\Lambda = \frac{1}{2} \frac{\Lambda + 1}{\Lambda - 1} \ln \Lambda. \tag{22}$$

For a recent derivation of this correction factor, see Campo and Oliveira (2005), where it was also shown that by a suitable modification of the discretization procedure, the factor $A_\Lambda$ can be taken into account from the outset.

In general, the discretization correction $A_\Lambda$ depends on the shape of $\Delta(\omega)$; for the soft-gap case, $\Delta(\omega) \propto |\omega|^r$, the corresponding result is given in Eq. (5.14) of Gonzalez-Buxton and Ingersent (1998).

### C. Mapping on a semi-infinite chain

According to Figs. 1(b) and 1(c), the next step is to transform the discretized Hamiltonian Eq. (20) into a semi-infinite chain form with the first site of the chain [filled circle in Fig. 1(c)] representing the impurity degrees of freedom. In the chain Hamiltonian, the impurity directly couples only to one conduction electron degree of freedom with operators $c_{0\sigma}^{(\dagger)}$, the form of which can be directly read off from the second and third lines in Eq. (20). With the definition

$$c_{0\sigma} = \frac{1}{\sqrt{\xi_0}} \sum_n (\gamma_n^+ a_{n\sigma} + \gamma_n^- b_{n\sigma}), \tag{23}$$

in which the normalization constant is given by

$$\xi_0 = \sum_n [(\gamma_n^+)^2 + (\gamma_n^-)^2] = \int_{-1}^{1} d\varepsilon \, \Delta(\varepsilon), \tag{24}$$

the hybridization term can be written as

$$\frac{1}{\sqrt{\pi}} f_\sigma^\dagger \sum_n (\gamma_n^+ a_{n\sigma} + \gamma_n^- b_{n\sigma}) = \sqrt{\frac{\xi_0}{\pi}} f_\sigma^\dagger c_{0\sigma} \tag{25}$$

(similarly for the Hermitian conjugate term). Note that, for a $k$-independent hybridization, $V_k = V$ in Eq. (2), the coupling in Eq. (25) reduces to $\sqrt{\xi_0/\pi} = V$.

The operators $c_{0\sigma}^{(\dagger)}$ represent the first site of the conduction electron part of the semi-infinite chain. These operators are of course not orthogonal to the operators $a_{n\sigma}^{(\dagger)}$ and $b_{n\sigma}^{(\dagger)}$. Constructing a new set of mutually orthogonal operators $c_{n\sigma}^{(\dagger)}$ from $c_{0\sigma}^{(\dagger)}$ and $a_{n\sigma}^{(\dagger)}$, $b_{n\sigma}^{(\dagger)}$ by a standard tridiagonalization procedure leads to the desired chain Hamiltonian, which takes the form

$$H = H_{\rm imp} + \sqrt{\frac{\xi_0}{\pi}} \sum_\sigma (f_\sigma^\dagger c_{0\sigma} + c_{0\sigma}^\dagger f_\sigma) + \sum_{\sigma n=0}^{\infty} [\varepsilon_n c_{n\sigma}^\dagger c_{n\sigma} + t_n (c_{n\sigma}^\dagger c_{n+1\sigma} + c_{n+1\sigma}^\dagger c_{n\sigma})], \tag{26}$$

with the operators $c_{n\sigma}^{(\dagger)}$ corresponding to the $n$th site of the conduction electron part of the chain. The parameters of the chain are the on-site energies $\varepsilon_n$ and the hopping matrix elements $t_n$. The operators $c_{n\sigma}^{(\dagger)}$ in Eq. (26) and the operators $\{a_{n\sigma}^{(\dagger)}, b_{n\sigma}^{(\dagger)}\}$ in Eq. (20) are related via an orthogonal transformation,

$$a_{n\sigma} = \sum_{m=0}^{\infty} u_{mn} c_{m\sigma}, \quad b_{n\sigma} = \sum_{m=0}^{\infty} v_{mn} c_{m\sigma},$$

$$c_{n\sigma} = \sum_{m=0}^{\infty} (u_{nm} a_{m\sigma} + v_{nm} b_{m\sigma}). \tag{27}$$

From the definition of $c_{0\sigma}$ in Eq. (23) we can read off the coefficients $u_{0m}$ and $v_{0m}$,

$$u_{0m} = \frac{\gamma_m^+}{\sqrt{\xi_0}}, \quad v_{0m} = \frac{\gamma_m^-}{\sqrt{\xi_0}}. \tag{28}$$

For the remaining coefficients $u_{nm}$, $v_{nm}$, as well as for the parameters $\varepsilon_n$, $t_n$, one can derive recursion relations fol-

lowing the scheme described in detail in, for example, Appendix A of Bulla *et al.* (2005). The starting point here is the equivalence of the free conduction electron parts

$$\sum_{n\sigma} (\xi_n^+ a_{n\sigma}^\dagger a_{n\sigma} + \xi_n^- b_{n\sigma}^\dagger b_{n\sigma}) = \sum_{\sigma n=0}^{\infty} [\varepsilon_n c_{n\sigma}^\dagger c_{n\sigma} + t_n (c_{n\sigma}^\dagger c_{n+1\sigma} + c_{n+1\sigma}^\dagger c_{n\sigma})]. \quad (29)$$

The recursion relations are initialized by

$$\varepsilon_0 = \frac{1}{\xi_0}\int_{-1}^{1} d\varepsilon\, \Delta(\varepsilon)\varepsilon,$$

$$t_0^2 = \frac{1}{\xi_0}\sum_m [(\xi_m^+ - \varepsilon_0)^2(\gamma_m^+)^2 + (\xi_m^- - \varepsilon_0)^2(\gamma_m^-)^2],$$

$$u_{1m} = \frac{1}{t_0}(\xi_m^+ - \varepsilon_0)u_{0m},$$

$$v_{1m} = \frac{1}{t_0}(\xi_m^- - \varepsilon_0)v_{0m}. \quad (30)$$

For $n \geq 1$, the recursion relations read

$$\varepsilon_n = \sum_m (\xi_m^+ u_{nm}^2 + \xi_m^- v_{nm}^2),$$

$$t_n^2 = \sum_m [(\xi_m^+)^2 u_{nm}^2 + (\xi_m^-)^2 v_{nm}^2] - t_{n-1}^2 - \varepsilon_n^2,$$

$$u_{n+1,m} = \frac{1}{t_n}[(\xi_m^+ - \varepsilon_n)u_{nm} - t_{n-1}u_{n-1,m}],$$

$$v_{n+1,m} = \frac{1}{t_n}[(\xi_m^- - \varepsilon_n)v_{nm} - t_{n-1}v_{n-1,m}]. \quad (31)$$

Note that for a particle-hole symmetric hybridization function, $\Delta(\omega)=\Delta(-\omega)$, the on-site energies $\varepsilon_n$ are zero for all $n$.

For a general hybridization function, the recursion relations have to be solved numerically. Although these relations are fairly easy to implement, it turns out that the iterative solution typically breaks down after about 20–30 steps. The source of this instability is the wide range of values for the parameters entering the recursion relations (e.g., the discretized energies $\xi_m^\pm$). In most cases this problem can be overcome using arbitrary precision routines for the numerical calculations. Furthermore, it is helpful to enforce the normalization of the vectors $u_{nm}$ and $v_{nm}$ after each step.

Analytical solutions for the recursion relations have so far been given only for a few special cases. Wilson derived a formula for the $t_n$ for a constant density of states of the conduction electrons in the Kondo version of the impurity model (Wilson, 1975a); this corresponds to a constant hybridization function $\Delta(\omega)$ in the interval $[-1,1]$. Here we have $\varepsilon_n=0$ for all $n$, and the expression for the $t_n$ reads

$$t_n = \frac{(1+\Lambda^{-1})(1-\Lambda^{-n-1})}{2\sqrt{1-\Lambda^{-2n-1}}\sqrt{1-\Lambda^{-2n-3}}}\Lambda^{-n/2}. \quad (32)$$

[Similar expressions have been given for the soft-gap model; see Bulla, Pruschke, and Hewson (1997).] In the limit of large $n$ this reduces to

$$t_n \to \frac{1}{2}(1+\Lambda^{-1})\Lambda^{-n/2}. \quad (33)$$

The fact that the $t_n$ fall off exponentially with the distance from the impurity is essential for the following discussion, so we briefly explain where this $n$ dependence comes from. Consider the discretized model Eq. (20) with a finite number $1+M/2$ ($M$ even) of conduction electron states for both positive and negative energies (the sum over $n$ then goes from 0 to $M/2$). This corresponds to $2+M$ degrees of freedom, which result in $2+M$ sites of the conduction electron part of the chain after the mapping to the chain Hamiltonian. The lowest energies in the discretized model Eq. (20) are the energies $\xi_{M/2}^\pm$ which, for a constant hybridization function, are given by $\xi_{M/2}^\pm = \pm\frac{1}{2}\Lambda^{-M/2}(1+\Lambda^{-1})$ [see Eq. (18)]. This energy shows up in the chain Hamiltonian as the last hopping matrix element $t_M$, so we have $t_M \sim \xi_{M/2}$ equivalent to Eq. (33).

Equation (26) is a specific one-dimensional representation of the single-impurity Anderson model Eq. (2) with the special feature that the hopping matrix elements $t_n$ fall off exponentially. As mentioned above, this representation is not exact since, in the course of its derivation, the $p \neq 0$ terms have been dropped. We should stress here that the dimensionality of the chain Hamiltonian is not related to that of the original model, which describes, for example, an impurity in a three-dimensional host (clearly, this holds only for a noninteracting conduction band). Nevertheless, the conduction electron sites of the chain do have a physical meaning in the original model, as they can be viewed as a sequence of shells centered around the impurity. The first site of the conduction electron chain corresponds to the shell with the maximum of its wave function closest to the impurity (Wilson, 1975a; Hewson, 1993a); this shell is coupled to a shell further away from the impurity, and so on.

### D. Iterative diagonalization

The transformations described so far are necessary to map the problem onto a form [the semi-infinite chain, Eq. (26)] for which an iterative renormalization group (RG) procedure can be defined. This is the point at which, finally, the RG character of the approach enters.

The chain Hamiltonian Eq. (26) can be viewed as a series of Hamiltonians $H_N$ ($N=0,1,2,\ldots$) which approaches $H$ in the limit $N \to \infty$:

$$H = \lim_{N\to\infty} \Lambda^{-(N-1)/2} H_N, \tag{34}$$

with

$$H_N = \Lambda^{(N-1)/2}\Bigg( H_{\rm imp} + \sqrt{\frac{\xi_0}{\pi}} \sum_\sigma (f_\sigma^\dagger c_{0\sigma} + c_{0\sigma}^\dagger f_\sigma) + \sum_{\sigma n=0}^{N} \varepsilon_n c_{n\sigma}^\dagger c_{n\sigma} + \sum_{\sigma n=0}^{N-1} t_n (c_{n\sigma}^\dagger c_{n+1\sigma} + c_{n+1\sigma}^\dagger c_{n\sigma}) \Bigg). \tag{35}$$

The factor $\Lambda^{(N-1)/2}$ in Eq. (35) [and, consequently, the factor $\Lambda^{-(N-1)/2}$ in Eq. (34)] has been chosen to cancel the $N$ dependence of $t_{N-1}$, the hopping matrix element between the last two sites of $H_N$. Such a scaling is useful for the discussion of fixed points, as described below. For a different $n$ dependence of $t_n$, as for the spin-boson model (Bulla *et al.*, 2005), the scaling factor has to be changed accordingly. (The $n$ dependence of $\varepsilon_n$ is, in most cases, irrelevant for the overall scaling of the many-particle spectra.)

Two successive Hamiltonians are related by

$$H_{N+1} = \sqrt{\Lambda} H_N + \Lambda^{N/2} \sum_\sigma \varepsilon_{N+1} c_{N+1\sigma}^\dagger c_{N+1\sigma} + \Lambda^{N/2} \sum_\sigma t_N (c_{N\sigma}^\dagger c_{N+1\sigma} + c_{N+1\sigma}^\dagger c_{N\sigma}), \tag{36}$$

and the starting point of the sequence of Hamiltonians is given by

$$H_0 = \Lambda^{-1/2}\Bigg( H_{\rm imp} + \sum_\sigma \varepsilon_0 c_{0\sigma}^\dagger c_{0\sigma} + \sqrt{\frac{\xi_0}{\pi}} \sum_\sigma (f_\sigma^\dagger c_{0\sigma} + c_{0\sigma}^\dagger f_\sigma) \Bigg). \tag{37}$$

This Hamiltonian corresponds to a two-site cluster formed by the impurity and the first conduction electron site. Note that, in the special case of the single-impurity Anderson model, one can also choose $H_{-1} = \Lambda^{-1} H_{\rm imp}$ as the starting point (with a proper renaming of parameters and operators) since the hybridization term has the same structure as the hopping term between the conduction electron sites.

The recursion relation Eq. (36) can now be understood in terms of a renormalization group transformation $R$:

$$H_{N+1} = R(H_N). \tag{38}$$

In a standard RG transformation, the Hamiltonians are specified by a set of parameters $\vec{K}$ and the mapping $R$ transforms the Hamiltonian $H(\vec{K})$ into another Hamiltonian of the same form $H(\vec{K}')$ with a new set of parameters $\vec{K}'$. In the context of the Kondo problem, it is the so-called poor man's scaling approach (Anderson, 1970) which works along these lines. In this approach, high-energy excitations close to the band edges of the conduction band are successively absorbed as renormalizations of the Hamiltonian parameters. When this is done to lowest order in perturbation theory, one obtains certain scaling equations, in the simplest case for the flow of the exchange coupling $J$ only. As it turns out, the exchange coupling scales to stronger and stronger values upon reducing the band cutoff, beyond the regime of the perturbation method used in the derivation.

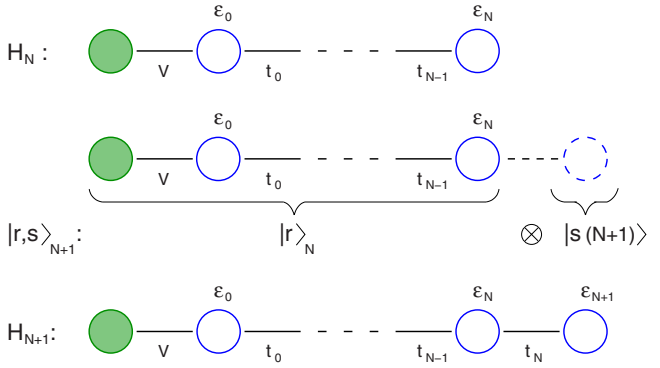


FIG. 2. (Color online) In each step of the iterative diagonalization scheme one site of the chain (with operators $c_{N+1}^{(\dagger)}$ and on-site energy $\varepsilon_{N+1}$) is added to the Hamiltonian $H_N$. A basis $|r;s\rangle_{N+1}$ for the resulting Hamiltonian $H_{N+1}$ is formed by the eigenstates of $H_N$, $|r\rangle_N$ and a basis of the added site $|s(N+1)\rangle$.

For more details and the physical interpretation of this result—a scaling of $J$ to strong coupling implies a screening of the impurity spin—we refer the reader to Hewson (1993a). We now come back to the RG transformation as it is performed with the NRG method.

A representation in which the Hamiltonian can be identified with a fixed set of parameters $\vec{K}$ does not exist, in general, for the $H_N$ which are obtained in the NRG iterations. Instead, we characterize $H_N$, and thereby also the RG flow, directly by the many-particle energies $E_N(r)$,

$$H_N|r\rangle_N = E_N(r)|r\rangle_N, \quad r = 1, \ldots, N_s, \tag{39}$$

with the eigenstates $|r\rangle_N$ and $N_s$ the dimension of $H_N$. This is particularly useful in the crossover regime between different fixed points, where a description in terms of an effective Hamiltonian with certain renormalized parameters is not possible. Only in the vicinity of the fixed points (except for certain quantum critical points) can one go back to an effective Hamiltonian description, as shown below.

Our primary aim now is to set up an iterative scheme for the diagonalization of $H_N$, in order to discuss the flow of the many-particle energies $E_N(r)$. Assume that, for a given $N$, the Hamiltonian $H_N$ has already been diagonalized, as in Eq. (39). We now construct a basis for $H_{N+1}$, as sketched in Fig. 2:

$$|r;s\rangle_{N+1} = |r\rangle_N \otimes |s(N+1)\rangle. \tag{40}$$

The states $|r;s\rangle_{N+1}$ are product states consisting of the eigenbasis of $H_N$ and a suitable basis $|s(N+1)\rangle$ for the added site (the new degree of freedom). From the basis Eq. (40) we construct the Hamiltonian matrix for $H_{N+1}$:

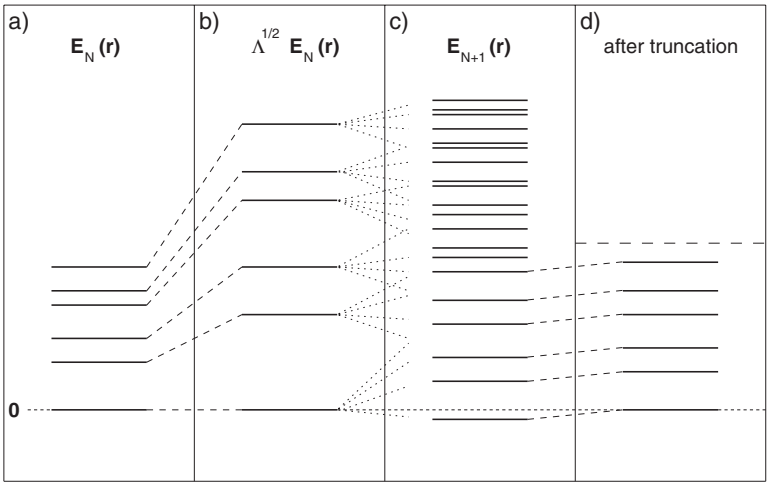


FIG. 3. (a) Many-particle spectrum $E_N(r)$ of the Hamiltonian $H_N$ with the ground-state energy set to zero. (b) The relation between successive Hamiltonians, Eq. (36), includes a scaling factor $\sqrt{\Lambda}$. (c) Many-particle spectrum $E_{N+1}(r)$ of $H_{N+1}$, calculated by diagonalizing the Hamiltonian matrix Eq. (41). (d) The same spectrum after truncation where only the $N_s$ lowest-lying states are retained.

$$H_{N+1}(rs,r's') = {}_{N+1}\langle r;s|H_{N+1}|r';s'\rangle_{N+1}. \tag{41}$$

For the calculation of these matrix elements it is useful to decompose $H_{N+1}$ into three parts:

$$H_{N+1} = \sqrt{\Lambda}H_N + \hat{X}_{N,N+1} + \hat{Y}_{N+1} \tag{42}$$

[see, for example, Eq. (36)], where the operator $\hat{Y}_{N+1}$ contains only the degrees of freedom of the added site, while $\hat{X}_{N,N+1}$ mixes these with the ones contained in $H_N$. The structure of the operators $\hat{X}$ and $\hat{Y}$, as well as the equations for the calculation of their matrix elements, depend on the model under consideration.

The following steps are illustrated in Fig. 3. In Fig. 3(a) we show the many-particle spectrum of $H_N$, that is, the sequence of many-particle energies $E_N(r)$. Note that, for convenience, the ground-state energy has been set to zero. Figure 3(b) shows the overall scaling of the energies by the factor $\sqrt{\Lambda}$; see the first term in Eq. (36).

Diagonalization of the matrix Eq. (41) gives the new eigenvalues $E_{N+1}(w)$ and eigenstates $|w\rangle_{N+1}$ which are related to the basis $|r;s\rangle_{N+1}$ via the unitary matrix $U$:

$$|w\rangle_{N+1} = \sum_{rs} U(w,rs)|r;s\rangle_{N+1}. \tag{43}$$

The set of eigenvalues $E_{N+1}(w)$ of $H_{N+1}$ is displayed in Fig. 3(c) (the label $w$ can now be replaced by $r$). The number of states increases on adding the new degree of freedom [when no symmetries are taken into account, the factor is the dimension of the basis $|s(N+1)\rangle$]. The ground-state energy is negative, but will be set to zero in the following step.

The increasing number of states is, of course, a problem for numerical diagonalization; the dimension of $H_{N+1}$ grows exponentially with $N$, even when we consider symmetries of the model so that the full matrix takes a block-diagonal form with smaller submatrices. This problem can be solved by a simple truncation scheme: after diagonalization of the various submatrices of $H_{N+1}$ one keeps only the $N_s$ eigenstates with the lowest many-particle energies. In this way, the dimension of the Hilbert space is fixed to $N_s$ and the computation time increases linearly with the length of the chain. Suitable values for the parameter $N_s$ depend on the model; for the single-impurity Anderson model, $N_s$ of the order of a few hundred is sufficient to get converged results for many-particle spectra, but the accurate calculation of static and dynamic quantities usually requires larger values of $N_s$. The truncation of high-energy states is illustrated in Fig. 3(d).

Such an *ad hoc* truncation scheme needs further explanation. First of all, there is no guarantee that this scheme will work in practical applications, and its quality should be checked for each individual application. An important criterion for the validity of this approach is whether the neglect of high-energy states spoils the low-energy spectrum in subsequent iterations—this can be easily seen numerically by varying $N_s$. The influence of the high-energy on the low-energy states turns out to be small since the addition of a new site to the chain can be viewed as a perturbation of relative strength $\Lambda^{-1/2} < 1$. This perturbation is small for large values of $\Lambda$, but for $\Lambda \to 1$ it is obvious that one has to keep more and more states to get reliable results. This also means that the accuracy of the NRG results decreases when $N_s$ is kept fixed and $\Lambda$ is reduced (vice versa, it is sometimes possible to improve the accuracy by increasing $\Lambda$ for fixed $N_s$).

From this discussion, we see that the success of the truncation scheme is intimately connected to the special structure of the chain Hamiltonian (that is, $t_n \propto \Lambda^{-n/2}$) which in turn is due to the logarithmic discretization of the original model. Note that a mapping to a one-dimensional chain can also be performed directly for a continuous conduction band, via a tridiagonalization scheme as described in detail by Hewson (1993a). The resulting chain Hamiltonian takes the same form as Eq. (26), but with $t_n \to$ const. For this Hamiltonian, the truncation scheme clearly fails. A similar observation is made when such a truncation is applied to the one-dimensional Hubbard model (see the discussion in Sec. V).

We now go into more details about construction of the basis $|r;s\rangle_{N+1}$. For this we have to decide, first of all, which of the symmetries of the Hamiltonian should be used in the iterative diagonalization. In the original calculations of Wilson (1975a) and Krishna-murthy *et al.* (1980a, 1980b), the following quantum numbers were used: total charge $Q$ (particle number with respect to half filling), total spin $S$, and $z$ component of the total spin $S_z$. It was essential in the 1970s to reduce the size of the matrices and hence the computation time as much as possible by invoking as many symmetries as possible. This is no longer necessary to such an extent on modern computer systems, i.e., one can, at least for single-band models, drop the total spin $S$ and classify the subspaces with the quantum numbers $(Q,S_z)$ only. This simplifies the program considerably, as one no longer has to worry about reduced matrix elements and the corresponding Clebsch-Gordan coefficients [see, for example, Krishna-murthy *et al.* (1980a)]. As we use this representation in Sec. III.A, here we explicitly state the form of $|r;s\rangle_{N+1}$:

$$|Q,S_z,r;1\rangle_{N+1} = |Q+1,S_z,r\rangle_N,$$

$$|Q,S_z,r;2\rangle_{N+1} = c^\dagger_{N+1\uparrow}\left|Q,S_z-\frac{1}{2},r\right\rangle_N,$$

$$|Q,S_z,r;3\rangle_{N+1} = c^\dagger_{N+1\downarrow}\left|Q,S_z+\frac{1}{2},r\right\rangle_N,$$

$$|Q,S_z,r;4\rangle_{N+1} = c^\dagger_{N+1\uparrow}c^\dagger_{N+1\downarrow}|Q-1,S_z,r\rangle_N. \quad (44)$$

Note that the quantum numbers $(Q,S_z)$ on the two sides of these equations refer to different systems; on the left-hand side they are for the system including the added site, and on the right-hand side without the added site. We do not go into the details of how to set up the Hamiltonian matrices Eq. (41), as this procedure is described in Appendix B in Krishna-murthy *et al.* (1980a).

For fermionic baths, the discretization parameter $\Lambda$ and the number of states $N_s$ kept in each iteration are the only parameters that govern the quality of the results of the NRG procedure. As discussed in Sec. IV.E, for the case of a bosonic bath the infinite-dimensional basis $|s(N+1)\rangle$ for the added bosonic site requires an additional parameter $N_b$, which determines the dimension of $|s(N+1)\rangle$.

### E. Renormalization group flow

The iterative diagonalization scheme yields the many-particle energies $E_N(r)$ with $r=1,\ldots,N_s$ (the number of states is less than $N_s$ for the very first steps before the truncation sets in). The index $N$ goes from 0 to a maximum number of iterations $N_{\max}$, which usually has to be chosen such that the system has approached its low-temperature fixed point.

As illustrated in Fig. 3, the sets of many-particle energies cover roughly the same energy range independent of $N$, due to the scaling factor $\Lambda^{(N-1)/2}$ in Eq. (35). The energy of the first excited state of $H_N$ is of the order of $\Lambda^{(N-1)/2}t_{N-1}$, a constant according to Eq. (33). The energy of the highest excited state kept after truncation depends on $N_s$—for typical parameters this energy is approximately 5–10 times larger than the lowest energy.

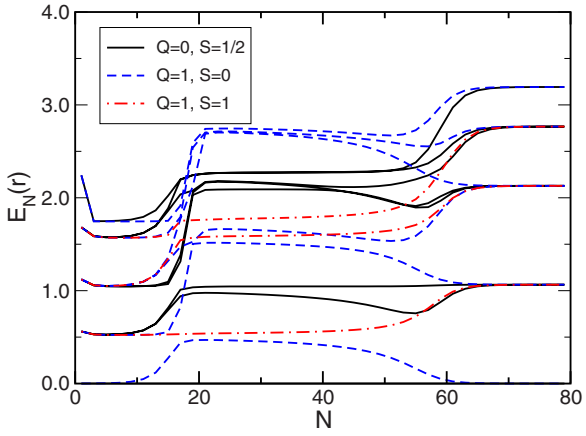


FIG. 4. (Color online) Flow of the lowest-lying many-particle levels of the single-impurity Anderson model for $\varepsilon_f=-0.5\times10^{-3}$, $U=10^{-3}$, $V=0.004$, and $\Lambda=2.5$. The states are labeled by the quantum numbers total charge $Q$ and total spin $S$. See text for a discussion of the fixed points.

When multiplied by the scaling factor $\Lambda^{-(N-1)/2}$ [see Eq. (34)], the energies $E_N(r)$ are an approximation to the many-particle spectrum of the chain Hamiltonian Eq. (26) within an energy window decreasing exponentially with increasing $N$. Note that the energies for higher-lying excitations obtained for early iterations are not altered in later iteration steps due to the truncation procedure. Nevertheless one can view the resulting set of many-particle energies and states from all NRG iterations $N$ as an approximation to the spectrum of the full Hamiltonian and use them to calculate physical properties in the whole energy range (see Sec. III).

Here we focus directly on the many-particle energies $E_N(r)$ and show how one can extract information about the physics of a given model by analyzing their flow, that is, the dependence of $E_N(r)$ on $N$. As a typical example for such an analysis, we show in Fig. 4 the flow of many-particle energies for the symmetric single-impurity Anderson model, with parameters $\varepsilon_f=-0.5\times10^{-3}$, $U=10^{-3}$, $V=0.004$, and $\Lambda=2.5$ [the same parameters as used in Fig. 5 in Krishna-murthy *et al.* (1980a); note that we show here a slightly different selection of the lowest-lying states]. The energies are plotted for odd $N$ only, that is, an odd total number of sites (which is $N+2$). This is necessary because the many-particle spectra show the usual even-odd oscillations of a fermionic finite-size system (the patterns for even $N$ look different but contain, of course, the same physics). The data points are connected by lines to visualize the flow. As in Krishna-murthy *et al.* (1980a), the many-particle energies are labeled by total charge $Q$ and total spin $S$.

What is the information one can extract from such a flow diagram? First of all we note the appearance of

three different fixed points of the RG transformation: for early iteration numbers $N<10$, for intermediate values of $N$, and for $N>60$ (strictly speaking, because we look at $N$ odd only, these are fixed points of $R^2$, not of $R$). The physics of these fixed points cannot be extracted by just looking at the pattern of the many-particle energies. This needs some further analysis, in particular the direct diagonalization of fixed point Hamiltonians (which usually have a simple structure) and the comparison of their spectrum with the numerical data. An excellent account of this procedure for the symmetric and asymmetric single-impurity Anderson model has been given by Krishna-murthy *et al.* (1980a, 1980b) and there is no need to repeat this discussion here. The analysis shows that, for $N\approx 3-9$, the system is very close to the free-orbital fixed point, with the fixed point Hamiltonian given by Eq. (26) for $U=0$ and $V=0$. This fixed point is unstable and for $N\approx 11-17$ we observe a rapid crossover to the local-moment fixed point in the range $N\approx 20-50$. This fixed point is characterized by a spin weakly coupled via a Kondo exchange to the conduction band. The local-moment fixed point is unstable as well, and after a characteristic crossover (see below), the system approaches the stable strong-coupling fixed point of a screened spin. Note that the terminology "strong coupling" was introduced originally because the fixed point Hamiltonian can be obtained from the limit $V\to\infty$, so "coupling" here refers to the hybridization, not the Coulomb parameter $U$.

The NRG method does not only allow one to match the structure of the numerically calculated fixed points with those of certain fixed point Hamiltonians. One can in addition identify the deviations from the fixed points (and thereby part of the crossover) with appropriate perturbations of the fixed point Hamiltonians. Again, we refer the reader to Krishna-murthy *et al.* (1980a, 1980b) for a detailed description of this analysis. The first step is to identify the leading perturbations around the fixed points. The leading operators can be determined by expressing them in terms of the operators that diagonalize the fixed point Hamiltonian; this tells us directly how these operators transform under the RG mapping $R^2$. One then proceeds with the usual classification into relevant, marginal, and irrelevant perturbations. The final results of this analysis perfectly agree with the flow diagram of Fig. 4: There is a relevant perturbation which drives the system away from the free-orbital fixed point, but for the local-moment fixed point there is only a marginally relevant perturbation, therefore the system only moves slowly away from this fixed point. Note that this marginal perturbation—which is the exchange interaction between the local moment and the spin of the first conduction electron site—gives rise to the logarithms observed in various physical quantities. Finally, there are only irrelevant operators which govern the flow to the strong-coupling fixed point. These are responsible for the Fermi-liquid properties at very low temperatures (Hewson, 1993a).

Having identified the leading operators for each fixed point, it is possible to calculate physical properties close to the fixed points perturbatively. We do not want to go into the calculational details here; see Krishna-murthy *et al.* (1980a) and also Sec. IV in Hewson (1993a).

Recently, Hewson *et al.* (2004) and Hewson (2005) developed an alternative approach to analyze the data from NRG calculations, based on the renormalized perturbation theory as developed by Hewson (1993b) for the single-impurity Anderson model. The ingredients of this method are an effective impurity model with renormalized parameters and a perturbation expansion in these parameters. As it turns out, the NRG method is a convenient (but not the only) way to calculate the renormalized parameters. The renormalized perturbation theory has been used to describe the physics close to the strong-coupling fixed point and is, in principle, applicable also on all energy scales. Higher-order expansions in the renormalized interactions require the careful use of counterterms, in order to avoid overcounting of renormalization effects. The approach has also been applied to study magnetic field effects in the Anderson impurity model (Hewson *et al.*, 2006) and for calculations of the conductance of quantum dots in nonequilibrium (Hewson *et al.*, 2005).

Flow diagrams as in Fig. 4 also give information about the relevant energy scales for the crossover between the fixed points. For example, an estimate of the Kondo temperature $T_K$ (the temperature scale that characterizes the flow to the strong-coupling fixed point) is given by $T_K\approx\omega_c\Lambda^{-\bar{N}/2}$, with $\bar{N}\approx 55$ for the parameters in Fig. 4.

The discussion of flow diagrams as in Fig. 4 concludes our introduction to the basics of the NRG approach. An important part is still missing, of course: the calculation of physical quantities from the flow of many-particle energies (and from certain additional matrix elements). This is the topic of the following section.

In Sec. IV we shall return to the discussion of flow diagrams and the structure of fixed points when studying various other quantum impurity systems, in particular the two-channel Kondo model, which displays a non-Fermi-liquid fixed point (see Sec. IV.B), and the soft-gap Anderson model, which has a quantum critical point separating the strong-coupling and local-moment phases (see Sec. IV.C.2).

We conclude this section with a few remarks on the relation between the NRG method and the density matrix renormalization group (DMRG) method, which is widely used for the investigation of one-dimensional interacting systems (Noack and Manmana, 2005; Schollwöck, 2005; Hallberg, 2006). The DMRG method works with a similar philosophy, that is, a stepwise increase of the system size within an iterative procedure, but it uses a different criterion for the selection of states, based on the density matrix. The DMRG method works for systems where the parameters do not fall off exponentially as one goes along the chain (a necessary requirement for the NRG method to work); therefore the range of applicability of the two methods is somewhat different. Note

that the DMRG method has been applied to quantum impurity systems as well (Nishimoto and Jeckelmann, 2004); nevertheless, the NRG approach is more suitable when it comes to describing the low-energy properties of impurity systems, in particular the appearance of fixed points and the crossover between fixed points.

## III. CALCULATION OF PHYSICAL PROPERTIES

In the previous section we discussed information that can be gained from the low-lying energy levels during the RG flow. Clearly, a lot can already be learned on this level about the physical properties of the system. However, an obvious aim of any method is also to calculate thermodynamic quantities like specific heat or susceptibilities, or even dynamical properties.

We start by reminding the reader that the coefficients $t_n$ appearing in the transformed Hamiltonian Eq. (26) decay like $\Lambda^{-n/2}$ for large $n$. This aspect can be used to relate a certain chain length $N$ with a temperature (energy) scale of the model in the following way (Wilson, 1975a; Krishna-murthy *et al.*, 1980a; Oliveira and Oliveira, 1994): Diagonalizing the scaled Hamiltonian (35) for a given chain length $N$ yields a set of eigenvalues $E_l^{(N)}$, where the spacing of the lowest eigenvalues is of order 1 due to the rescaling with $\Lambda^{(N-1)/2}$. Clearly, for a given temperature $T$, the eigenvalues $E_l^{(N)}-E_0^{(N)} \gg \Lambda^{(N-1)/2}k_BT$, where $E_N^{(0)}$ is the ground-state energy, will not contribute significantly to the calculation of physical properties because they will be exponentially suppressed by the Boltzmann factor. Thus, for an inverse temperature $\beta_N=(k_BT_N)^{-1}$ with

$$\beta_N\Lambda^{-(N-1)/2} =: \bar{\beta} \tag{45}$$

and $\bar{\beta}$ of order 1, it is permissible to approximate the full Hamiltonian $H_N$ by the truncated one for the same $N$, provided that enough states are kept to ensure $E_l^{(N)}-E_N^{(0)} \gg \Lambda^{(N-1)/2}k_BT_N$ for large eigenvalue index $l$.

On the other hand, longer chains will significantly modify only the first few eigenvalues $E_l^{(N)}-E_N^{(0)} \ll \Lambda^{(N-1)/2}k_BT_N$, i.e., for the calculation of impurity properties on the temperature or energy scale $k_BT_N$ they do not introduce significant contributions, and it will thus be sufficient to use the truncated Hamiltonian $H_N$ instead of the full Hamiltonian (26). The actual choice of $\bar{\beta}$ depends on the value of the discretization parameter $\Lambda$ and the number of states kept. In practice, a value $\bar{\beta}=0.5–1$ has been proven to be appropriate.

Thus, provided we can keep enough states in the truncation scheme introduced in Sec. II, it is permissible to use the truncated Hamiltonian at level $N$ obtained from the iterative diagonalization to calculate thermodynamic properties for the impurity on the temperature scale $k_BT_N=\Lambda^{-(N-1)/2}/\bar{\beta}$ (see the next section).

The situation becomes more complicated when one is interested in quantities that mix information on different energy scales, as is the case for dynamical response functions. Here a more elaborate scheme has to be developed, which will be discussed in Sec. III.B.

### A. Thermodynamic and static properties

#### 1. Entropy, specific heat, and susceptibility

The simplest physical quantities related to the impurity degrees of freedom are the impurity contribution to the entropy $S_{\mathrm{imp}}$, specific heat $C_{\mathrm{imp}}$, and magnetic susceptibility $\chi_{\mathrm{imp}}$.

The entropy and specific heat are the first derivatives of the free energy $F=-k_BT\ln Z$ and internal energy $U=\langle H\rangle$ with respect to temperature, i.e.,

$$S=-\frac{\partial F}{\partial T}$$

and

$$C=\frac{\partial U}{\partial T}.$$

From a numerical point of view, performing differentiations is something to avoid if possible. For the numerical implementation of the NRG method, another complication arises. To avoid an exponential increase of energies, it is necessary to subtract the ground-state energy at each NRG level $N$, i.e., one would have to keep track of these subtractions. Clearly, a more convenient approach is to evaluate the derivative analytically, yielding

$$S/k_B=\beta\langle H\rangle+\ln Z$$

for the entropy and

$$C/k_B=\beta^2(\langle H^2\rangle-\langle H\rangle^2)$$

for the specific heat.

Other local properties usually involve the calculation of correlation functions. Here one has to distinguish between equal-time correlators and susceptibilities. In the following we will concentrate on the latter and address the former in Sec. III.A.2.

The prescription to calculate the impurity contribution to the isothermal magnetic susceptibility requires some more thought. The standard definition for the isothermal magnetic susceptibility is (we set $g\mu_B=1$)

$$\chi(T)=\int_0^\beta \langle S_z[\tau]S_z\rangle d\tau-\beta\langle S_z\rangle^2, \tag{46}$$

with $\tau$ the imaginary time ($0<\tau<\beta$), $S_z$ the $z$ component of the impurity spin operator, and

$$\langle S_z[\tau]S_z\rangle=\frac{1}{Z}\,\mathrm{Tr}(e^{-\beta H}e^{\tau H}S_ze^{-\tau H}S_z).$$

However, evaluation of the latter expectation value is equivalent to the calculation of a dynamical correlation function. This, as well as the calculation of the adiabatic static susceptibility from the dynamic response function in the limit $\omega\to 0$, is in general a much more complex task and will be discussed in the next section.

Alternatively, one can apply a finite magnetic field $B$ to the model and calculate numerically the derivative $\partial m/\partial B$, where $m$ is the local magnetization due to the presence of $B$. This approach requires at least two NRG calculations (one with and one without the field $B$). Furthermore, as we need $\partial m(B)/\partial B$ in the limit $B\to 0$, it is often necessary to calculate a series of $B$ values to be sure that one has indeed reached this limit with a linear dependence $m(B)\propto B$. From this point of view, this approach appears to be rather costly in computer resources.

Here we employ a different approach, which in turn is also more closely related to the experimental definition of this quantity. In general, experiments address the susceptibility of the whole system. Since the total spin commutes with the Hamiltonian, i.e., $\langle S_{\mathrm{tot},z}[\tau]S_{\mathrm{tot},z}\rangle = \langle S_{\mathrm{tot},z}S_{\mathrm{tot},z}\rangle$ is time independent, Eq. (46) simplifies to

$$\chi_{\mathrm{tot}}(T) = \beta(\langle S_{\mathrm{tot},z}^2\rangle - \langle S_{\mathrm{tot},z}\rangle^2)$$

in this case. From this, one subtracts the susceptibility of a reference system, i.e., one without impurity, leading to Wilson's definition (Wilson, 1975a) of the impurity contribution to the susceptibility,

$$\chi_{\mathrm{imp}}(T) = \chi_{\mathrm{tot}}(T) - \chi_{\mathrm{tot}}^{(0)}(T). \tag{47}$$

Since $S_{\mathrm{tot},z}$ is a quantum number used to classify the states in the calculation, the expectation values in Eq. (47) can be evaluated straightforwardly.

Similarly, the impurity contributions to the entropy and specific heat can be calculated as

$$S_{\mathrm{imp}}(T) = S_{\mathrm{tot}}(T) - S_{\mathrm{tot}}^{(0)}(T) \tag{48}$$

and

$$C_{\mathrm{imp}}(T) = C_{\mathrm{tot}}(T) - C_{\mathrm{tot}}^{(0)}(T), \tag{49}$$

where $S_{\mathrm{tot}}^{(0)}(T)$ and $C_{\mathrm{tot}}^{(0)}(T)$ are again the entropy and specific heat of a suitable reference system.

We discuss the details of the actual calculation for the entropy as a specific example. Following the introductory remarks, we can—for a given temperature $k_BT$—restrict the Hilbert space to the NRG iteration $N$ satisfying Eq. (45). If we denote the corresponding Hamiltonian by $H^{(N)}$, we can introduce the quantity

$$S^{(N)}/k_B := \beta\langle H^{(N)}\rangle + \ln Z^{(N)}, \tag{50}$$

where, using the notation of Sec. II [see, for example, Eq. (40)],

$$\langle\cdots\rangle^{(N)} := \frac{1}{Z^{(N)}}\sum_{Q,S_z}\sum_{r} e^{-\beta E_N(Q,S_z,r)} \times {}_N\langle Q,S_z,r|\cdots|Q,S_z,r\rangle_N \tag{51}$$

and

$$Z^{(N)} := \sum_{Q,S_z}\sum_{r} e^{-\beta E_N(Q,S_z,r)}. \tag{52}$$

The impurity contribution to the entropy for a temperature $k_BT_N := \Lambda^{-(N-1)/2}/\bar{\beta}$ can then be obtained as

$$S_{\mathrm{imp}}(T_N)/k_B \approx S^{(N)}/k_B - S_{\mathrm{cb}}^{(N)}/k_{\mathrm{B}}. \tag{53}$$

Here we introduced the free entropy

$$S_{\mathrm{cb}}^{(N)}/k_B := \beta\langle H_{\mathrm{cb}}^{(N)}\rangle^{(N)} + \ln Z_{\mathrm{cb}}^{(N)}, \tag{54}$$

obtained from the bare conduction Hamiltonian

$$H_{\mathrm{cb}}^{(N)} = \sum_{\sigma n=0}^{N}[\epsilon_n c_{n\sigma}^\dagger c_{n\sigma} + t_n(c_{n\sigma}^\dagger c_{n+1\sigma} + c_{n+1\sigma}^\dagger c_{n\sigma})]. \tag{55}$$

Similarly, for $k_BT_N = \Lambda^{-(N-1)/2}/\bar{\beta}$, the specific heat and magnetic susceptibility are obtained as

$$C_{\mathrm{imp}}(T_N)/k_B \approx C_{\mathrm{tot}}^{(N)} - C_{\mathrm{cb}}^{(N)} \tag{56}$$

and

$$\chi_{\mathrm{imp}}(T_N) \approx \chi_{tot}^{(N)} - \chi_{\mathrm{cb}}^{(N)}. \tag{57}$$

Since the Hamiltonian (55) is a noninteracting system, these quantities $S_{\mathrm{cb}}^{(N)}$, etc., can be expressed via the eigenvalues $\eta_{l\sigma}$ of Eq. (55) in standard fashion.

For $T\to 0$ the behavior of $S_{\mathrm{imp}}(T)$ and $\chi_{\mathrm{imp}}(T)$ given by Eqs. (56) and (57) can be obtained analytically from the fixed point spectra. We refer the reader interested in this derivation to Wilson (1975a) and concentrate here on the actual numerical calculations.

Another aspect is that the fixed points and the flow to them are different for $N$ even and odd. This in turn means that one in principle has to calculate thermodynamic properties for either $N$ even or odd only and thus lose half of the temperature values. One can, however, use all information by averaging odd and even steps.

- For a given $N$, calculate the quantities $O^{(N-1)}$, $O^{(N)}$, and $O^{(N+1)}$.
- Approximate $O(T_N)$ as

$$O(T_N) \approx \frac{1}{2}\left(O^{(N)} + O^{(N-1)} + \frac{O^{(N+1)} - O^{(N-1)}}{T_{N+1} - T_{N-1}} \times (T_N - T_{N-1})\right).$$

  The first term in the large parentheses is the observable calculated at step $N$. The second and third terms are a linear interpolation of the values at $N-1$ and $N+1$ to iteration $N$.
- Continue with $N+1$.

As a positive side effect, this averaging also improves the accuracy of the thermodynamic quantities calculated (see, e.g., Fig. 5).

At this point some remarks about potential numerical problems should be made. The arguments given in the introduction to this section rely on the assumption that one can keep states with high enough energy to ensure (i) the accuracy of the states at medium and low energies and (ii) the convergence of the partition function and expectation values. Depending on the actual quantity to be calculated, the latter point can in principle lead to problems. As an example, consider $\langle H\rangle$ and $\langle H^2\rangle$. While for a given energy cutoff $E_{\mathrm{cut}}$ the contribution

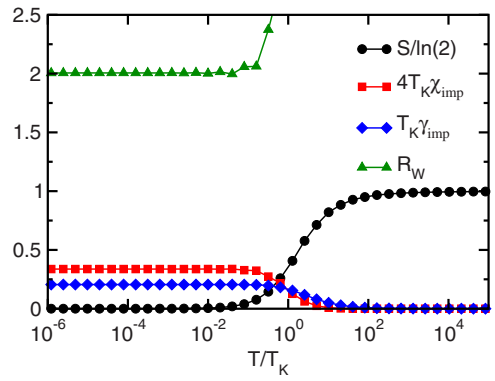


FIG. 5. (Color online) Entropy $S_{\rm imp}(T)$, susceptibility $\chi_{\rm imp}(T)$, Sommerfeld coefficient $\gamma_{\rm imp}=C_{\rm imp}(T)/T$, and Wilson ratio $R_W$ for the single-channel Kondo model. The Kondo temperature is defined by the Wilson relation $\chi_{\rm imp}(0)=0.413/4T_K$.

$\bar{\beta}E_{\rm cut}e^{-\bar{\beta}E_{\rm cut}}$ to $\langle H\rangle$ can already be small enough to use the sum up to $E_{\rm cut}$ as an approximation to $\langle H\rangle$, this need not necessarily be true for $\langle H^2\rangle$. Thus the resulting values for the specific heat $\bar{\beta}(\langle H^2\rangle-\langle H\rangle^2)$ can be rather poor, although the entropy and susceptibility are much more accurate. In this case numerical differentiation of the entropy is the better choice (Costi *et al.*, 1994a).

### 2. Other local properties

While entropy, specific heat, and impurity susceptibility can be obtained directly from the spectra of the Hamiltonian, other local quantities require the calculation of the corresponding local matrix elements. As an example, we discuss here the local occupancy $n_\sigma=\langle f_\sigma^\dagger f_\sigma\rangle$ and double occupancy $D=\langle f_\uparrow^\dagger f_\uparrow f_\downarrow^\dagger f_\downarrow\rangle$ for the single-impurity Anderson model Eq. (2). Both quantities are of interest in actual applications. Expectation values of other local operators can be calculated in a similar manner.

As before, on a given temperature scale $k_BT_N=\Lambda^{-(N-1)/2}/\bar{\beta}$, we approximate the expectation values by

$$n_\sigma(T_N)\approx\frac{1}{Z^{(N)}}\sum_{Q,S_z}\sum_r e^{-\beta E_N(Q,S_z,r)}\times{}_N\langle Q,S_z,r|f_\sigma^\dagger f_\sigma|Q,S_z,r\rangle_N \tag{58}$$

for the occupancy and a corresponding expression for the double occupancy. The matrix elements

$$n_\sigma(Q,S_z,r,r';N):={}_N\langle Q,S_z,r|f_\sigma^\dagger f_\sigma|Q,S_z,r'\rangle_N \tag{59}$$

at a given step $N$ can be calculated from those of the previous step $N-1$ with the help of the basis transformation (43) for the step $N$. The same scheme works for the matrix elements of the double occupancy $D(Q,S_z,w,w',N)$ and the matrix elements of general local operators—like $f_\sigma^\dagger$ needed in the calculation of the single-particle Green's function (see Sec. III.B).

All that is left to specify are the initial values for $n_\sigma(Q,S_z,w,w';-1)$ and $D(Q,S_z,w,w';-1)$ on the level of the impurity. For the Anderson model Eq. (2) they are explicitly given as

$$\begin{aligned}
&n_\sigma(0,0,0,0;-1)=0,\\
&n_\sigma(1,\sigma,0,0;-1)=1,\\
&n_\sigma(2,0,0,0;-1)=2,\\
&D(0,0,0,0;-1)=0,\\
&D(1,\sigma,0,0;-1)=0,\\
&D(2,0,0,0;-1)=1.
\end{aligned} \tag{60}$$

With these prerequisites we are now in the position to do actual calculations for the thermodynamic properties of quantum impurity models using the NRG method.

### 3. Example: The Kondo model

As an example for the method we present results for the Kondo model,

$$H=\sum_{k\sigma\alpha}\varepsilon_k c_{k\sigma\alpha}^\dagger c_{k\sigma\alpha}+J\sum_\alpha \mathbf{S}\cdot\mathbf{s}_\alpha, \tag{61}$$

with $\alpha$ the channel index and $\mathbf{S}$ ($\mathbf{s}_\alpha$) the spin operators of the impurity (the conduction band electrons at the impurity site with channel index $\alpha$). Depending on the number of bands coupling to the local spin, one observes a conventional Kondo effect with the formation of a local Fermi-liquid or non-Fermi-liquid fixed point with anomalous temperature dependencies of the specific heat and susceptibility as well as a residual entropy $S(0)=\frac{1}{2}\ln 2$ at $T=0$ (Cragg *et al.*, 1980; Nozières and Blandin, 1980) (this will be discussed in Secs. IV.A and IV.B).

In Fig. 5 we show the entropy $S_{\rm imp}(T)$, susceptibility $\chi_{\rm imp}(T)$, Sommerfeld coefficient $\gamma_{\rm imp}=C_{\rm imp}(T)/T$, and Wilson ratio $R_W:=4\pi^2\chi_{\rm imp}(T)/[3\gamma_{\rm imp}(T)]$ as a function of $T/T_K$ for the single-channel Kondo model. As the Kondo coupling we choose $J=0.05D$, where $D$ is the half-bandwidth of the conduction band, for which we assume a density of states $\rho_{\rm cb}(\epsilon)=N_F\Theta(D-|\epsilon|)$. The value of $T_K$ is obtained from Wilson's definition (Wilson, 1975a) $4T_K\chi_{\rm imp}(0)=0.413$. Calculations are performed with a discretization parameter $\Lambda=4$, keeping 400 states at each NRG step. Although this value of $\Lambda$ seems to be fairly large, experience tells us that for static properties such large values of $\Lambda$ are still permissible, considerably reducing the number of states one has to keep in the truncation procedure.

One sees in Fig. 5 the quenching of the local moment by the Kondo effect for temperatures of the order of $T_K$. The high-temperature values for the entropy $S_{\rm imp}(T\to\infty)=\ln 2$ and the Wilson ratio $R_W=2$ below $T_K$ (Wilson, 1975a) are also obtained with high precision.

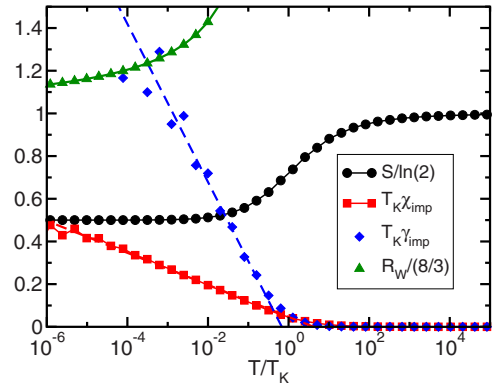


FIG. 6. (Color online) Entropy $S_{\rm imp}(T)$, susceptibility $\chi_{\rm imp}(T)$, Sommerfeld coefficient $\gamma_{\rm imp}=C_{\rm imp}(T)/T$, and Wilson ratio $R_W$ for the two-channel Kondo model. The value for the Kondo temperature is the same as in Fig. 5.

If one adds a second screening channel to the Kondo model, one arrives at the so-called two-channel Kondo model. The rather interesting physics of this model will be discussed in Sec. IV.B. Here we want to demonstrate that NRG calculations for this model are possible too; however, the additional bath degrees of freedom, which lead to Hilbert spaces larger by a factor of 4, make calculations more cumbersome and for some quantities also less accurate. In Fig. 6 we show as before the impurity contributions to the entropy, susceptibility, and Sommerfeld coefficient as well as the Wilson ratio as a function of $T/T_K$. The impurity parameters are the same as in Fig. 5; for the NRG method we again choose $\Lambda=4$ but keep 8100 states per iteration. The value of $T_K$ is that of the corresponding single-channel model. As emphasized before, the entropy and susceptibility come out quite accurately; in particular, the residual entropy $S(0)=\frac{1}{2}\ln 2$ is obtained as well as the logarithmic increase of $\chi_{\rm imp}(T)\propto\ln(T/T_K)$ for $T<T_K$ (Cragg *et al.*, 1980; Pang and Cox, 1991; Affleck *et al.*, 1992). The specific heat, however, is less accurate; it does show the logarithmic increase as expected, although with strong oscillations superimposed. By fitting both quantities with a logarithmic form, one can recover the correct Wilson ratio $R_W=8/3$ for $T\to 0$. Note, however, that the latter value is approached only logarithmically.

#### 4. Improving the accuracy: The $z$ averaging

For more complex quantum impurity models, like the two-channel Kondo model (discussed in the previous section and in Sec. IV.B) or multiorbital models, the Hilbert space per NRG step increases more strongly than for single-channel models. Consequently, the fraction of states kept in the truncation procedure has to be reduced. As has been pointed out by Oliveira and Oliveira (1994), this leads to an exponential decrease of accuracy, which can, however, be compensated by an increase of the discretization parameter $\Lambda$. However, the use of a large $\Lambda$ (i) takes one further away from the continuum limit $\Lambda\to 1$ of interest and (ii) introduces oscillations into the thermodynamic expectation values. A way out of this dilemma, proposed by Oliveira and Oliveira (1994), is as follows.

- Instead of the discretization Eq. (6) choose
$$x_n=\Lambda^{-n+z},\quad n\geq 1,\quad z\in[0,1). \tag{62}$$
The mapping to a semi-infinite chain is done as before (see Sec. II.C) with the replacement $\Lambda^{-n}\to\Lambda^{-n+z}$ for $n\geq 1$.
- For fixed $z\in[0,1)$ perform a NRG calculation for a fixed set of temperatures $T_N=\Lambda^{-(N-1)/2}/\bar{\beta}$ as before.
- Average over several calculations for different $z$. This averaging is meant to reintroduce the continuum limit to some extent (Oliveira and Oliveira, 1994) and also can be shown to remove oscillations introduced by the use of large $\Lambda\gg 1$.

For two different values of $z$ this procedure already removes spurious oscillations in thermodynamic quantities and reproduces the exact result with good accuracy for $\Lambda$ as large as $\Lambda=10$. This technique can be incorporated straightforwardly into the NRG code [for applications, see Silva *et al.* (1996); Costa *et al.* (1997); Paula *et al.* (1999); Campo and Oliveira (2003, 2004); Ramos *et al.* (2003)].

### B. Dynamic properties

As for static properties, there exist a variety of interesting local dynamical quantities, for example, the single-particle Green's function, the dynamical magnetic susceptibility, or the density-density response function. Depending on the actual model and questions at hand, one may also be interested in response functions of other observables.

In Sec III.B.1 we discuss the application of the NRG method to the calculation of the equilibrium single-particle Green's function and the corresponding spectral density as a specific example (Frota and Oliveira, 1986; Sakai *et al.*, 1989; Costi and Hewson, 1992b; Costi *et al.*, 1994a). Calculations can be carried out at both $T=0$ and finite temperature, thereby allowing the calculation also of transport properties (Costi *et al.*, 1994a). The scheme can also be applied to other observables; one just has to replace the annihilation and creation operators by the corresponding observables and respect the differences between fermionic and bosonic operators in the Lehmann representation [see Eq. (67)]. Two improvements to dynamics, using the correlation self-energy (Bulla *et al.*, 1998) and the reduced density matrix (Hofstetter, 2000), are described in Sec. III.B.2. Section III.B.3 deals with the calculation of the transient dynamics of impurities subject to sudden local perturbations.

#### 1. Equilibrium dynamics and transport

For definiteness we consider the Anderson impurity model and illustrate the procedure for the impurity spectral density $A_\sigma(\omega,T)=-\frac{1}{\pi}\,\mathrm{Im}\,G_\sigma(\omega,T)$, with

$$G_\sigma(\omega,T)=\int_{-\infty}^{+\infty}d(t-t')e^{i\omega(t-t')}G_\sigma(t-t'), \tag{63}$$

$$G_\sigma(t-t')=-i\theta(t-t')\langle[f_\sigma(t),f_\sigma^\dagger(t')]_+\rangle_\varrho, \tag{64}$$

with $\varrho$ the density matrix of the system and $f_\sigma(t)=e^{iHt}f_\sigma(0)e^{-iHt}$ the $f$-electron annihilation operator in the Heisenberg representation. Suppose, for the moment, that we know all the many-body eigenstates $|r\rangle$ and eigenvalues $E_r$ of the Anderson impurity Hamiltonian $H$ exactly. Then the density matrix $\varrho(T)$ and partition function $Z(T)$ of the full system at temperature $k_BT=1/\beta$ are given by

$$\varrho(T)=\frac{1}{Z(T)}\sum_r e^{-\beta E_r}|r\rangle\langle r|, \tag{65}$$

$$Z(T)=\sum_r e^{-\beta E_r}, \tag{66}$$

and the impurity spectral density $A_\sigma$ can be written in the Lehmann representation as

$$A_\sigma(\omega,T)=\frac{1}{Z(T)}\sum_{r,r'}|M_{r,r'}|^2(e^{-E_r/k_BT}+e^{-E_{r'}/k_BT})\times\delta(\omega-(E_{r'}-E_r)), \tag{67}$$

with $M_{r,r'}=\langle r|f_\sigma|r'\rangle$ the relevant many-body matrix elements.

Consider first the $T=0$ case ($T>0$ is described below). Then

$$A_\sigma(\omega,T=0)=\frac{1}{Z(0)}\sum_r|M_{r,0}|^2\delta(\omega+(E_r-E_0))+\frac{1}{Z(0)}\sum_{r'}|M_{0,r'}|^2\delta(\omega-(E_{r'}-E_0)), \tag{68}$$

with $E_0=0$ the ground-state energy. In order to evaluate this from the information that is obtained from an iterative diagonalization of $H$, we consider the impurity spectral densities corresponding to the sequence of Hamiltonians $H_N$, $N=0,1,\ldots$, whose characteristic scale is $\omega_N=\frac{1}{2}(1+\Lambda^{-1})\Lambda^{-(N-1)/2}$,

$$A_\sigma^N(\omega,T=0)=\frac{1}{Z_N(0)}\sum_r|M_{r,0}^N|^2\delta(\omega+E_r^N)+\frac{1}{Z_N(0)}\sum_{r'}|M_{0,r'}^N|^2\delta(\omega-E_{r'}^N). \tag{69}$$

Here $E_r^N$ and $|r\rangle_N$ are the eigenvalues and eigenstates of $H_N$, i.e.,

$$H_N|r\rangle_N=E_r^N|r\rangle_N \tag{70}$$

and

$$M_{r,r'}^N={}_N\langle r|f_\sigma|r'\rangle_N \tag{71}$$

are the relevant many-body matrix elements, whose calculation will be outlined below. Since the spectrum of $H_N$ is truncated, the range of excitations it describes is limited to $0\le\omega\le K(\Lambda)\omega_N$, where $K(\Lambda)$ depends on both $\Lambda$ and the actual number of states retained at each iteration and is typically 5–10 for $\Lambda=1.5$–$2.0$ and $N_s=500$–$1000$ retained states. Moreover, excitations and eigenstates below the characteristic scale $\omega_N$ of $H_N$ will only be approximations to the excitations and eigenstates of the infinite system described by $H$. These excitations and eigenstates are refined in subsequent iterations. Hence, for each $N=1,2,\ldots$, we can evaluate the spectral density from $A_\sigma^N$ at a frequency $\omega$ chosen to lie in the window $\omega_N\le\omega\le K(\Lambda)\omega_N$,

$$A_\sigma(\omega,T=0)\approx A_\sigma^N(\omega,T=0). \tag{72}$$

A typical choice, for $\Lambda=1.5$–$2.0$, is $\omega=2\omega_N$.

The above procedure still only yields discrete spectra. For comparison with experiment, smooth spectra are required, so we replace the delta functions $\delta(\omega\pm E_r^N)$ appearing in Eq. (69) by smooth distributions $P(\omega\pm E_r^N)$. A natural choice for the width $\eta_N$ of $P$ is $\omega_N$, the characteristic scale for the energy level structure of $H_N$. Two commonly used choices for $P$ are the Gaussian, $P_G$, and the logarithmic Gaussian, $P_{\rm LG}$, distribution (Sakai *et al.*, 1989; Costi *et al.*, 1994a; Bulla *et al.*, 2001):

$$P_G(\omega\pm E_r^N)=\frac{1}{\eta_N\sqrt{\pi}}e^{-[(\omega\pm E_r^N)/\eta_N]^2}, \tag{73}$$

$$P_{\rm LG}(\omega\pm E_r^N)=\frac{e^{-b^2/4}}{bE_r^N\sqrt{\pi}}e^{-[\ln(|\omega|/E_r^N)/b]^2}. \tag{74}$$

For the Gaussian, a width $\eta_N=0.3\omega_N$–$0.8\omega_N$ is typically used (Costi *et al.*, 1994a), whereas, for the logarithmic Gaussian, a typical width parameter $b=0.3$–$0.7$ is used (Sakai *et al.*, 1989; Bulla *et al.*, 2001). Note that the logarithmic Gaussian gives little weight to excitations below $\omega_N$ and more weight to higher-energy excitations. Due to the logarithmic discretization, this might appear to be the better choice. In practice, the difference in using a Gaussian is small.

In general, spectra for even and odd $N$ differ by a few percent at most as a result of finite-size effects (see also the discussion of the reduced density matrix approach in Sec. III.B.2), so generally either even $N$ or odd $N$ spectra are calculated (as for thermodynamics). It is also possible to combine information from shells $N$ and $N+2$ by an appropriate weighting (Bulla *et al.*, 2001). We note also that, since the broadening is proportional to the energy, a peak of intrinsic width $\Gamma$ at frequency $\Omega_0$ will be well resolved by the above procedure provided that $\Omega_0\ll\Gamma$, which is the case for the Kondo resonance and other low-energy resonances. In the opposite case, the low (logarithmic) resolution at higher frequencies may be insufficient to resolve the intrinsic widths and heights of such peaks, although their weights are correctly cap-

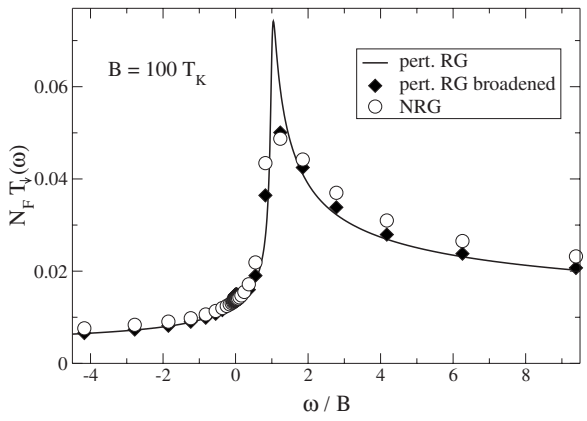


FIG. 7. Spin-resolved Kondo resonance at high magnetic fields calculated with the NRG method and perturbative RG. The large Gaussian broadening used at $\omega=g\mu_B B=100T_K$ reduces the height of the sharp peak and overestimates its width, as is evident on applying the NRG broadening procedure to the analytic perturbative RG result (Rosch *et al.*, 2003).

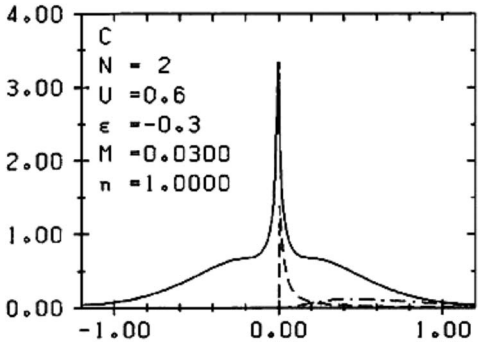


FIG. 8. $T=0$ spectral densities for single-particle (solid line), magnetic (dashed line), and charge (dot-dashed line) excitations of the spin degenerate symmetric, Anderson model versus energy $\omega/D$ for $U=0.6D$, $D=1.0$, and $\Delta/\pi=M=0.03D$. From Sakai *et al.*, 1989.

tured. In cases where the width of such high-energy peaks is due to single-particle effects, e.g., the resonant level in the empty orbital regime of the Anderson model, one can use the representation of the spectral density in terms of the correlation self-energy, as described in the next section, with the single-particle broadening explicitly included so that essentially the correct peak widths and heights are obtained. In other cases, when the width of such peaks is due to correlations, one inevitably has some overbroadening. An extreme example is the spin-resolved Kondo resonance at high magnetic fields $B\gg T_K$, which is sharply peaked at $\omega=B$ and is highly asymmetrical, as shown in Fig. 7. The extent of the problem is quantified here by comparison with analytic perturbative results with and without the NRG broadening procedure.

A procedure for obtaining smooth spectra that resolves finite-frequency peaks without broadening the discrete spectra involves an averaging over many different discretizations of the band (the $z$ averaging discussed in the previous section on thermodynamics). We refer the reader to Yoshida *et al.* (1990) for details.

In calculating the impurity spectral density, one requires the matrix elements $M^N_{r,r'}$ at each iteration. The matrix elements are obtained recursively using the unitary transformation Eq. (43), yielding

$$M^N_{r,r'}=\sum_{p,s_N}\sum_{p',s'_N}U_N(r,ps_N)U_N(r',p's'_N)\delta_{s_N,s'_N}M^{N-1}_{p,p'}. \tag{75}$$

Hence the matrix elements $M^N_{r,r'}$ can be evaluated recursively from knowledge of the eigenstates of finite-size Hamiltonians up to $H_N$ starting from the initial matrix elements ${}_{-1}\langle r|f_\sigma|r'\rangle_{-1}$ of the isolated impurity $H_{\rm imp}=\varepsilon_f\Sigma_\sigma f^\dagger_\sigma f_\sigma+Uf^\dagger_\uparrow f_\uparrow f^\dagger_\downarrow f_\downarrow$. Similar considerations apply to other local dynamical quantities such as dynamical spin and charge susceptibilities. Figure 8 shows $T=0$ spectral densities for single-particle, magnetic, and charge excitations calculated using the above procedure. These NRG calculations have been shown to satisfy exact Fermi-liquid relations, such as the Friedel sum rule for the single-particle spectral density and the Shiba relation for the magnetic excitation spectrum, to within a few percent irrespective of the interaction strength $U/\pi\Delta$ in the Anderson model or the value of the exchange $J$ in the Kondo model [see Costi *et al.* (1994a) and Costi (1998) for a discussion]. We note that fulfillment of these low-energy and low-temperature Fermi-liquid relations is indication that the recursive evaluation of matrix elements and excitations, inherent to the NRG procedure, remains stable and accurate down to the lowest energies, i.e., for large iterations $N\gg 1$. In the case of excitations, the accuracy and stability of the recursive diagonalization scheme can also be judged by the exact results obtained for fixed point eigenvalues [see Sec. II and Wilson (1975a)].

The case of finite-temperature dynamics is more complicated. Contributions to the spectral density at frequency $\omega\sim\omega_N$ now arise from excitations between arbitrary excited states, i.e., $\omega=E_r-E_0=E_{r'}-E_{p'}=E_{r''}-E_{p''}=\cdots$ with $E_0=0<E_{p'}<E_{p''}<\cdots$; see Fig. 9. Consequently, the finite-$T$ spectral density at $\omega\sim\omega_N$ will have contributions from all energy shells $n=1,\ldots,N$. These

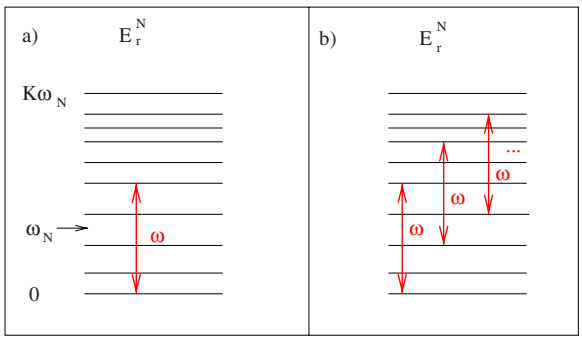


FIG. 9. (Color online) Excitations of $H_N$ contributing to the spectral function at frequency $\omega$ for (a) $T=0$ and (b) $T>0$.

need to be summed up, as in the calculation of transient quantities described in Sec. III.B.3. It is clear, however, that in the case of equilibrium spectral densities the contributions from shells $n<N$ will be suppressed by Boltzmann factors. This motivates the following approximation. At $\omega=2\omega_n>k_BT$ one can calculate $A_\sigma(\omega,T)$ as in the $T=0$ case,

$$A_\sigma(\omega_n,T)\approx A_\sigma^n(\omega_n,T)$$
$$=\frac{1}{Z_n(T)}\sum_{r,r'}|M_{r,r'}^n|^2(e^{-E_r^n/k_BT}+e^{-E_{r'}^n/k_BT})\delta(\omega_n-(E_{r'}^n-E_r^n)). \quad (76)$$

In the other limit, $\omega=2\omega_n\leq k_BT$, there is no completely satisfactory procedure. One approach assumes that the main contribution to the spectral density for $\omega=2\omega_n\leq k_BT$ comes from the energy window containing thermal excitations $O(k_BT)$ (Costi and Hewson, 1992b; Costi *et al.*, 1994a). In this case, the relevant shell $M$ is determined by temperature via $\omega_M\approx\bar{\beta}k_BT$, as in the evaluation of thermodynamic properties in the previous section, so that, for $\omega=2\omega_n\leq k_BT$, we use

$$A_\sigma(\omega_n,T)\approx A_\sigma^M(\omega_n,T)$$
$$=\frac{1}{Z_M(T)}\sum_{r,r'}|M_{r,r'}^M|^2(e^{-E_r^M/k_BT}+e^{-E_{r'}^M/k_BT})\delta(\omega_n-(E_{r'}^M-E_r^M)). \quad (77)$$

In practice, this procedure gives a smooth crossover as $\omega$ is lowered below $k_BT$ for temperatures comparable to the Kondo scale and higher, but becomes less reliable at $\omega<k_BT\ll T_K$.

Once the finite-$T$ spectral density is known, one can also calculate transport properties, since the transport time $\tau_{tr}$ for electrons scattering from a small concentration $n_i$ of magnetic impurities is given in terms of the spectral density by

$$\frac{1}{\tau_{tr}(\omega,T)}=\frac{2n_i\Delta}{N_F}A_\sigma(\omega,T), \quad (78)$$

where $N_F$ is the conduction electron density of states and $\Delta$ is the hybridization strength. For example, the resistivity $R(T)$ due to Kondo impurities in a clean metal is given by

$$R(T)=\frac{1}{e^2\int d\omega(-\partial f/\partial\omega)\tau_{tr}(\omega,T)}, \quad (79)$$

and the conductance through a quantum dot (or the resistivity of Kondo impurities in a dirty metal) modeled by an Anderson impurity model is given by

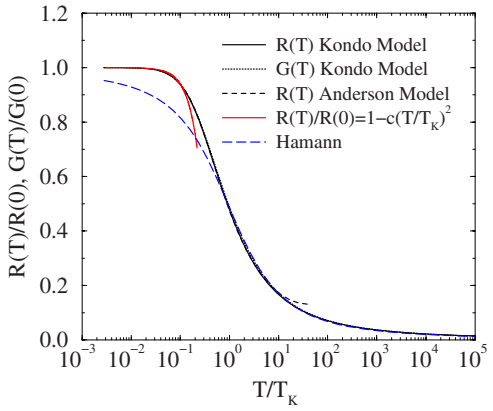


FIG. 10. (Color online) Scaled resistivity and conductance of the $S=1/2$ Kondo model. For comparison the resistivity of the symmetric Anderson model for $U/\pi\Delta=4$ is also shown (Costi and Hewson, 1993) and seen to be identical to that for the Kondo model, up to nonuniversal corrections arising from charge fluctuations at higher temperatures (for $U/\pi\Delta=4$ these corrections occur for $T>10T_K$). Adapted from Costi, 2000.

$$G(T)/G(0)=\sum_\sigma\int d\omega\left(-\frac{\partial f}{\partial\omega}\right)A_\sigma(\omega,T). \quad (80)$$

Figure 10 compares the scaled resistivity $R(T)/R(0)$ for the Kondo and Anderson models with the scaled conductance $G(T)/G(0)$ for the Kondo model. The conductance and resistivity are seen to be almost identical universal functions of $T/T_K$. At finite magnetic field, the two quantities deviate from each other in the region $T\approx B$ (Costi, 2000). The NRG results can be compared to analytic results at low and high temperatures. The resistivity of the Anderson model in the low-temperature Fermi-liquid regime is given by the result of Nozières (1974),

$$R(T)/R(0)=G(T)/G(0)=1-c\left(\frac{T}{T_K}\right)^2,\quad T\ll T_K, \quad (81)$$

where $c=\pi^4/16=6.088$ and $T_K$ is the low-temperature Kondo scale defined from the static spin susceptibility via

$$\chi(T=0)=(g\mu_B)^2/4k_BT_K. \quad (82)$$

At high temperatures $T>T_K$, Hamann used the Nagaoka-Suhl approximation (Hewson, 1993a) to obtain for the resistivity of the Kondo model

$$R(T)/R(0)=\frac{1}{2}\left(1-\frac{\ln(T/T_{KH})}{[\ln(T/T_{KH})^2+\pi^2S(S+1)]^{1/2}}\right), \quad (83)$$

where $S$ is the impurity spin and $T_{KH}$ is a Kondo scale defined by

$$R(T=T_{KH})=R(0)/2. \quad (84)$$

Micklitz *et al.* (2006) found numerically that $T_{KH}\approx 0.91T_K$. We see from Fig. 10 that the NRG result for

the resistivity of the Kondo model agrees with the Hamann result for $T \geq T_K$. The $T^2$ Fermi-liquid behavior at low temperature $T \ll T_K$ is also recovered. In contrast, the Hamann result violates Fermi-liquid behavior and cannot be reliable for $T < T_K$. Numerical determination of the coefficient $c$ in Eq. (81) requires obtaining $\tau_{\rm tr}(\omega, T)$ accurately up to second order in both $\omega$ and $T$ (Costi *et al.*, 1994a). Typical errors for $c$ can be as large as 10–30 % so there is room for further improvement of the finite-$T$ dynamics in the Fermi-liquid regime $T \ll T_K$. Recent multiple-shell techniques, described in Sec. III.B.3, look promising in this respect. For a discussion of other transport properties of Kondo systems, such as thermopower and thermal conductivity, see Costi and Hewson (1993), Zlatić *et al.* (1993), and Costi *et al.* (1994a).

### 2. Self-energy and reduced density matrix approach

We now describe two improvements to the calculation of dynamical quantities. The first of these, a direct calculation of the correlation part of the self-energy of the Anderson impurity model (Bulla *et al.*, 1998), is particularly important for applications to DMFT, where the impurity self-energy plays a central role. The second, introduction of the reduced density matrix into the calculation of dynamics, is important, for example, in correcting large finite-size errors in spin-resolved spectra of the Anderson and Kondo models when a magnetic field perturbs the ground state (Hofstetter, 2000).

The correlation part of the self-energy for the Anderson impurity model $\Sigma_\sigma$ is defined via

$$G_\sigma(\omega, T) = \frac{1}{\omega - \varepsilon_f + i\Delta - \Sigma_\sigma(\omega, T)} \tag{85}$$

and can be expressed, via the equation of motion for $G_\sigma$ (Bulla *et al.*, 1998), as the ratio of a two-particle and a one-particle Green's function,

$$\Sigma_\sigma(\omega, T) = U\langle\langle f_\sigma f^\dagger_{-\sigma} f_{-\sigma}; f^\dagger_\sigma\rangle\rangle / \langle\langle f_\sigma; f^\dagger_\sigma\rangle\rangle, \tag{86}$$

where the notation $\langle\langle A; B\rangle\rangle$ represents the retarded Green's function for the operators $A, B$. Evaluating the spectral densities of the two Green's functions in Eq. (86) as in the previous section, and calculating from these, via a Kramers-Kronig transformation, the corresponding real parts of the Green's functions one obtains the self-energy, shown in Fig. 11. Using this in Eq. (85), one is able to obtain the impurity spectral density with improved resolution of high-energy peaks, since in this procedure the single-particle broadening $\Delta$ is included exactly. In particular, this scheme recovers the limit $U \to 0$ exactly. It is also found to improve the spectral sum rule

$$-\frac{1}{\pi}\int_{-\infty}^{+\infty} d\omega\, \mathrm{Im}\left(\frac{1}{\omega - \varepsilon_f + i\Delta - \Sigma_\sigma(\omega, T)}\right) = 1, \tag{87}$$

with typical errors as low as 0.1% or less.

Evaluation of spectral densities described in the previous section is subject to systematic errors due to neglect of high-energy states in constructing $H_N$. These are the same as for thermodynamic properties, and they can be controlled by decreasing $\Lambda$ and increasing the number of retained states $N_s$. Another source of error, specific to the method used to calculate the dynamics, is that, while we chose the frequency $\omega$ in evaluating spectra from $H_N$ carefully so that $\omega > \omega_N$, nevertheless the eigenstates in the range $0 \leq E_r^N \leq \omega_N$, which for small $N$ are only crude approximations to the eigenstates of $H$, are also used in the evaluation. They enter the calculation directly, as can be seen from Fig. 9, and also via the density matrices (e.g., at $T=0$ via $\varrho_N = |0\rangle_{NN}\langle 0|$) which are used to find Eqs. (69), (76), and (77). As a result, the spectral density is subject to errors for small $N$, i.e., for high energies, due to the use of low-lying states which are not converged (Hofstetter, 2000). With increasing $N$, i.e., lower energies, this error will decrease. An improvement, due to Hofstetter (2000), is to use in place of $\varrho_N$ the reduced density matrix $\varrho^{N,\rm red}$ of $H_N$, obtained from the density matrix of the largest finite-size Hamiltonian diagonalized, $H_{N_{\rm max}}$, i.e.,

$$\varrho^{N,\rm red} = \mathrm{Tr}_{s_{N+1},\ldots,s_{N_{\rm max}}}[\varrho_{N_{\rm max}}], \tag{88}$$

where $s_{N+1}, \ldots, s_{N_{\rm max}}$ are the extra degrees of freedom contained in $H_{N_{\rm max}}$ but absent in $H_N$. As $\varrho^{N,\rm red}$ for $N < N_{\rm max}$ is not diagonal in the eigenbasis of $H_N$, the resulting spectral function takes on a more complicated form,

$$A_\sigma^N(\omega, 0) = \sum_{r',r} C_{r',r} M^N_{r,r'} \delta(\omega - (E^N_{r'} - E^N_r)), \tag{89}$$

$$C_{r',r} = \sum_p \rho^{N,\rm red}_{p,r} M^N_{r',p} + \sum_p \rho^{N,\rm red}_{r',p} M^N_{p,r}. \tag{90}$$

The reduced density matrices $\varrho^{n,\rm red}$ are calculated iteratively backward starting from the density matrix of $H_{N_{\rm max}}$. One situation where the reduced density matrix is important is in obtaining correctly the spin-resolved spectral density of the Anderson model in a magnetic

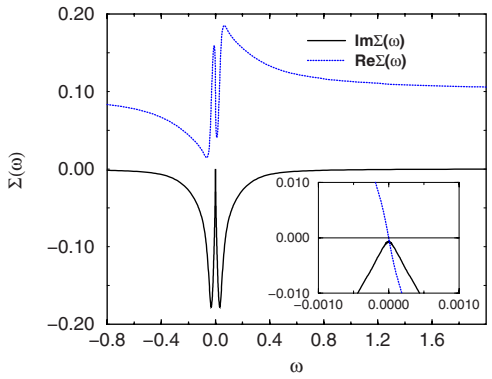


FIG. 11. (Color online) Real and imaginary parts of the self-energy for the Anderson impurity model for $\varepsilon_f = -0.1$, $U = 0.2$, and a constant hybridization strength $\Delta = 0.015$. The inset shows the region around the Fermi level where the Hartree term was subtracted off the real part. From Bulla *et al.*, 1998.

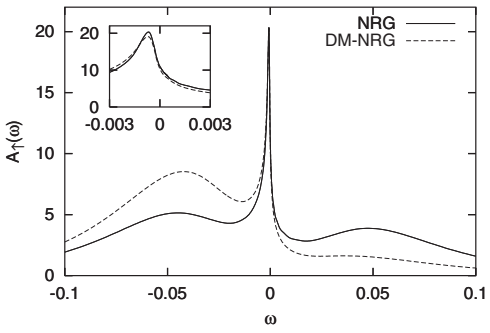


FIG. 12. Comparison of the spectral function for the Anderson impurity model calculated in a magnetic field with and without the reduced density matrix: $\Delta=0.01, U=0.1, \varepsilon_f=-0.05$, and $B=0.001$. From Hofstetter, 2000.

field (Hofstetter, 2000). A magnetic field comparable to $T_K$ changes the magnetization and therefore the occupation of up and down states by $O(1)$, so large shifts in spectral weight occur at high energies in the impurity spectral density which are captured correctly only using the reduced density matrix (see Fig. 12). Results for dynamical susceptibilities in a magnetic field using the reduced density matrix have been discussed by Hewson (2006). The reduced density matrix also eliminates to a large extent the difference between the spectra calculated for even and odd $N$ and allows a correct description of the asymptotics of the Kondo resonance in high magnetic fields (Rosch *et al.*, 2003).

### 3. The x-ray problem and transient dynamics

We consider here the calculation of the response of a system to a sudden local perturbation, such as the excitation of an electron from a core level to the conduction band of a metal in the x-ray problem (Mahan, 1974), or the time-dependent response of a spin in the spin-boson model following an initial-state preparation (Leggett *et al.*, 1987). These problems represent a special kind of nonequilibrium problem where one is interested in the relaxation of the system to a new equilibrium state following a sudden local perturbation. As shown below, one can calculate the nonequilibrium dynamics of these special kinds of problem within the NRG method because one needs only the information contained in the initial- and final-state Hamiltonians. In this review, we do not address the more difficult problem of global perturbations giving rise to nonequilibrium steady states, as, for example, in transport through a quantum dot far from the linear response regime.

The NRG approach to the x-ray problem (Oliveira and Wilkins, 1981) was the first application of the method to dynamical quantities. The approach developed by Oliveira and Wilkins (1981) treats the localized core-hole potential exactly and calculates the absorption spectrum within linear response theory using the techniques of Sec. III.B.1. It uses the idea of formulating the calculation of the absorption spectrum in terms of initial- and final-state Hamiltonians (Nozières and De Dominicis, 1969), which is also inherent in the recent NRG approach to transient dynamics (Costi, 1997a; Anders and Schiller, 2005), so we discuss both problems together in this section.

A simple model for describing the x-ray absorption spectra in metals is given by the following spinless Hamiltonian:

$$H=\sum_k \varepsilon_k c_k^\dagger c_k + E_d d^\dagger d + \sum_{k,k'} U_{dc} c_k^\dagger c_{k'} d d^\dagger, \tag{91}$$

where $d^\dagger$ creates a core electron with energy $E_d$, and the attractive screening interaction $U_{dc}$ acts only when the core level is empty ($dd^\dagger=1$). The core-level lifetime is assumed infinite, and the interaction with the x-ray field is taken to be of the form

$$H_x = w(c_0^\dagger d e^{-i\omega t} + \text{H.c.}), \tag{92}$$

where $c_0=\Sigma_k c_k$. The x-ray absorption spectrum $\mu(\omega)$ is obtained using linear response theory from the imaginary part of the optical conductivity $\chi_{cd}=\langle\langle c_0^\dagger d; d^\dagger c_0\rangle\rangle$. At zero temperature, one finds for the absorption spectrum a power-law singularity of the form

$$\mu(\omega) \sim (\omega - E_T)^{-\alpha}, \tag{93}$$

where $E_T$ is the absorption threshold and $\alpha$ is an exponent which depends on the strength of the core-hole potential. The exponent $\alpha$ has two contributions, $\alpha=\alpha'-\varepsilon$, an excitonic part $\alpha'$ due to Mahan (1967) and an orthogonality part $\varepsilon$ which follows from Anderson's orthogonality catastrophe theorem (Anderson, 1967). An exact solution of the x-ray problem for the asymptotically low-energy regime has been obtained by Nozières and De Dominicis (1969) using the decomposition of Eq. (91) into single-particle initial-state $H_I$ and final-state $H_F$ Hamiltonians, corresponding to the situations before ($dd^\dagger=0$) and after ($dd^\dagger=1$) a core electron is excited to the conduction band:

$$H_I=\sum_k \varepsilon_k c_k^\dagger c_k + E_d, \tag{94}$$

$$H_F=\sum_k \varepsilon_k c_k^\dagger c_k + \sum_{k,k'} U_{dc} c_k^\dagger c_{k'}. \tag{95}$$

For the spinless model, Eq. (91), Nozières and De Dominicis (1969) found the exponents

$$\alpha' = 2\delta/\pi, \quad \varepsilon = (\delta/\pi)^2, \tag{96}$$

where the phase shift $\delta=\arctan(-\pi N_F U_{dc})$ is that for conduction electrons scattering from the additional potential created by the core hole, and $N_F$ is the conduction electron density of states at the Fermi level. In addition to the absorption spectrum, the core-level photoemission spectrum $A_d(\omega)=-\text{Im}(\langle\langle d; d^\dagger\rangle\rangle)/\pi$ is also of interest. In the core-level photoemission spectrum, only the orthogonality effect is operative and the core-electron spectral function, which has the quasiparticle form $A_d(\omega)=\delta(\omega-E_d)$ in the absence of screening, is replaced by an incoherent spectrum of the form

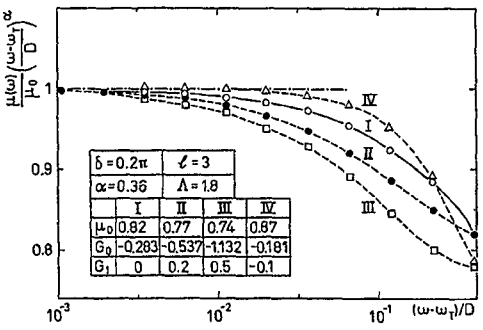


FIG. 13. Absorption spectrum normalized by the Nozières–De Domenicis result [Eq. (93)] for several screening potentials of the form $U_{dc}(k,k')=G_0+G_1(k+k')$ (Oliveira and Wilkins, 1981).

$$A_d(\omega) \sim \theta(\tilde{E}_d-\omega)(\tilde{E}_d-\omega)^{-(1-\varepsilon)} \tag{97}$$

in the presence of screening (Doniach and Šunjić, 1970).

Oliveira and Wilkins (1981) applied the NRG method to the initial-state and final-state Hamiltonians (94) and (95) and calculated the zero-temperature linear response absorption spectrum,

$$\mu(\omega) = 2\pi w^2 \sum_{m_F} |\langle m_F|c_0^\dagger d|m_{I,GS}\rangle|^2 \times \delta(\omega-(E_{m_F}-E_{m_{I,GS}})), \tag{98}$$

with $H_{I,F}|m_{I,F}\rangle=E_{m_{I,F}}|m_{I,F}\rangle$ and $|m_{I,GS}\rangle$ the ground state of $H_I$. In evaluating $\mu(\omega)$, truncated Hamiltonians $H_{I,F}^N$ were used and the spectrum was evaluated at an appropriate frequency $\omega=\omega_N$ as in Sec. III.B.1 but with a box broadening function on a logarithmic scale. They were able to recover the exact threshold exponent of Nozières and De Dominicis (1969) [see Líbero and Oliveira (1990a) for similar calculations of the photoemission spectra]. They also extended the calculation of absorption spectra to core-hole potentials of finite range $U_{dc} \to U_{dc}(k,k')$, finding (see Fig. 13) that the threshold exponent remains universal, i.e., it depends only on the phase shift $\delta$ at the Fermi level, but that the asymptotic scale for the onset of power-law behavior depends on both the range (Oliveira and Wilkins, 1981) and the strength of the core-hole potential (Cox *et al.*, 1985). It also depends on any energy dependence in the density of states (Chen *et al.*, 1995). These results reflect the fact that the crossover scale to the low-energy fixed point, determining universal properties, depends on details of the density of states and the core-hole potential.

X-ray singularities also play an important role in the dynamics of auxiliary particles in the slave-boson approach to the infinite-$U$ Anderson impurity model (Coleman, 1984; Müller-Hartmann, 1984). A NRG calculation of the $T=0$ photoemission spectra for slave bosons $A_b(\omega)$ and pseudofermions $A_{f\sigma}(\omega)$ showed that these diverge with the exponents given above for the photoemission and absorption spectra, respectively, generalized to include spin (Costi *et al.* 1994b, 1996):

$$A_{f\sigma}(\omega) \sim (\omega-E_T)^{-\alpha_f}, \tag{99}$$

$$A_b(\omega) \sim (\omega-E_T)^{-\alpha_b}, \tag{100}$$

$$\alpha_f = 2\frac{\delta_\sigma}{\pi} - \sum_\sigma \left(\frac{\delta_\sigma}{\pi}\right)^2, \tag{101}$$

$$\alpha_b = 1 - \sum_\sigma \left(\frac{\delta_\sigma}{\pi}\right)^2, \tag{102}$$

with the phase shift $\delta_\sigma=\pi n_{f\sigma}$ and $n_{f\sigma}$ the occupancy per spin of the local level. Here, also, the scale for the onset of power-law behavior is determined by the relevant low-energy crossover scale, e.g., the Kondo scale in the Kondo regime.

We turn now to a problem which is formally similar to the x-ray problem, namely, the dynamics of a spin subject to an initial-state preparation, as in the case, for example, of the dynamics of the spin in the spin-boson model Eq. (141). Further discussion of the effects of screening on the spectra of impurity models is given in Sec. IV.A.1. In the spin-boson model one is interested in the dynamics of a spin $\sigma_z$ described by $P(t)=\langle\sigma_z(t)\rangle_{\varrho_I}$, following an initial-state preparation of the system described by an initial density matrix $\varrho_I$ (Leggett *et al.*, 1987). For example, the spin $\sigma_z$ in Eq. (141) could be prepared in state $|\uparrow\rangle$ at $t<0$ by an infinite bias $\varepsilon=\infty$ with the environment fully relaxed about this state, and the bias could subsequently be switched off at $t=0$, allowing the spin to evolve. The time evolution of the spin for $t>0$ is then described by

$$\langle\sigma_z(t)\rangle_{\varrho_I} = \frac{1}{\mathrm{Tr}\,\varrho_I}\mathrm{Tr}(\varrho_I e^{-iH_F t/\hbar}\sigma_z e^{iH_F t/\hbar}), \tag{103}$$

where $\varrho_I=e^{-\beta H_I}$ and the initial- and final-state Hamiltonians are given by

$$H_I = H_{\mathrm{SB}}(\varepsilon=\infty), \tag{104}$$

$$H_F = H_{\mathrm{SB}}(\varepsilon=0), \tag{105}$$

where $H_{\mathrm{SB}}$ is the spin-boson Hamiltonian (141).

This approach has been investigated within the NRG method using, for the Ohmic case, in place of $H_{\mathrm{SB}}$, the equivalent anisotropic Kondo model (Costi, 1997a). Despite the similarity with the x-ray problem, the exact formulation indicates the difficulties that have to be overcome in calculating transient dynamical quantities. Consider the spectral function

$$P(\omega) = \frac{1}{Z_I}\sum_{m_I,m_F,m_F'} e^{-\beta E_{m_I}}\langle m_I|m_F\rangle\langle m_F'|m_I\rangle \times \langle m_F|\sigma_z|m_F'\rangle\delta(\omega-(E_{m_F}-E_{m_F'})), \tag{106}$$

with

$$P(t) = \int_0^{+\infty} P(\omega)\cos(\omega t)d\omega. \tag{107}$$

We see that even at $T=0$, no ground state enters the delta functions in Eq. (106), in contrast to the linear response expression (98) for $\mu(\omega)$ in the x-ray problem. This implies that, in evaluating $P(\omega)$ at a frequency $\omega \sim \omega_N$, contributions will arise from energy shells $n=1,2,\ldots,N$, as discussed previously for finite-$T$ dynamics. In the present situation, however, contributions from higher-energy shells (i.e., $n<N$) are not suppressed by Boltzmann factors, so it is not clear *a priori* that using a single-shell approximation will give meaningful results. Such an approximation shows that the short-time dynamics of the spin-boson model can be recovered and that in order to obtain the long-time dynamics one has to sum up contributions from all shells (Costi, 1997a). Adding up such contributions using the retained states of successive Hamiltonians $H_{I,F}^N, H_{I,F}^{N+1},\ldots$ is problematic due to the overlap of the spectra at low energies. An elegant solution of this problem, allowing multiple-shell NRG calculations to be carried out, has been found by Anders and Schiller (2005). Their idea was to recognize that the set of states discarded $|r\rangle_{m,\mathrm{disc}}$ at each NRG iteration $m \geq m_{\min}$, with $m_{\min}$ the first iteration where truncation starts, supplemented with the degrees of freedom $|e;m\rangle = |s_{m+1}\rangle \otimes \cdots \otimes |s_{N_{\max}}\rangle$, for $m=m_{\min},\ldots,N_{\max}$, with $N_{\max}$ the size of the largest Hamiltonian diagonalized, forms a complete basis set,

$$\sum_{m=m_{\min}}^{N_{\max}} \sum_{r\in\{\mathrm{disc}\}} |r,e;m\rangle\langle r,e;m| = 1. \tag{108}$$

Using this identity, their result for $P(t)$ in the basis of final states is

$$P(t) = \sum_{m=m_{\min}}^{N} \sum_{m_F,m_F'}^{\mathrm{trun}} e^{i(E_{m_F}^m - E_{m_F'}^m)t/\hbar} \langle m_F|\sigma_z|m_F'\rangle \varrho_{m_F,m_F'}^{m,\mathrm{red}}, \tag{109}$$

where $\varrho_{r_F,s_F}^{m,\mathrm{red}}$ are the matrix elements of the reduced density matrix of $H_I^m$ introduced in the previous section and the sum $\Sigma_{m_F,m_F'}^{\mathrm{trun}}$ implies that at least one of the states $m_F,m_F'$ is in the discarded sector for iteration $m$. Rotating $\varrho_{r_F,s_F}^{m,\mathrm{red}}$ to the initial-state basis gives overlap matrix elements $\langle m_I|m_F\rangle$, $\langle m_I|m_F'\rangle$ as in Eq. (106). Within this approach the time-dependent transient dynamics of a number of models has been investigated, including the Anderson and resonant level models (Anders and Schiller, 2005), the Kondo model (Anders and Schiller, 2006), and the sub-Ohmic spin-boson model (Anders *et al.*, 2007).

The use of a complete basis set (108) has the potential to improve the finite-$T$ calculation of spectral densities also, particularly in the problematic range $\omega<T$ (Weichselbaum and von Delft, 2007). Further improvement in using a complete basis set is that the sum rule for spectral densities $\int_{-\infty}^{\infty} d\omega\, A_\sigma(\omega,T)=1$ is, by construction, satisfied exactly when applied to the spectral density in discrete form and with an error of $10^{-4}$ due to numerical integration when applied to the broadened form (Peters *et al.*, 2006; Weichselbaum and von Delft, 2007). In contrast, the higher-moment spectral sum rules $\int_{-\infty}^{\infty} d\omega\, \omega^m A_\sigma(\omega,T)=\mu_m$ with $\mu_m=\langle\{[f_\sigma,H]_m,f_\sigma^\dagger\}\rangle$, $[f_\sigma,H]_1=[f_\sigma,H]$, $[f_\sigma,H]_2=[[f_\sigma,H],H]$, etc., and $\{\cdots\}$ denoting an anticommutator, are expected to be less well satisfied. These involve summations over expressions containing factors $(E_r^N-E_{r'}^N)^m$ where the eigenvalues $E_r^N$ are those of the finite-size Hamiltonian $H_N$ in the NRG procedure. Such eigenvalues are subject to truncation errors for $N\geq N_{\mathrm{trun}}$, where $N_{\mathrm{trun}}$ is the first NRG iteration at which states are truncated. Consequently, the above sum rules are expected to acquire errors. One expects, however, that these errors will decrease with increasing $N_{\mathrm{trun}}$. For application of these sum rules to spectral functions of the Hubbard model, see White (1991). For the Anderson impurity model, the first two moments are $\mu_1=\varepsilon_f+U\langle n_{-\sigma}\rangle$ and $\mu_2=V^2+\varepsilon_f^2+2\varepsilon_f U\langle n_{-\sigma}\rangle+U^2\langle n_{-\sigma}\rangle$, where $n_{-\sigma}=f_{-\sigma}^\dagger f_{-\sigma}$. For $m\geq 3$, the moments involve increasingly complex correlation functions, so their evaluation and subsequent calculation within the NRG method will become increasingly difficult and impractical. We note that, in testing the above sum rules, one should use the discrete spectra as the broadened spectra have modified tails (and consequently altered higher moments) due to the particular broadening function used.

## IV. APPLICATION TO IMPURITY MODELS

In this section we review the application of the NRG method to a range of quantum impurity models. Section IV.A reviews work on models with conduction electron screening (Sec. IV.A.1), underscreened and fully screened Kondo models (Sec. IV.A.2), and models exhibiting the Kondo effect in nanostructured devices (Sec. IV.A.3). Section IV.B deals with the prototypical overscreened Kondo model, the two-channel Kondo model, which is often encountered as an effective model describing the quantum criticial point of more complex quantum impurity models, e.g., certain double-quantum-dot systems (Zarand *et al.*, 2006). Impurity quantum phase transitions are reviewed in Sec. IV.C in the contexts of multi-impurity systems IV.C.1, soft-gap systems IV.C.2, and in the context of magnetic impurities in superconductors IV.C.3. Section IV.D reviews work on multiorbital systems, including the effects of crystal-field splittings in Anderson impurity models. Finally, models with bosonic degrees of freedom are reviewed in Sec. IV.E. Note also that a number of models of nanostructured devices, for example, the single-electron box, quantum dots with phonons, or multiorbital quantum dots, are discussed in Secs. IV.B–IV.E.

### A. Kondo effect and related phenomena

#### 1. Charge screening and photoemission

Charge screening effects are important whenever an electron is excited from a localized core or valence state into the conduction band or removed completely, leaving behind a hole which attracts conduction electrons. Such effects can have a drastic influence on the photoemission and absorption spectra of impurity systems. In this section we consider a number of extensions to the basic screening model (91) introduced in Sec. III.B.3. We consider first the generalization of Eq. (91) to a simplified model of an atom adsorbed on a metallic surface (Oliveira and Wilkins, 1985). In addition to a core level, as in Eq. (91), the atom has a resonant level (created by $b^\dagger$) whose position, $E_{bI}$ or $E_{bF}$, depends on the occupancy of the core level according to

$$H_{db} = E_{bI} b^\dagger b d^\dagger d + E_{bF} b^\dagger b (1 - d^\dagger d), \tag{110}$$

and the level hybridizes with the conduction band via

$$H_{\rm mix} = V \sum_k (c_k^\dagger b + \text{H.c.}). \tag{111}$$

Note that $H_{db}$ represents screening of the core hole by electrons in the resonant level. Excitation of an electron from the core level by an x ray can proceed either directly or via the resonant level, leading to a Fano antiresonance in the x-ray absorption at finite energy (in addition to the usual edge singularity at $\omega = E_T$). This Fano antiresonance, present also without the core hole potential, is found to be significantly narrowed and shifted in the presence of the core hole potential (Oliveira and Wilkins, 1985). It would be of interest to investigate also the core-level photoemission spectrum of this model using the NRG method, as both this and the absorption spectrum are accessible in experiments. Brito and Frota (1990) have carried out such a calculation for an appropriately generalized spinful version of the above model, i.e., the Anderson model (2) in the presence of both an interaction

$$H_{dc} = U_{dc} d d^\dagger \sum_{kk'\sigma} c_{k\sigma}^\dagger c_{k'\sigma} \tag{112}$$

between the core hole and conduction electrons, and an interaction

$$H_{df} = U_{df} d d^\dagger \sum_\sigma f_\sigma^\dagger f_\sigma \tag{113}$$

between the core hole and the valence level. Signatures of the valence states could be identified in the x-ray photoelectron spectroscopy (XPS) spectra and their dependence on $U_{dc}$ was investigated in the mixed valence and empty orbital regimes. A reduction of the hybridization between the valence level and the conduction band, arising from orthogonality effects, was found with increasing $U_{dc}$. The corresponding calculation in the Kondo regime is still lacking. The x-ray absorption spectrum of the same model has been investigated by Helmes *et al.* (2005) in the context of excitons in Kondo-correlated quantum dots and the expected absorption exponent from the Nozières–De Domenicis theory was recovered.

In the models discussed so far, the core level was assumed to have infinite lifetime. Consequently, the screening interaction gave rise to true singularities in the core-level absorption and photoemission spectra. These singularities are cut off as soon as the core-level lifetime is finite (Doniach and Šunjić, 1970). Another situation where the singularities due to screening are cut off, but where screening effects may nevertheless be important, is in the valence band photoemission spectra of heavy fermions within a local impurity approach, which we now address.

It is often assumed that the effects of conduction electron screening on the *f*-electron photoemission spectra of heavy fermions can be taken into account by renormalizing the bare parameters of an effective Anderson impurity model. However, this is not *a priori* clear, as the screening interaction in these systems can be an appreciable fraction of the local Coulomb repulsion. One of the merits of the NRG method, which allows such questions to be investigated, is that it can deal with all local Coulomb interactions on an equal footing and in a nonperturbative manner, and some examples of this have already been given above. For the particle-hole symmetric Anderson model, Eq. (2), it was shown by Costi and Hewson (1991, 1992a) that the effect of a screening term of the form

$$H_{fc} = U_{fc} \sum_{kk'\sigma\sigma'} f_\sigma^\dagger f_\sigma c_{k\sigma'}^\dagger c_{k'\sigma'} \tag{114}$$

on the valence band photoemission spectrum could be well-accounted for by a renormalization of the bare parameters of the Anderson model, both the local level position $\varepsilon = -U/2$ and the hybridization. An excitonic-like enhancement of the hybridization was found with increasing $U_{fc}$. Similar effects are reflected in the scanning tunneling microscopy (STM) conductance of a magnetic adatom modeled by the screened Anderson model (Cornaglia and Balseiro, 2003). Calculations for the infinite-$U$ Anderson impurity model, for thermodynamics (Alascio *et al.*, 1986; Zhuravlev *et al.*, 2007) and dynamics (Takayama and Sakai, 1993), are consistent with the above findings.

The above model for screening in heavy fermions assumes that the largest contribution to screening of *f* holes arises from conduction electrons in states that hybridize with the *f* states. These hybridizing states are usually the *p* levels from neighboring ligand ions, so the screening from these (denoted $U_{fc}$ above) should be expected to be smaller than the on-site screening $U_{df}$ from *d* electrons of the rare-earth ion. In the presence of inversion symmetry, the latter do not hybridize with *f* states. Neglecting $U_{fc}$ and representing *d* electrons by a spinless *s*-wave band, we represent the screening of *f* holes by *d* electrons by adding to the Anderson model (2) the term

$$H_{\rm scr} = \sum_k \varepsilon_k d_k^\dagger d_k + U_{df} \sum_{kk'} (n_f - 1) d_k^\dagger d_{k'}, \tag{115}$$

where $n_f = \Sigma_\sigma f_\sigma^\dagger f_\sigma$. The result is a two-channel Anderson model, in which one channel screens but does not hybridize (the $d$ electrons) and the other channel hybridizes but does not screen. Assuming localized $d$ electrons gives the model studied by Brito and Frota (1990) and discussed above. For the full model, Takayama and Sakai (1993, 1997) calculated the valence band photoemission spectrum and, surprisingly, found that the effect of $U_{dc}$ in the Kondo regime could be absorbed into a renormalization of the Anderson model parameters. This result was for infinite $U$, but should remain valid in the Kondo regime for any finite $U$ provided $U_{dc}$ remains smaller than or comparable to $U$. In contrast to the model (114) described above, where screening occurs in the hybridizing channel, the effect of the screening interaction in the present model (115) is to reduce the effective hybridization of valence electrons to the conduction band, which can be understood as an orthogonality effect. We conclude from these NRG calculations that in the Kondo regime, and with realistic values of $U_{df}$ ($U_{fc}$), the valence band photoemission spectra of the above screening models can be well accounted for by an Anderson model with renormalized parameters.

The two-channel screening model discussed above has also been studied for finite $U$ (Perakis *et al.*, 1993; Perakis and Varma, 1994). At particle-hole symmetry, increasing $U_{dc}$ reduces both $U$ and the effective hybridization, resulting, for sufficiently large $U_{dc}$, in an effective attractive local Coulomb interaction and a charge Kondo effect. For still larger $U_{dc}$, a Kosterlitz-Thouless transition to a non-Fermi-liquid state occurs (Perakis *et al.*, 1993; Perakis and Varma, 1994) with a collapse of the Kondo resonance in the valence band photoemission spectrum (Costi, 1997b).

It is natural to ask whether the x-ray singularity in the core-level photoemission spectrum of the spinless x-ray model (91) persists on going to its periodic counterpart, the Falicov-Kimball model (Freericks and Zlatić, 2003), whose Hamiltonian is given by

$$H = -\sum_{ij} t_{ij} c_i^\dagger c_j + E_d \sum_i d_i^\dagger d_i + \sum_i U_{dc} c_i^\dagger c_i d_i^\dagger d_i. \tag{116}$$

Here $t_{ij}$ are the hopping matrix elements of the itinerant conduction electrons and $E_d$ is the energy of the localized (core-level) electrons. In the particle-hole symmetric case ($E_d = 0$) this question has been answered by Anders and Czycholl (2005) within a DMFT approach using the NRG method as the impurity solver (see Sec. V for applications of the NRG method to DMFT). In the metallic regime of the model, they find that the core-level photoemission spectrum diverges at the threshold $\omega = E_d = 0$ as in the usual x-ray problem, as a power law $|\omega|^{-\alpha}$, and with an exponent $\alpha$ depending on $U_{dc}$. It would be interesting to carry out similar calculations away from particle-hole symmetry, $E_d < 0$. Recently Cornaglia and Georges (2007) have used the DMFT in combination with the NRG method to study the x-ray singularity in the core-level photoemission spectrum across the metal-insulator transition in the Hubbard model.

### 2. Kondo effect in the bulk and underscreened models

Real magnetic impurities in metals have both orbital and spin degrees of freedom and the resulting low-energy effective impurity models can be very complicated (Hewson, 1993a). The NRG method has been applied so far to models with at most three orbitals (see Sec. IV.D). In cases where the ground state is an orbital singlet, e.g., for dilute Mn ions in metals, Nozières and Blandin (1980) have given a classification of the resulting effective single-impurity Kondo models in terms of the size of the impurity spin $S$ and the number of conduction channels, $n$, that couple to the spin via the Kondo exchange. These multichannel Kondo models are described by

$$H = \sum_{k\sigma\alpha} \varepsilon_k c_{k\sigma\alpha}^\dagger c_{k\sigma\alpha} + J \sum_\alpha \mathbf{S} \cdot \mathbf{s}_\alpha, \tag{117}$$

where $\alpha = 1, \ldots, n$ is the channel index and the exchange constant $J$ is antiferromagnetic. For $n = 2S$, complete screening of the impurity spin takes place, leading to a local Fermi liquid at low temperatures. The overscreened case $n > 2S$ exhibits non-Fermi-liquid behavior and is reviewed in Sec. IV.B. In this section, we deal with some recent developments in the fully screened $S = 1/2$ Kondo model, relevant to bulk Kondo impurities, and also describe work on the single-channel underscreened case $n = 1 < 2S$.

One of the signatures of the Kondo effect is the appearance of the Kondo resonance in the impurity spectral density at the Fermi level. Point contact spectroscopy on Cu wires containing magnetic impurities, using the mechanically controllable break junction technique, shows a zero-bias anomaly, which is attributed to the Kondo resonance (Yanson *et al.*, 1995). In addition, these experiments show that the Kondo resonance splits in a magnetic field. NRG calculations for the $S = 1/2$ Kondo model in a magnetic field show that the Kondo resonance splits in a magnetic field $B$, provided the Zeeman splitting $g_i \mu_B B$ exceeds $0.5 T_K$ (Costi, 2000). Here $g_i$ and $\mu_B$ are the impurity $g$ factor and Bohr magneton, and $T_K$ is the Kondo scale defined from the half width at half maximum of the $T = 0$ Kondo resonance. The latter is obtained from the imaginary part of the many-body $T$ matrix $T_{kk'\sigma}$ for spin $\sigma$, defined by

$$G_{kk'\sigma}(\omega) = \delta_{kk'} G^0_{kk'\sigma} + G^0_{kk\sigma} T_{kk'\sigma} G^0_{k'k'\sigma}, \tag{118}$$

where $G_{kk'\sigma}(\omega) = \langle\langle c_{k\sigma}; c_{k'\sigma}^\dagger \rangle\rangle$ is the full conduction electron Green's function and $G^0_{kk'}$ is the corresponding unperturbed Green's function. From the equations of motion for $G_{kk'}$ one finds for the orbitally isotropic Kondo model

$$T_{kk'\sigma}(\omega) = \sigma \frac{J}{2} \langle S_z \rangle + \left(\frac{J}{2}\right)^2 \langle\langle O_\sigma; O_\sigma^\dagger \rangle\rangle, \tag{119}$$

$$O_\sigma = \sum_k \vec{S} \cdot \vec{\tau}_{\sigma\sigma'} c_{k\sigma'}, \tag{120}$$

with $\vec{\tau}$ the Pauli matrices. From the $T$ matrix one can also extract the transport time and thereby the magnetoresistivity. The latter is found to agree well with experimental data on diluted Ce impurities in $LaAl_2$ (Costi, 2000).

A recent development has been the realization by Zaránd *et al.* (2004) that one can use the NRG method to extract from the many-body $T$ matrix both elastic and inelastic scattering rates and cross sections. The total scattering cross section $\sigma_{\rm tot}(\omega)$ is related to the imaginary part of the $T$ matrix by the optical theorem

$$\sigma_{\rm tot}(\omega = \varepsilon_k) = -\frac{2}{v_k} \mathrm{Im}[T_{kk\sigma}(\omega)], \tag{121}$$

with $v_k$ the velocity of electrons with wave vector $k$. Consequently, by using the expression for the elastic scattering cross section

$$\sigma_{\rm el}(\omega = \varepsilon_k) = \frac{2\pi}{v_k} \sum_{k'} \delta(\varepsilon_{k'} - \varepsilon_k) |T_{kk'\sigma}(\omega)|^2, \tag{122}$$

Zaránd *et al.* (2004) were able to calculate the inelastic scattering cross section $\sigma_{\rm inel} = \sigma_{\rm tot} - \sigma_{\rm el}$ and the inelastic scattering time $\tau_{\rm inel} \sim \sigma_{\rm inel}^{-1}$. In order to shed light on the expression for $\sigma_{\rm inel}$, consider the Anderson model for a flat band with density of states $N_F = \Sigma_{k'} \delta(\varepsilon_{k'} - \varepsilon_k)$ and resonant level width $\Delta = \pi N_F V^2$. We have $T_{kk'} = V^2 G_d$, with $G_d = [\omega - \varepsilon_d + i\Delta - \Sigma(\omega)]^{-1}$ and $\Sigma$ the correlation part of the self-energy. The inelastic scattering cross section for $\omega = \varepsilon_k$ reduces to (Zaránd *et al.*, 2004)

$$\sigma_{\rm inel} = -\frac{2}{v_k} \frac{V^2 \Sigma''(\omega)}{[\omega - \varepsilon_d - \Sigma'(\omega)]^2 + [\Delta - \Sigma''(\omega)]^2}, \tag{123}$$

which shows that the inelastic scattering rate vanishes at $T = 0$ for electrons at the Fermi level due to the Fermi-liquid property of the self-energy $\Sigma''(\omega) \sim -\omega^2$ for $\omega \to 0$. Zaránd *et al.* (2004) evaluated $\sigma_{\rm inel}$ for the $S = 1/2$ Kondo model via the NRG method using the $T$ matrix in Eq. (119) at $T = 0$ and for both zero and finite magnetic fields. The maximum in the inelastic scattering rate occurs close to $\omega \approx T_K$ (see Fig. 14).

A quantity closely related to the inelastic scattering time $\tau_{\rm inel}(\omega, T) \sim \sigma_{\rm inel}^{-1}$ is the dephasing time $\tau_\phi(T)$ for electrons scattering from magnetic impurities and measured in weak-localization experiments on diffusive conductors (Mohanty *et al.*, 1997; Pierre *et al.*, 2003; Schopfer *et al.*, 2003; Bäuerle *et al.*, 2005). A derivation of the connection between these two quantities and exact expressions relating them can be found in Micklitz *et al.* (2006). For samples of dimensionality $d = 1, 3$,

$$\frac{1}{\tau_\phi(T)} = \left( -\int d\omega f'(\omega) \tau_{\rm inel}(\omega, T)^{(2-d)/2} \right)^{2/(d-2)}, \tag{124}$$

where $f'(\omega)$ is the derivative of the Fermi function at temperature $T$ (Micklitz *et al.*, 2006). For similar expressions in $d = 2$ and dephasing rates in mesoscopic ring geometries see Micklitz *et al.* (2006, 2007).

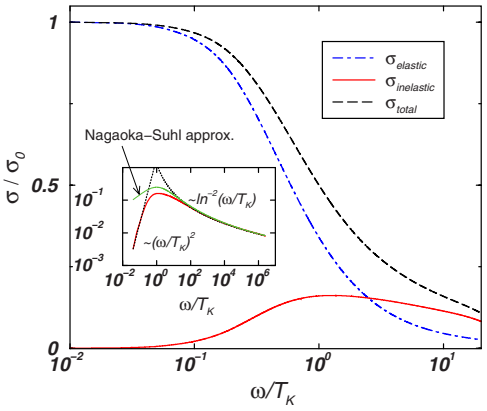


FIG. 14. (Color online) Elastic, inelastic, and total scattering rates for the $S = 1/2$ fully screened Kondo model at $T = 0$. The Kondo scale $T_K$ is that from the half width at half maximum of the Kondo resonance and is approximately twice that from the $T = 0$ susceptibility defined in Eq. (82). From Zaránd *et al.*, 2004.

Figure 15 shows the dephasing rate as a universal function of $T/T_K$ for the $S = 1/2$ Kondo model, obtained by using the NRG method for finite-temperature dynamics. The maximum dephasing rate occurs at $T \approx T_K$ and decreases at first linearly with temperature below $T_K$ and eventually as $T^2$ in the Fermi-liquid region $T \ll T_K$. The magnetic field dependence of the dephasing time $\tau_\phi(B, T)$ has also been calculated, and the expression for the dephasing rate has been generalized to arbitrary dynamical scatterers (Micklitz *et al.*, 2007). Recent experiments on Fe impurities in Ag wires show better than expected agreement with the theoretical predictions for the dephasing rate of the $S = 1/2$ Kondo model (Alzoubi and Birge, 2006; Mallet *et al.*, 2006). Fe

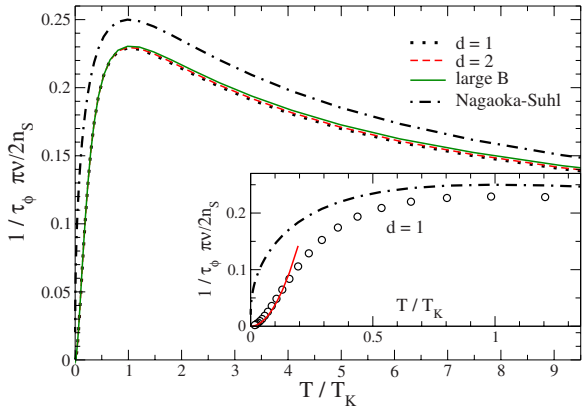


FIG. 15. (Color online) Universal dephasing rate for the $S = 1/2$ fully screened Kondo model calculated via the NRG method for Kondo impurities in $(d = 1, 2)$-dimensional conductors. The solid line in the inset is the analytic $T^2$ result from Fermi-liquid theory valid for $T \ll T_K$, where $T_K$ is the scale defined in Eq. (82). From Micklitz *et al.*, 2006.

impurities in Ag will have both an orbital moment and a spin $S>1/2$ in the absence of crystal-field and spin-orbit interactions. Inclusion of the latter, may, however, result in an effective $S=1/2$ single-channel Kondo model at the low temperatures $T\approx 1$ K of the experiments, thereby helping to explain the good agreement with the $S=1/2$ theory. At the very lowest temperatures, $T<0.1T_K$, a slower decay of the dephasing rate has been reported in these experiments, as compared to that expected from a fully screened model. One possible explanation for this is that a small fraction of Fe impurities is only partially screened. Underscreened Kondo models, to which we now focus, are known to give a much slower decay of the dephasing rate below the Kondo scale [see below and Vavilov and Glazman (2003)].

Cragg and Lloyd (1979) investigated the single-channel $S=1$ underscreened Kondo model and showed that its low-energy fixed point corresponds to the spectrum of the ferromagnetic $S'=1/2$ Kondo model. Deviations from the fixed point at iteration $N$ are of the form $\tilde{J}(N)\vec{S}'\cdot\vec{s}_0$ with $\tilde{J}(N)$ being $O(-A/[N+C(J)])$ with $A$ being a constant and $C(J)$ depending on $J$, i.e., the deviations are marginally irrelevant. These calculations were extended by Koller, Hewson, and Meyer (2005) to models with $S=1,\ldots,5/2$. They also determined $C(J)$ explicitly for the different cases. Using the relation of $N$ to energy $\omega\sim\Lambda^{-N/2}$, the effective coupling can be written as $\tilde{J}(\omega)\sim 1/\ln(\omega/T_0)$, with $T_0$ an appropriate Kondo scale (Koller, Hewson, and Meyer, 2005). Consequently, there are logarithmic corrections to thermodynamic quantities at low temperature, instead of the power-law corrections characteristic of fully screened Kondo models. Nonanalytic corrections are also found in dynamical quantities (Koller, Hewson, and Meyer, 2005; Mehta *et al.*, 2005), so underscreened Kondo models have been termed singular Fermi liquids (Mehta *et al.*, 2005). For example, the spectral density $\rho_t(\omega)$ obtained from the $T$ matrix (119) takes a finite value at the Fermi level, but the approach to this value is nonanalytic (Koller, Hewson, and Meyer, 2005):

$$\rho_t(\omega)=\rho_t(0)-b/\ln(\omega/T_0)^2. \tag{125}$$

Similarly, the $T=0$ inelastic cross section, also calculated by Koller, Hewson, and Meyer (2005), decays as $1/\ln(\omega/T_0)^2$ at low energies, and consequently the dephasing rate decays as $\tau_\phi^{-1}(T)\sim 1/\ln(T/T_0)^2$. As mentioned above, a small fraction of underscreened Fe impurities may explain the excess dephasing observed at the lowest temperatures in the experiments of Mallet *et al.* (2006) and Alzoubi and Birge (2006). Calculations for the temperature dependence of the resistivity and dephasing rates of the spin $S>1/2$ underscreened Kondo models and their relevance to Fe impurities in Ag can be found in Mallet *et al.* (2006). It is also interesting to note that calculations for ferromagnetic Kondo models (Koller, Hewson, and Meyer, 2005) show that all cross sections vanish at the Fermi level, with the inelastic part contributing nearly all the scattering in this limit and the elastic part being negligibly small.

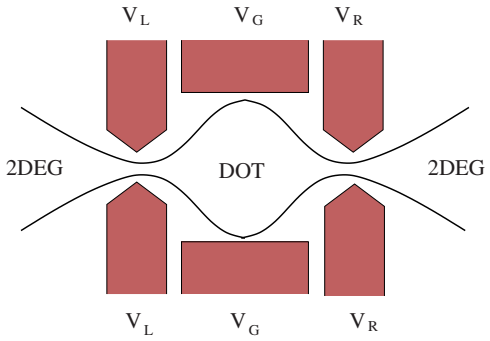


FIG. 16. (Color online) Schematic top view of a lateral quantum dot, consisting of a confined region of typical size 10–100 nm defined in the two-dimensional electron gas (2DEG) of a GaAs/AlGaAs heterostructure. The dot is connected to the left and right electron reservoirs. Gate voltages $V_{L,R}$ control the tunnel barriers into and out of the dot, while $V_G$ controls the dot level positions.

Finally we mention recent work on calculating spatial correlations such as spin-density correlations $C(x)=\langle\vec{S}\cdot\vec{s}_x\rangle$ around Kondo impurities, where $\vec{s}_x$ is the electron spin density at distance $x$ from the impurity [for earlier work involving perturbative aspects combined with the NRG method see Chen *et al.* (1987, 1992)]. Borda (2007) worked with Wannier states centered at both the impurity and $x$, thereby reducing the problem to a two-impurity-type calculation (Sec. IV.C.1). At $T=0$ and in one dimension, the decay of $C(x)$ is found to change from $1/x$ to $1/x^2$ around $x=\xi_K=\hbar v_F/T_K$, where the coherence length $\xi_K$ describes the size of the Kondo screening cloud. At finite temperature, the expected exponential decay of $C(x)$ for $x>\xi_T=\hbar v_F/k_BT$ is recovered.

### 3. Kondo effect in nanostructures

Experimental work has demonstrated the importance of the Kondo effect in determining the low-temperature transport properties of nanoscale size devices such as quantum dots (Cronenwett *et al.*, 1998; Goldhaber-Gordon *et al.*, 1998; van der Wiel *et al.*, 2000). An example of such a device, a quantum dot, is shown in Fig. 16. More complicated devices, such as capacitively coupled double dots or dots contained in one or two arms of an Aharanov-Bohm interferometer, can be built up from this basic unit. A quantum dot consists of a confined region of electrons coupled to leads via tunnel barriers. It may be viewed as an artificial multielectron atom, in which the different levels (filled, partially filled, or empty) couple to electron reservoirs via one or more channels. A quantum dot can be described, in general, by the following multilevel Anderson impurity model:

$$H=H_{\rm dot}+H_c+H_{\rm tun},$$

$$H_{\rm dot}=\sum_{i\sigma}\varepsilon_{i\sigma}d_{i\sigma}^\dagger d_{i\sigma}+E_C(\hat{N}-\mathcal{N})^2-J_H\vec{S}^2,$$

$$H_c = \sum_{k\alpha\sigma} \varepsilon_{k\sigma} c^\dagger_{k\alpha\sigma} c_{k\alpha\sigma},$$

$$H_{\rm tun} = \sum_{k\alpha i\sigma} t_{\alpha i}(d^\dagger_{i\sigma} c_{k\alpha\sigma} + c^\dagger_{k\alpha\sigma} d_{i,\sigma}), \tag{126}$$

where $\epsilon_{i\sigma}, i=1,2,\ldots$ are the dot level energies for spin $\sigma$ electrons, $\mathcal{N}=\langle\hat{N}\rangle=\Sigma_{i\sigma}\langle d^\dagger_{i\sigma} d_{i\sigma}\rangle$ is the dot occupancy, $E_C$ is the charging energy, $\vec{S}=\frac{1}{2}\Sigma_{i\mu\nu} d^\dagger_{i\mu}\vec{\sigma}_{\mu\nu} d_{i\nu}$ is the total spin of the dot, and $J_H>0$ is the Hund's exchange coupling. In the above, $\alpha=L,R$ labels left (right) lead degrees of freedom and $k$ labels the wave vector of a single transverse channel propagating through the constriction between the two-dimensional electron gas and the quantum dot. Electrons tunnel into and out of the dot with amplitudes $t_{\alpha i}$ and give rise to a single-particle broadening $\Gamma_i$ of the levels.

The model above is essentially the same model as the multiorbital model of Sec. IV.D, used to describe bulk Kondo systems. The novel situation in quantum dots is that parameters such as the tunnel couplings and level positions can be controlled by gate voltages. This allows such models to be experimentally investigated in all physically interesting regimes, such as spin and charge fluctuation regimes, and in principle also to be tuned through quantum phase transitions. In addition, different realizations of quantum dots (nanotubes, vertical dots) may have level degeneracies or near level degeneracies, allowing the effects of Hund's exchange to be investigated. Finally, the devices described by Eq. (126) can be driven out of equilibrium by a finite transport voltage, allowing the study of nonequilibrium effects in relatively simple quantum many-body systems. This would be one motivation to further develop the NRG method to steady-state nonequilibrium situations.

*a. Single-level quantum dots*

In the low-temperature limit, only one or two partially filled levels close to the Fermi level of the leads will be important for transport. The remaining levels will be either filled or empty, and, at the low temperatures of interest for quantum transport, they may be neglected. The simplest model, therefore, to describe low-temperature transport through a quantum dot is the single-level Anderson impurity model (2) with level position $\varepsilon_1=\varepsilon_f=-eV_G$ controlled by the gate voltage and Coulomb repulsion $U$ given by the charging energy $E_C=U/2$. Only one conduction channel, the even combination of left and right electron states, $a_{k\sigma}$ below, couples to the local level, as can be seen by using the canonical transformation

$$a_{k\sigma} = (t_L c_{kL\sigma} + t_R c_{kR\sigma})/\sqrt{t_L^2 + t_R^2}, \tag{127}$$

$$b_{k\sigma} = (-t_R c_{kL\sigma} + t_L c_{kR\sigma})/\sqrt{t_L^2 + t_R^2}, \tag{128}$$

with $t_\alpha = t_{\alpha i}\delta_{i,1}$. We note that treating the Coulomb interaction classically implies that, for an integer number of electrons on the dot, transport is blocked for large $U$, since transferring electrons through the dot requires overcoming the large Coulomb repulsion. Glazman and Raikh (1988) and Ng and Lee (1988) pointed out, however, that in the situation where the total spin on the dot is finite, as happens for an odd number of electrons (i.e., for $\mathcal{N}=1$ in the effective single-level model), one should expect, on the basis of Eq. (2), an enhancement of the conductance to its maximum possible value of $G=2e^2/h$ via the Kondo effect in the limit of zero temperature. A device representing a tunable Anderson impurity model has been realized (Cronenwett *et al.*, 1998; Goldhaber-Gordon *et al.*, 1998), and the predicted enhancement of the low-temperature conductance for dots with an odd number of electrons was measured and compared (Goldhaber-Gordon *et al.*, 1998) to quantitative NRG calculations (Costi *et al.*, 1994b), such as those shown in Fig. 10 for the conductance in the Kondo regime [see also Izumuda, Sakai, and Suzuki (2001)]. Tuning the quantum dot to the mixed valence and empty orbital regimes has also enabled comparisons with theory in those regimes (Schoeller and König, 2000; Costi, 2003).

The frequency dependence of the linear conductance $G'(\omega)$ of a single-level quantum dot described by Eq. (2) has been considered (Izumida *et al.*, 1997; Campo and Oliveira, 2003; Sindel *et al.*, 2005). Sindel *et al.* (2005) calculated $G'(\omega)$, in the Kondo regime at $T=0$, and also extracted the current noise

$$C(\omega) = \int_{-\infty}^{+\infty} dt\, e^{i\omega t}[\langle I(0)I(t)\rangle - \langle I\rangle^2] \tag{129}$$

by making use of the fluctuation-dissipation theorem

$$C(\omega) = \frac{2\hbar\omega}{e^{\hbar\omega/k_B T}-1} G'(\omega). \tag{130}$$

The conductance and spin-resolved conductances of single-level quantum dots in a magnetic field have also been calculated and a strong spin-filtering effect has been observed in the mixed valence regime (Costi, 2001). For spin-filtering effects in quantum dots with ferromagnetic leads, see Martinek *et al.* (2003) and Simon *et al.* (2007).

One of the hallmarks of the $S=1/2$ single-channel Kondo effect is the flow of the exchange coupling to strong coupling (Wilson, 1975a). This can be interpreted as resulting in a phase shift of the conduction electrons at the Fermi level, at $T=0$, of $\delta_\sigma=\pi/2$ (Nozières, 1974). A direct measurement of this phase shift is possible if one embeds a quantum dot in one arm of an Aharanov-Bohm interferometer. Assuming a single-level Anderson model for the quantum dot and a multiterminal open geometry, Gerland *et al.* (2000) carried out NRG calculations for the interference term $G_{\rm AB}$ whose measurement can be used to extract $\delta_\sigma$. A similar setup has been investigated by Hofstetter *et al.* (2001) for the flux dependence $G(\phi)$ of the conductance at $T=0$ and by Kang *et al.* (2005) for the complex transmission. Izumida *et al.* (1997) calculated $G(\phi)$ for two single-level quantum dots embedded in the arms of an Aharanov-Bohm interfer-

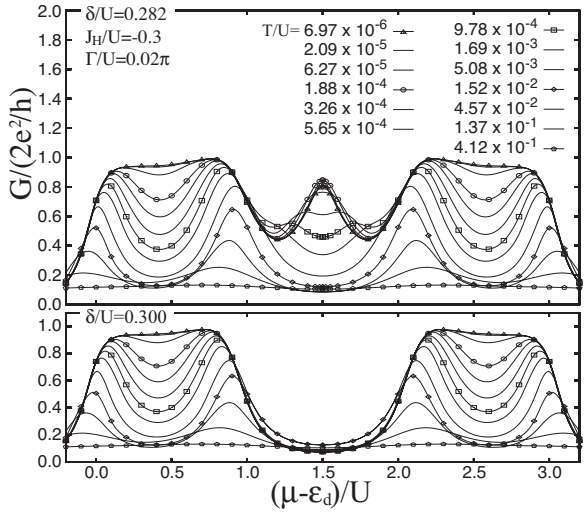


FIG. 17. The singlet-triplet crossover in the linear conductance of the two-channel two-orbital Anderson model including Hund's exchange $J_H$, intraorbital and interorbital Coulomb energy $U$, levels $\varepsilon_d \pm \delta/2$, and temperature $T$. Top (bottom) panel show $G(T)$ on the triplet (singlet) side of the crossover and $(\mu-\varepsilon_d)/U=0.5,1.5,2.5$ correspond to $\mathcal{N}=1.0,2.0,3.0$ electrons on the dot. Adapted from Sakai and Izumida, 2003.

ometer. This model reduces, in general, to a two-channel two-orbital Anderson model, which we discuss next.

*b. Two-level quantum dots*

A quantum dot with two active levels for transport introduces some new physics due to the competition between the level spacing $\delta=\varepsilon_2-\varepsilon_1$, the charging energy $E_C$, and the Hund's exchange $J_H$. In particular, a Kondo effect with an even number of electrons on the dot can be realized. This can occur when the dot is occupied with two electrons and $\delta<2J_H$ so that the ground state of the dot has $S=1$. Such a two-level dot will, in general, couple to two channels so an $S=1$ Kondo effect will result, leading to a singlet ground state and an enhanced conductance $G(T)$ at low temperatures. In the opposite case $\delta>2J_H$, the dot has $S=0$, the Kondo effect is absent, and the conductance is low. This behavior was measured in the experiments of Sasaki *et al.* (2000) on vertical quantum dots, where a magnetic field was used to decrease the energy splitting $\Delta_{TS}=\delta-2J_H$ between the triplet and singlet states, thereby leading to the above mentioned crossover behavior in the conductance at $\mathcal{N}=2$. Theoretical calculations by Izumida, Sakai, and Tarucha (2001), shown in Fig. 17, are consistent with the experimental results.

The singlet-triplet crossover behavior in a two-level quantum dot can become a quantum phase transition when only one conduction channel couples to the leads, e.g., when all lead couplings are equal (Pustilnik and Glazman, 2001; Hofstetter and Schoeller, 2002). In this case, for large Hund's exchange, an effective single-channel $S=1$ underscreened Kondo model results, which has a doubly degenerate many-body ground state. For small Hund's exchange, a model with $S=0$ results, having a nondegenerate many-body ground state. A sharp transition separates these two different ground states. As discussed above, however, two channels will, in general, couple to the dot and this will result in perfect screening of the $S=1$ spin so that the ground state is always a singlet. Nevertheless, proximity to the singlet-triplet transition can still be seen as a signature in various quantities, such as a nonmonotonic dependence of the conductance as a function of magnetic field on the triplet side of the crossover (Hofstetter and Zaránd, 2004). Experiments on lateral quantum dots at the singlet-triplet crossover point (van der Wiel *et al.*, 2002) show behavior in the differential conductance similar to predictions for the spectral density (Hofstetter and Schoeller, 2002).

The above is only a brief account of the simplest nanostructured devices studied using the NRG method. Further applications include numerous studies of double-dot systems, including realizing an SU(4) Kondo state (Borda *et al.*, 2003) and quantum critical points of two-impurity Kondo models (Garst *et al.*, 2004; Zaránd *et al.*, 2006; Zhu and Varma, 2006) (see Sec. IV.C.1), static and dynamics of double dots (Galpin *et al.*, 2006a, 2006b), double dots with only one dot coupled to the leads (Cornaglia and Grempel, 2005b), applications to quantum tunneling in molecular magnets (Romeike *et al.*, 2006a, 2006b), a novel Kondo effect in a $\nu=1$ integer quantum Hall system (Choi, Hwang, and Yang, 2003), and the conductance of ultrasmall tunnel junctions (Frota and Flensberg, 1992; Frota, 2004). Crossover from two-channel Kondo behavior to Fermi-liquid behavior on lowering the temperature has recently been investigated for triple quantum dots attached to leads (Žitko and Bonča, 2007).

### B. Two-channel Kondo physics

Nozières and Blandin (1980) have proposed a variation of the Kondo model in which the localized spin couples to two conduction bands [see Eq. (117) with $\alpha=1,2$]. An important feature of this model is the overscreening of the impurity spin: in the strong-coupling limit, the spins of both conduction bands try to screen the impurity spin, so that again a net spin-1/2 object is formed. In other words, the strong-coupling fixed point at $J=\infty$ (which gives rise to the Fermi-liquid fixed point in the single-channel case) is unstable, and an intermediate-coupling fixed point is realized. This new fixed point shows a variety of non-Fermi-liquid properties such as a divergence of the specific heat ratio $C/T=\gamma\propto\ln T$ and of the spin susceptibility $\chi\propto\ln T$ for $T\to 0$; an anomalous Wilson ratio $R=\chi/\gamma=8/3$, in contrast to the result for the standard Kondo model, $R=8/4=2$; and a zero-point entropy of $\frac{1}{2}\ln 2$, indicating that half-fermionic excitations (Majorana fermions) play a crucial role for the structure of the fixed point.

We have discussed these features in the section on the calculation of thermodynamic and static quantities (see

Fig. 6). An extensive review of the two-channel Kondo model, its physical properties, and its relevance for non-Fermi-liquid behavior in real materials has been given by Cox and Zawadowski (1998). This paper also reviews earlier NRG calculations for this model.

Historically, the two-channel Kondo model has been the first application of the NRG method to a quantum impurity model in which the physics is not governed by the Fermi-liquid fixed point of the standard Kondo model. In this sense, the early work of Cragg *et al.* (1980) on the two-channel Kondo model opened the way for a variety of investigations of more complex impurity models, displaying both Fermi-liquid and non-Fermi-liquid fixed points. Due to the importance of this and following work, we focus this section purely on two-channel Kondo physics and postpone the discussion of other multiband models to Sec. IV.D.

As discussed already in Sec. II, the truncation of states within the iterative diagonalization scheme severely limits the applicability of the NRG method to multiband models. In the calculations of Cragg *et al.* (1980), iterations were observed to break down after only a few (approximately 12) steps. The source of this problem is mainly the small number of states ($N_s \approx 400$) used in this work, which corresponds to keeping $N_s \approx \sqrt{400} = 20$ states in a one-channel calculation. Specific symmetries of the two-channel Kondo model, such as the total axial charge, have been used to reduce the matrix sizes in the diagonalization (Pang and Cox, 1991), but later calculations showed that by increasing the number of states the iterations can be stabilized sufficiently. Independent of the value of $N_s$, it is important to avoid any symmetry breaking due to the truncation of states.

In order to approach the non-Fermi-liquid fixed point within only a few iterations, Cragg *et al.* (1980) and Pang and Cox (1991) used large values of either the exchange coupling $J$ or the discretization parameter (up to $\Lambda = 9.0$). Nevertheless, these calculations give the correct fixed point spectrum of the (isotropic) two-channel Kondo model with the characteristic structure of excitations at energies 1/8, 1/2, 5/8, 1, etc., at least for the lowest-lying excited states. Figure 18 shows a typical flow diagram for parameters $J = 0.05D$, where $2D$ is the bandwidth of the featureless conduction band density of states, $\Lambda = 4$, and $N_s = 4900$, for both even (dashed curves) and odd NRG iterations (full curves) [for similar plots, see Fig. 1 in Cragg *et al.* (1980) and Figs. 1 and 2 in Pang and Cox (1991)]. After some initial even-odd oscillations, the flow reaches the non-Fermi-liquid fixed point which does not show any even-odd effect.

Comparison with conformal field theory calculations (Affleck *et al.*, 1992) gave an excellent agreement with the NRG method for both the excitation spectrum and corresponding degeneracies. Such a comparison, however, requires the extrapolation of the NRG fixed point spectra for $\Lambda \to 1$ [see Fig. 9 in Affleck *et al.* (1992); the analysis is not quite satisfactory for $\Lambda < 2$ and it would be interesting to repeat these calculations using larger values of $N_s$]. This work, and that by Pang and Cox (1991), also focused on the stability of the non-Fermi-liquid fixed point against various perturbations. As it turns out, the non-Fermi-liquid fixed point is stable against anisotropy in the exchange interaction ($J_z \neq J_\perp$) but unstable against both the presence of a magnetic field and the lifting of the exchange symmetry between the two channels ($J_a \neq J_b$). In the latter case, a temperature scale $T^* \propto (J_a - J_b)^2$ for the crossover between the non-Fermi-liquid fixed point at intermediate temperatures and the stable Fermi-liquid fixed point at $T \to 0$ has been found. These instabilities were later investigated by Yotsuhashi and Maebashi (2002), via calculation of the impurity entropy and the crossover temperature.

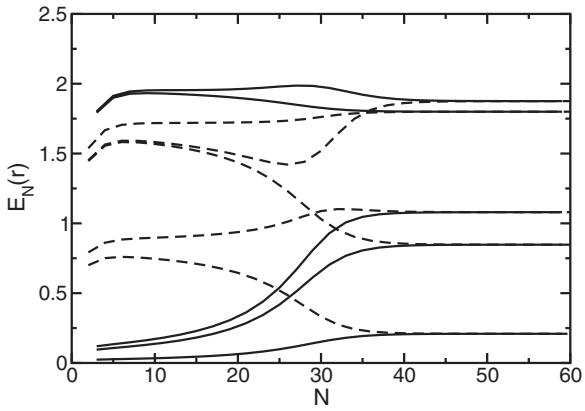


FIG. 18. Flow diagram of the lowest-lying many-particle levels for the isotropic two-channel Kondo model (even iterations dashed curves, odd iterations full curves).

Further investigations concerning the stability of the non-Fermi-liquid fixed point have been performed by Pang (1994) (flavor exchange coupling) and Kusunose and Kuramoto (1999) and Kusunose *et al.* (1996) (effect of repulsion among conduction electrons and potential scattering).

A pedestrian approach for understanding the two-channel Kondo model was introduced by Coleman *et al.* (1995). These authors argued that the two conduction bands in the two-channel Kondo model can be replaced by a single conduction band, with a coupling between impurity spin $\mathbf{S}$ to both spin $\boldsymbol{\sigma}$ and isospin $\boldsymbol{\tau}$ of the conduction band. The isospin $\boldsymbol{\tau}$ takes into account the charge degrees of freedom of the conduction band and the compactified $\sigma$-$\tau$ model takes the form

$$H = \sum_{k\sigma} \varepsilon_k c^\dagger_{k\sigma} c_{k\sigma} + J(\mathbf{S} \cdot \boldsymbol{\sigma} + \mathbf{S} \cdot \boldsymbol{\tau}). \tag{131}$$

This model can be related to an Anderson-type model [the O(3)-symmetric Anderson model] via a Schrieffer-Wolff transformation (Coleman and Schofield, 1995).

It was later verified with the NRG approach (Bulla and Hewson, 1997) that these compactified models indeed show many of the anomalous non-Fermi-liquid properties of the two-channel Kondo model, although these models do not allow for an overscreening of the impurity spin. Furthermore, the structure of the non-Fermi-liquid fixed point has been studied in detail. It

turns out that the many-particle spectrum of this fixed point is composed of single Majorana fermion excitations (Bulla, Hewson, and Zhang, 1997). This information can then be extended to the fixed point structure of the two-channel Kondo model, which can be described by two towers of excitations which are both composed of Majorana fermions [see Sec. 8 in Bulla, Hewson, and Zhang (1997)].

Naturally, we expect that the non-Fermi-liquid properties of the two-channel Kondo model are also visible in its dynamic properties, but, unfortunately, detailed and comprehensive NRG calculations for the dynamics have not been performed so far. Apart from a brief sketch of the results for the $T$ matrix and the magnetic susceptibility by Sakai, Shimizu, and Kaneko (1993), the published data are only for models equivalent to the two-channel Kondo model in certain limits.

It has been argued by Bradley *et al.* (1999) that the dynamical spin susceptibility $\chi(\omega)$ of the compactified models introduced above is exactly equivalent to that of the two-channel Kondo model, and that this equivalence holds for the *full* frequency range. The NRG results show, for example, a $\ln(\omega)$ divergence of $\chi'(\omega)$ for $\omega \rightarrow 0$, in agreement with the results of Sakai, Shimizu, and Kaneko (1993). On the other hand, there is no counterpart of the single-particle dynamics calculated by Bradley *et al.* (1999) in the two-channel Kondo model.

The two-channel Anderson model shows a line of fixed points of the two-channel Kondo type when the local level position is varied (Bolech and Andrei, 2002). In the Kondo limit, this model is connected to the two-channel Kondo model via a Schrieffer-Wolff transformation (note that this holds only when the impurity degrees of freedom in the Anderson model are written in terms of Hubbard operators that include the channel index). This connection is visible in thermodynamic properties, such as the zero-point entropy of $\frac{1}{2}\ln 2$. Anders (2005) investigated the single-particle dynamics (spectral function and self-energy) of the two-channel Anderson model, quantities which, again, do not have a counterpart in the two-channel Kondo model. Concerning the results for the dynamic susceptibility $\chi(\omega)$ presented by Anders (2005), comparison to the corresponding results of the two-channel Kondo model has not yet been done.

There is an ongoing discussion about the observability of two-channel Kondo physics in experiments for a variety of systems. We stress here that the instability of the non-Fermi-liquid fixed point itself does not exclude its observation. As for any system with a quantum critical point, the corresponding anomalous properties dominate a significant fraction of the finite-temperature phase diagram (determined by the critical exponent) so that a precise tuning of the Hamiltonian parameters is not required. Nevertheless, two-channel Kondo physics is now mainly discussed within systems in which alternative degrees of freedom (such as orbital quantum numbers) take the role of the spin or channel in the Hamiltonian, Eq. (61); one example is the quadrupolar Kondo model, which is discussed by Cox and Zawadowski (1998).

Here we discuss NRG calculations for two-channel Kondo physics in quantum dot systems (Lebanon *et al.*, 2003a, 2003b; Anders *et al.*, 2004, 2005). Within a model of a quantum box coupled to the leads via a single-mode point contact [see Fig. 1 in Lebanon *et al.* (2003b)], the physics at the degeneracy points of the Coulomb blockade staircase can be directly connected to that of the two-channel Kondo model. Here the two charge configurations in the box play the role of the impurity spin and the physical spin of the conduction electrons corresponds to the channel index. For such a system, the NRG method allows the nonperturbative calculation of the charge inside the box and the capacitance in the whole parameter regime. The results show, for example, that the shape of the charge steps is governed by the non-Fermi-liquid fixed point of the two-channel Kondo model.

To conclude this section we mention that there are models involving a more complicated orbital structure of the impurity—including, for example, excited crystalline electric field levels—which reduce to the two-channel Kondo model in certain limits or which display non-Fermi-liquid fixed points of the two-channel Kondo type. NRG studies of such models can be found in Koga and Shiba (1995, 1996); Sakai *et al.* (1997); Koga and Cox (1999); and Hattori (2005). Overscreening can also be realized in single-channel models when the conduction electron spin exceeds the impurity spin; for a discussion of this issue see, for example, Kim *et al.* (1997). We note also a recent study (Kolf and Kroha, 2007) showing an exponential dependence of the Kondo scale on $-1/JN_F$ and $-JN_F$, for small and large coupling cases, respectively, which may explain the absence of a broad distribution of Kondo scales in nanoconstrictions with two-channel Kondo impurities.

### C. Impurity quantum phase transitions

In this section, we focus on models which, as a function of one or more couplings in the model, give rise to a phase transition in the ground state. Typically, this is due to a competition between the Kondo effect, which tends to favor a strong-coupling ground state with a screened or partially screened local moment, and some competing mechanism, which leads to a ground state with a free or almost free local moment. In general, such phase transitions are termed impurity quantum phase transitions [for reviews, see Bulla and Vojta (2003) and Vojta (2006)], as they are observable only in the *impurity* contribution to physical properties and not connected to possible phase transitions in the bulk to which the impurity couples.

As impurity quantum phase transitions are usually associated with a vanishing low-energy scale, the NRG method is ideally suited to their investigation, allowing their detection and characterization with very high accuracy. This is most evident for continuous transitions where the critical exponents connected to the quantum critical point can only be calculated when a large range of energy or temperature scales is accessible. In this sec-

tion we give an overview of NRG results for multi-impurity models (Sec. IV.C.1), models with locally critical behavior (Sec. IV.C.2), and models with magnetic impurities in superconductors (Sec. IV.C.3). Note that impurity quantum phase transitions are also observed in models which are discussed in other sections of this review: the non-Fermi-liquid fixed point of the two-channel Kondo model, Sec. IV.B, can be viewed as a quantum critical point when the control parameter "channel anisotropy" is tuned through zero; locally critical behavior is also connected to models with coupling to a bosonic bath as discussed in Sec. IV.E.

#### 1. Multi-impurity physics

An early extension of the NRG method to more complex systems was the study of the two-impurity $S=1/2$ Kondo model (Jones and Varma, 1987; Jones *et al.*, 1988), whose Hamiltonian is given by

$$H = \sum_{k\sigma} \varepsilon_k c^\dagger_{k\sigma} c_{k\sigma} + J_K \sum_{l=1}^{2} \mathbf{S}(\mathbf{R}_l) \cdot \mathbf{s}(\mathbf{R}_l) + I_D \mathbf{S}(\mathbf{R}_1) \cdot \mathbf{S}(\mathbf{R}_2). \tag{132}$$

Here $\mathbf{s}(\mathbf{R}_l)$ is the conduction electron spin density at the impurity site $\mathbf{R}_l$ and $J_K>0$ is the antiferromagnetic Kondo exchange. The first two terms in Eq. (132) are sufficient to generate an indirect Ruderman-Kittel-Kasuya-Yosida (RKKY) interaction $I_{\mathrm{RKKY}}$ between the impurity spins. In some contexts a direct exchange interaction among the impurity spins of strength $I_D$ can arise (Jones and Varma, 1987), so the last term has been added. The net effective exchange interaction between the spins is given by $I_{\mathrm{eff}}=I_D+I_{\mathrm{RKKY}}$ and can be either ferromagnetic $I_{\mathrm{eff}}<0$ or antiferromagnetic $I_{\mathrm{eff}}>0$. The properties of the model then depend solely on the ratio $I_{\mathrm{eff}}/T_K$, where $T_K$ is the single-ion Kondo scale, and the details of the dispersion relation $\varepsilon_k$. The model in Eq. (132) also arises in the Schrieffer-Wolff limit (Schrieffer and Wolff, 1966) of the two-impurity Anderson model, which in the notation introduced in Eq. (2) reads

$$H = \sum_{k\sigma} \varepsilon_k c^\dagger_{k\sigma} c_{k\sigma} + \sum_{l=1}^{2} \sum_{\sigma} \varepsilon_{l\sigma} f^\dagger_{l\sigma} f_{l\sigma} + U \sum_{l=1}^{2} f^\dagger_{l\uparrow} f_{l\uparrow} f^\dagger_{l\downarrow} f_{l\downarrow} + \frac{1}{\sqrt{N}} \sum_{l=1}^{2} \sum_{k\sigma} V_k (e^{i\mathbf{R}_l\cdot\mathbf{k}} f^\dagger_{l\sigma} c_{k\sigma} + \mathrm{H.c.}) + I_{\mathrm{D}} \mathbf{S}(\mathbf{R}_1) \cdot \mathbf{S}(\mathbf{R}_2). \tag{133}$$

The motivation to study such two-impurity models originally arose in the context of heavy fermions. In these systems, the competition between the local Kondo exchange and the intersite RKKY interaction is expected to lead to a phase transition between nonmagnetic and magnetically ordered ground states as a function of $I_{\mathrm{eff}}/T_K$ (Doniach, 1977). The nature of this quantum phase transition remains an open question in heavy fermion physics (v. Löhneysen *et al.* 2007). It is therefore of some interest to investigate the possibility of a transition in the two-impurity problem as this might shed light on the physics of heavy fermions.

Jones *et al.* (1988) have established that such a phase transition can occur under certain conditions (see below) in the particle-hole symmetric two-impurity Kondo model. This can be seen by considering the strong-coupling limits $I_{\mathrm{eff}}\to\pm\infty$ (Affleck *et al.*, 1995). For $I_{\mathrm{eff}}\to-\infty$ the two spins combine to form a spin $S=1$ interacting antiferromagnetically with two conduction channels (characterized by even and odd parity) with, in general, energy-dependent coupling strengths $J_e(k)$ and $J_o(k)$ replaced in Jones *et al.* (1988) by constants (see below). The resulting two-stage Kondo effect progressively screens the $S=1$ spin down to a singlet and leads to a Fermi-liquid ground state characterized by phase shifts $\delta_{e,o}$ for electrons in the even (odd) parity channels. The assumed particle-hole symmetry and the nature of the strong-coupling ground state ensures that these phase shifts will be exactly $\pi/2$ (Millis *et al.*, 1990). In the other limit, $I_{\mathrm{eff}}\to\infty$, the spins form an intersite singlet $S=0$ and the Kondo effect is absent so that the phase shifts are exactly zero. Since the fixed points at $I_{\mathrm{eff}}=\pm\infty$ are both stable and characterized by different (constant) phase shifts, it follows that there can be an unstable fixed point at some critical intermediate value of the intersite exchange $I_c$ at which the phase shifts change discontinuously. This phase transition has also been found in the particle-hole symmetric two-impurity Anderson model (Sakai and Shimizu, 1992a; Paula *et al.*, 1999). Jones *et al.* (1988) estimated $I_c/T_K\approx 2.2$. The associated critical point has been characterized using conformal field theory (Affleck and Ludwig, 1992; Affleck *et al.*, 1995) and bosonization (Gan, 1995), and the physics is found to be similar to that of the two-channel Kondo model. In particular, the staggered susceptibility $\chi_s(T)$ diverges logarithmically at low temperature and the residual entropy has the same value as in the two-channel Kondo model $S(T=0)=\ln\sqrt{2}$ (Gan, 1995). However, the low-temperature form $C(T)=\gamma T$ persists through the critical point, in contrast to the behavior in the two-channel Kondo model $C(T)=-T\ln T$. Close to the critical point, conformal field theory predicts $\gamma\sim(I_{\mathrm{eff}}-I_c)^{-2}$, in agreement with numerical results (Jones, 1990). The level structure of the fixed point at quantum criticality agrees well with NRG calculations and is rather complex, exhibiting a hidden SO(7) symmetry (Affleck *et al.*, 1995).

For generic situations, the natural energy dependence of $J_{e/o}$ obtained from transforming the Kondo model (132) or Anderson model (133) as described below in Eq. (134), as well as a charge transfer term of the form $t\Sigma_\sigma(f^\dagger_{1\sigma}f_{2\sigma}+\mathrm{H.c.})$ in the two-impurity Anderson model, breaks particle-hole symmetry and destroys the critical point (Sakai *et al.*, 1990; Affleck *et al.*, 1995). A similar charge transfer term involving conduction electrons has the same effect in the two-impurity Kondo model (Zaránd *et al.*, 2006; Zhu and Varma, 2006). Potential scattering, if it does not induce charge transfer, breaks particle-hole symmetry but may not affect the critical

point [for a discussion see Affleck *et al.* (1995), Zaránd *et al.* (2006), and Zhu and Varma (2006)]. Thus in general the quantum phase transition discussed above will be absent in the two-impurity models (132) and (133), although signatures of it might still be observable as crossover behavior in various properties. We note briefly here the case of Ising coupled spins $IS_z(\mathbf{R}_1)S_z(\mathbf{R}_2)$. In this case, the ground state for large $I$ will be doubly degenerate as compared to that for small $I$, where the Kondo effect screens the individual spins to singlets, so a quantum phase transition separating these two different ground states arises and is found to be of the Kosterlitz-Thouless type (Garst *et al.*, 2004).

In order to formulate Eq. (132) or Eq. (133) as a linear chain problem for treatment with the NRG method, one needs an orthonormal basis set. The local conduction electron states on the impurity sites in Eq. (132) are not orthogonal. Following Jones and Varma (1987), the Kondo exchange part of Eq. (132) is rewritten in terms of orthonormal even ($e$) and odd ($o$) parity states for the conduction electrons. This results in more complicated interaction terms; in particular, one will obtain two exchange couplings $J_{e/o}(k)$, with $J_e(k) \neq J_o(k)$ in general, which will depend on momentum or energy (Jones and Varma, 1987). The precise form of $J_{e/o}(k)$ will depend on the details of the band structure of the conduction electrons. For free electrons in $D=3$ they can be approximated as (Jones and Varma, 1987; Sakai *et al.*, 1990)

$$J_{e/o}(k) \approx J_K\left(1 \pm \frac{\sin kR}{kR}\right),$$

where $R=|\mathbf{R}_1-\mathbf{R}_2|$. Jones and Varma (1987) used constant couplings $J_{e/o}(k) \approx J_{e/o}(k_F)$ to obtain for the interaction part of the Hamiltonian (132)

$$\begin{aligned} H_{\text{int}} &= \mathbf{S}^{(e)} \cdot \sum_{\alpha\beta} (J_e c^\dagger_{e\alpha} \boldsymbol{\sigma}_{\alpha\beta} c_{e\beta} + J_o c^\dagger_{o\alpha} \boldsymbol{\sigma}_{\alpha\beta} c_{o\beta}) \\ &+ \mathbf{S}^{(o)} \cdot \sum_{\alpha\beta} (\sqrt{J_e J_o} c^\dagger_{e\alpha} \boldsymbol{\sigma}_{\alpha\beta} c_{o\beta} + \text{H.c}) \\ &+ I_D \mathbf{S}(\mathbf{R}_1) \cdot \mathbf{S}(\mathbf{R})_2, \end{aligned} \tag{134}$$

where $\mathbf{S}^{(e/o)} := \mathbf{S}(\mathbf{R}_1) \pm \mathbf{S}(\mathbf{R}_2)$. The conduction electron Hamiltonian now consists of two decoupled linear chains with even and odd parity symmetry. By neglecting the energy dependence of the couplings a particle-hole symmetric model results. This is the form used by Jones *et al.* (1988) to investigate the phase transition discussed above. The results of retaining the full energy dependence of the couplings, using, for example, the formulation of Sec. II, will be described below. We note here that from the NRG point of view the two-impurity models (133) and (132) present a challenging task because, as in the case of the two-channel Kondo model (61), the "impurity" now couples to *two semi-infinite chains*. Consequently, the Hilbert space grows by a factor of 16 in each NRG step. While this is still manageable with modern computer resources, it is apparent that larger clusters or more complex situations quickly become too expensive to be treated with the NRG method with sufficient accuracy, although the flow of the many-body eigenstates can still be used to identify fixed points and thus qualitatively describe the physics of more complicated systems, like the two-channel two-impurity Kondo model (Ingersent *et al.*, 1992) and the three-impurity Kondo model (Paul and Ingersent, 1996; Ingersent *et al.*, 2005). A reliable calculation of dynamics for more complex quantum impurities coupled to many channels will likely require additional tools like the ones described in Sec. III.A.4, allowing one to work with large $\Lambda \gg 1$ and so maintain low truncation errors.

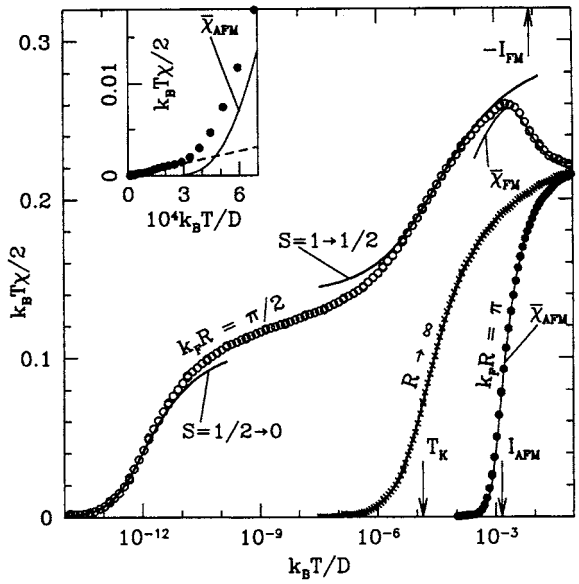


FIG. 19. Effective local moment $\mu^2(T) := T\chi_{\text{imp}}(T)$ for the two-impurity Kondo model (133) for the three regimes described in the text. Arrows indicate the Kondo scale $T_K = 1.4 \times 10^{-4}$, and the RKKY interactions for ferromagnetic ($I_{\text{FM}} = -8 \times 10^{-3}$) and antiferromagnetic cases ($I_{\text{AFM}} = 3 \times 10^{-3}$). From Silva *et al.*, 1996.

The generic two-impurity Anderson model (133), including a charge transfer term, has been studied by Sakai and co-workers (Sakai *et al.*, 1990; Sakai and Shimizu, 1992a, 1992b) using the NRG method. Single-particle and magnetic excitation spectra were calculated, and in the case of particle-hole symmetry, Sakai, Shimizu, and Kaneko (1993) showed that on passing through the transition, a peak in the impurity single-particle spectra sharpened at $I_{\text{eff}} = I_c$ into a cusp and turned into a dip for $I_{\text{eff}} > I_c$. In the generic case, the regime with Kondo screening, $|I_{\text{eff}}| \ll T_K$, and the nonlocal singlet regime, $I_{\text{eff}} \gg T_K$, are connected via a smooth crossover (Sakai *et al.*, 1990; Sakai and Shimizu, 1992a, 1992b; Silva *et al.*, 1996; Campo and Oliveira, 2004).

Results from thermodynamic calculations are shown in Fig. 19 for the squared effective magnetic moment from Silva *et al.* (1996) for the two-impurity Kondo model with $I_D = 0$. In these calculations $I_{\text{eff}} = I_{\text{RKKY}}$ and the energy dependence of $J_{e/o}(k)$ is crucial to generate the intrinsic RKKY exchange interaction $I_{\text{RKKY}}$. Using the result for free electrons in three dimensions (Sakai *et al.*, 1990), an approximate formula for the energy depen-

dence of the coupling constants is (Silva *et al.*, 1996)

$$J_{e/o}(\epsilon) = J_K\left(1 \pm \frac{\sin[k_F R(1+\epsilon)]}{k_F R(1+\epsilon)}\right) \tag{135}$$

with $\epsilon \in [-1,1]$; $k_F$ is the Fermi momentum of the conduction electron states. For the derivation of Eq. (135) a linearized dispersion relation $\epsilon_k \approx D(k-k_F)/k_F$ was assumed and $D=1$ used as the energy scale.

Depending on the value of $k_F R$, different regimes can then be identified (see, for example, Fig. 19). For $k_F R \to \infty$ we have $I_{\mathrm{RKKY}}=0$, single-impurity physics dominates, and no nonlocal magnetic exchange is generated, as expected (Jones and Varma, 1987). For $k_F R=\pi/2$, the RKKY exchange $I_{\mathrm{RKKY}}=I_{\mathrm{FM}}$ is ferromagnetic, with $|I_{\mathrm{RKKY}}|/T_K \gg 1$ and a two-stage screening scenario arises. First, the system locks into an $S=1$ state at high temperatures due to the RKKY interaction. In the intermediate temperature regime this triplet is screened to a doublet via the even channel, which then is further screened to a singlet by the odd channel. Finally, for $k_F R=\pi$, the RKKY exchange $I_{\mathrm{RKKY}}=I_{\mathrm{AFM}}$ is antiferromagnetic with $I_{\mathrm{RKKY}}/T_K \gg 1$ and a nonlocal singlet is formed eventually. Similar results for entropy and specific heat of the two-impurity Kondo model, exhibiting a smooth change of physical properties with changing $I_{\mathrm{RKKY}}$, can be found in Campo and Oliveira (2004).

We note here that, while two-impurity models with energy-independent coupling constants are crude approximations in the context of bulk Kondo impurities and heavy fermions, these can, however, be realized in quantum dots. Correspondingly, they have been proposed to describe various extensions of single quantum dots and studied in this context with the NRG method by several groups (Boese *et al.*, 2002; Hofstetter and Schoeller, 2002; Vojta, Bulla, and Hofstetter, 2002; Borda *et al.*, 2003; Zaránd *et al.*, 2006; Žitko and Bonča, 2006) over the past years. Since modern nanostructure technology permits a rather broad tailoring of such mesoscopic objects, the models discussed typically introduce additional interactions as compared to the conventional two-impurity Anderson model (133) like capacitive couplings (Boese *et al.*, 2002; Hofstetter and Schoeller, 2002; Borda *et al.*, 2003) or direct hopping (Dias da Silva *et al.*, 2006; Žitko and Bonča, 2006). Consequently, these extended models show a much larger variety in intermediate- and low-temperature fixed points than the bare model (133), ranging from the conventional Kondo effect over a two-stage Kondo effect (Jayaprakash *et al.*, 1981; Vojta, Bulla, and Hofstetter, 2002), two-channel physics as an intermediate fixed point (Žitko and Bonča, 2006, 2007), to quantum phase transitions (Vojta, Bulla, and Hofstetter, 2002; Dias da Silva *et al.*, 2006; Zaránd *et al.*, 2006; Zhu and Varma, 2006; Žitko and Bonča, 2006).

### 2. Local criticality

The term local criticality was first used in the context of phase transitions in certain heavy fermion systems, such as $CeCu_{6-x}Au_x$ (Si *et al.*, 1999, 2001; v. Löhneysen *et al.*, 2007). It has been argued that the quantum critical point separating the magnetically ordered and paramagnetic phases at $T=0$ is characterized by critical excitations which are local. This observation raised considerable interest in models which show such locally critical behavior: these are either lattice models studied within certain extensions of DMFT (see also Sec. V.B) or impurity models as discussed in this section. Such impurity models might not be directly connected to the locally critical behavior in heavy fermion systems; nevertheless, the insights gained in studying impurity models might be helpful in constructing theories for lattice systems [for a general discussion of the relation between quantum impurity physics and the physics of lattice systems, see Bulla (2006)].

We focus here on the soft-gap Anderson model, originally proposed by Withoff and Fradkin (1990). The Hamiltonian is the same as the one for the standard single-impurity Anderson model Eq. (2), but the hybridization function is assumed to have a power-law form

$$\Delta(\omega) = \Delta_0 |\omega|^r \quad \text{with } r > -1, \tag{136}$$

either valid over the whole frequency range or restricted to some low-frequency region. The competing mechanisms leading to a quantum phase transition in this model are local moment formation (favored by increasing $U$) and screening of the local moments. For values of the exponent $r>0$, corresponding to a soft gap in $\Delta(\omega)$, there are fewer degrees of freedom available to screen the moment, and a quantum phase transition occurs at some finite value of $\Delta_0$.

This quantum phase transition and the physical properties in the whole parameter regime have been studied with a variety of techniques [for an overview, see Bulla and Vojta (2003); Vojta (2006); Lee *et al.* (2005)]. The NRG method has been particularly helpful in clarifying the physics of the soft-gap Anderson model (and the related Kondo version of the model) as we briefly discuss in the following. The technical details necessary to apply the NRG method to the soft-gap Anderson model have already been introduced in Sec. II [see also Bulla, Pruschke, and Hewson (1997)].

Thermodynamic and static properties of the various phases of the soft-gap Anderson and Kondo models have been presented by Chen and Jayaprakash (1995a); Ingersent (1996); Bulla, Pruschke, and Hewson (1997); and Gonzalez-Buxton and Ingersent (1998). The most comprehensive review of these results is given by Gonzalez-Buxton and Ingersent (1998). This paper covers the discussion of thermodynamic properties and the analysis of the various fixed points also for the underscreened spin-1 Kondo model and the (overscreened) two-channel Kondo model (both with a soft gap in the conduction electron density of states).

The key role of particle-hole symmetry has been identified by Ingersent (1996) and investigated in more detail by Gonzalez-Buxton and Ingersent (1998). As shown, for example, in Fig. 5 of that work, the line of quantum critical points separating the local moment (LM) and strong-coupling (SC) phases is restricted to $0<r<1/2$ in

the particle-hole symmetric case (for $r>1/2$, only the LM phase exists). This is different in the asymmetric case where the transition line extends up to $r\to\infty$. Particle-hole symmetry also influences the physical properties of the various fixed points. The symmetric SC fixed point, for example, shows a residual magnetic moment of $\chi_{\rm imp}=(r/8)k_BT$ and a residual entropy of $S_{\rm imp}=2rk_B\ln 2$, whereas both values are zero in the asymmetric SC fixed point. The appearance of unstable fixed points is particularly complex in the asymmetric case; see, for example, the schematic flow diagrams of Fig. 16 in Gonzalez-Buxton and Ingersent (1998).

The impurity spectral function of the symmetric soft-gap Anderson model was first investigated by Bulla, Pruschke, and Hewson (1997): the spectral function shows a divergence $A(\omega)\propto|\omega|^{-r}$ for both the SC and quantum critical phases, whereas it varies as $A(\omega)\propto|\omega|^r$ in the LM phase (for the behavior in the asymmetric case, see the discussion in Sec. IV.C.3).

In the symmetric SC phase, the product $F(\omega)=c|\omega|^rA(\omega)$ (where the prefactor cancels the divergence in the spectral function) contains a generalized Kondo resonance at the Fermi level with a pinning of $F(\omega=0)$ (for a properly chosen constant $c$) and a width that goes to zero upon approaching the quantum critical point. This feature, together with the scaling properties and the low-energy asymptotics has been discussed by Bulla *et al.* (2000), based on the results both from the NRG method and from the local moment approach [also described earlier by Logan and Glossop (2000)].

Dynamical properties at the quantum critical point are particularly interesting: Ingersent and Si (2002) have shown that the dynamical susceptibility at the critical point exhibits $\omega/T$ scaling with a fractional exponent, similar to the locally critical behavior in the heavy fermion systems mentioned above. This result also implies that the critical fixed point is interacting, in contrast to the stable fixed points (SC and LM) which both can be composed of noninteracting single-particle excitations.

The interacting fixed point of the symmetric soft-gap model has been further analyzed by Lee *et al.* (2005). The general idea of this work can be best explained with Fig. 20, which shows the dependence of the many-particle spectra for the various fixed points on the exponent $r$.

For the limits $r\to 0$ and $r\to 1/2$, the many-particle spectra of the quantum critical point approach those of the LM and SC fixed points, respectively. The deviations and splittings of the spectra at the quantum critical point close to these limits can then be understood from a proper perturbational analysis using suitable marginal operators. Information on these operators can be extracted from epsilon-expansion techniques, as shown by Lee *et al.* (2005).

The case of negative exponents in the hybridization function $\Delta(\omega)\propto|\omega|^r$ with $-1<r<0$, where the soft gap turns into a divergence at the Fermi level, has been analyzed by Vojta and Bulla (2002a) in the context of the Kondo model with both ferromagnetic and antiferromagnetic values of $J$. The behavior of this class of models turns out to be rather complex; see the schematic flow diagrams of Fig. 1 in that work. A remarkable feature here is the appearance of a *stable* intermediate-coupling fixed point with universal properties corresponding to a fractional ground-state spin.

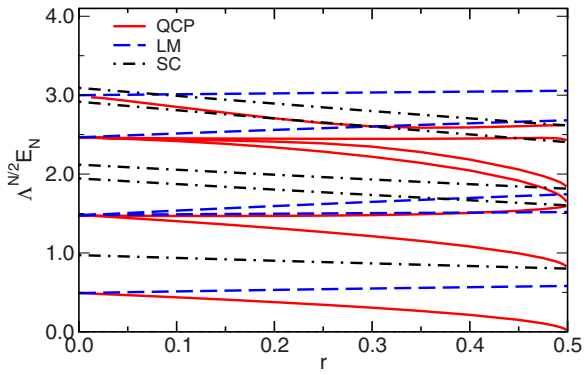


FIG. 20. (Color online) Dependence of the many-particle spectra for three fixed points of the particle-hole symmetric soft-gap Anderson model on the exponent $r$: SC (dot-dashed lines), LM (dashed lines), and the (symmetric) quantum critical point (solid lines). From Lee *et al.*, 2005.

The case of a hard gap in the hybridization function, that is, $\Delta(\omega)=0$ within a certain gap region around the Fermi level, can be viewed as the $r\to\infty$ limit of the soft-gap case, provided the power law is restricted to the gap region $|\omega|\le E_g/2$, with $E_g$ the width of the gap. From a technical point of view, two different strategies have been developed to apply the NRG method to the hard-gap case. Takegahara *et al.* (1992, 1993) considered the case of a small but finite value of $\Delta(\omega)$ in the gap region $\Delta(\omega)=\bar{\Delta}$ for $|\omega|\le E_g/2$, and based their conclusions on the extrapolation $\bar{\Delta}\to 0$. In this approach, the standard NRG method for nonconstant hybridization functions as described in Sec. II can be applied.

If, on the other hand, the value of $\bar{\Delta}$ is set to zero from the outset, the NRG approach has to be modified. As discussed by Chen and Jayaprakash (1998), the logarithmic discretization of a $\Delta(\omega)$ with a hard gap results in a discretized model which maps onto a chain with a *finite* number of sites $M$, with $E_g$ of the order of $\Lambda^{-M}$. The iterative diagonalization then has to be terminated at site $M$. Thermodynamic properties at temperatures $T<E_g$ can nevertheless be computed using the Hamiltonian of the final iteration [see Chen and Jayaprakash (1998) where a variety of correlation functions have been calculated for both the Kondo and the Anderson model with a hard gap].

Certain features of the soft-gap case with finite $r$ are also visible in the fully gapped case. As expected from the discussion above, there is no transition in the particle-hole symmetric case, but a transition exists as soon as one is moving away from particle-hole symmetry (Takegahara *et al.*, 1992; Ingersent, 1996; Chen and

Jayaprakash, 1998). This transition turns out to be of first order.

### 3. Kondo effect in superconductors

We now consider magnetic impurities in superconducting hosts [for a general review on impurity effects in conventional and unconventional superconductors, see Balatsky *et al.* (2006)]. In this case, the screening of the magnetic moments competes with Cooper pair formation of the conduction electrons. We therefore expect a quantum phase transition from a screened phase to a local moment phase upon increasing the value of the superconducting gap $\Delta_{sc}$ similar to the phase transitions in the soft-gap (and hard-gap) impurity models discussed in Sec. IV.C.2. In fact, a relation between impurity models in superconductors and those in metallic hosts with a soft or hard gap can be established as discussed below.

The first applications of the NRG method to magnetic impurities in superconductors focused on the *s*-wave case (Satori *et al.*, 1992; Sakai, Shimizu, *et al.*, 1993), with the standard Kondo Hamiltonian Eq. (117) supplemented by the BCS pairing interaction

$$-\Delta_{sc}\sum_k (c^\dagger_{k\uparrow}c^\dagger_{-k\downarrow} + c_{-k\downarrow}c_{k\uparrow}).$$

Several strategies have been developed to transform the Hamiltonian including the BCS term onto a semi-infinite chain which can then be diagonalized iteratively in the usual way. Satori *et al.* (1992) performed a sequence of transformations, including a Bogoliubov and a particular particle-hole transformation, to map the original model onto a Hamiltonian that conserves particle number (this is somewhat easier for the numerical implementation though not absolutely necessary). The approach in Sakai, Shimizu, *et al.* (1993) leads to the same Hamiltonian; the difference here is that the Bogoliubov transformation is performed before the logarithmic discretization. In both cases, the semi-infinite chain contains a staggered potential of the form

$$-\Delta_{sc}\sum_{n=0}^{\infty} (-1)^n(c^\dagger_{n\uparrow}c_{n\uparrow} + c^\dagger_{n\downarrow}c_{n\downarrow}).$$

This term does not fall off exponentially like the other terms in the chain Hamiltonian so that the NRG iterations should be terminated a few steps after the characteristic scale $\omega_N$ of the chain Hamiltonian $H_N$ has reached the superconducting gap $\Delta_{sc}$. This procedure still allows one to access the properties of the localized excited state within the energy gap, whose position and weight can now be determined in the full parameter space [in contrast to previous investigations; see the references in Satori *et al.* (1992)]. Figure 21 shows the position and weight of the localized excited state as a function of $T_K/\Delta_{sc}$ ($T_K$ is determined from the corresponding Kondo model with $\Delta_{sc}=0$). The position changes its sign when $T_K$ is of the order of $\Delta_{sc}$ (the precise value depends on the model), corresponding to a change of the ground state from a doublet for small $T_K/\Delta_{sc}$ to a singlet for large $T_K/\Delta_{sc}$. This quantum phase transition can be characterized as a level crossing transition [see Fig. 5 in Satori *et al.* (1992)] and is not connected to quantum critical behavior.

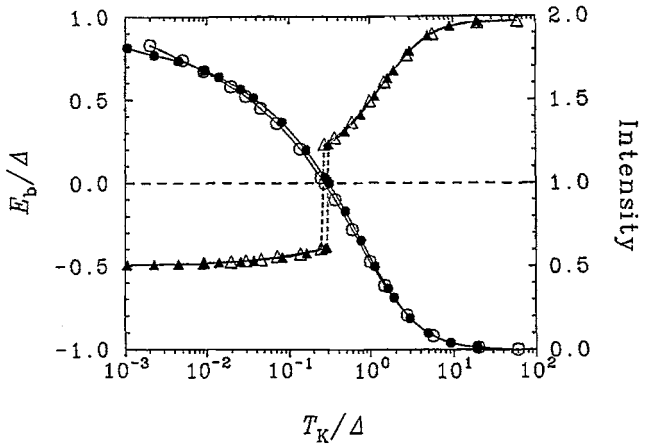


FIG. 21. Position $E_b$ and weight (intensity) of the localized excited state as a function of $T_K/\Delta_{sc}$ for the Kondo model in an *s*-wave superconductor. At $T_K/\Delta_{sc}\approx 0.2$, the position changes its sign and the weight jumps by a factor of 2; see also Fig. 2(A) in Sakai, Shimizu, *et al.* (1993). In this work, the notation $\Delta$ is used for the superconducting gap $\Delta_{sc}$.

These studies of impurities in *s*-wave superconductors were later extended to more complex impurity models. Yoshioka and Ohashi (1998) investigated the case of an anisotropic interaction between the impurity and the conduction electron spin, with basically the same NRG approach as in Sakai, Shimizu, *et al.* (1993). The phase diagram of this model turns out to be much more complex than the one for the isotropic case. For example, two localized excited states with different energies appear in certain regions of the parameter space.

Yoshioka and Ohashi (2000) considered the Anderson version of the impurity model with coupling to an *s*-wave superconductor. From a technical point of view, this case is different from the corresponding Kondo model, since the sequence of transformations used in, for example, Sakai, Shimizu, *et al.* (1993) now produce an extra impurity term of the form $\delta(f^\dagger_\uparrow f^\dagger_\downarrow + \text{H.c.})$, so that the whole Hamiltonian no longer conserves charge (note that the parameter $\delta$ is zero for the particle-hole symmetric case). The results for the Kondo regime of this model are, as expected, the same as those obtained previously, but the approach of Yoshioka and Ohashi (2000) also allows one to study other parameter ranges of the model, such as the mixed valent regime.

It is important to note here that the final Hamiltonian used by Satori *et al.* (1992) and Sakai, Shimizu, *et al.* (1993) for the NRG iteration is the same as the one for an impurity in a nonsuperconducting host with a gapped density of states (which corresponds to the quasiparticle density of states of the superconductor). In addition, the sequence of transformations also generates a potential scattering term. In light of the results for the hard-gap impurity models (Sec. IV.C.2), this potential scattering

term is essential to observe the quantum phase transition from a screened to an unscreened phase.

The question now arises whether the quasiparticle density of states can be used as the sole bath characteristic (possibly supplemented by a potential scattering term) in more general situations, such as impurities in unconventional superconductors. Before we address this issue, we look at what happens when a similar sequence of transformations as in the *s*-wave case is applied to impurity models in *p*- or *d*-wave superconductors.

Matsumoto and Koga (2001, 2002) considered the Kondo model with a coupling of the impurity spin to superconductors with $p_x+ip_y$ and $d_{x^2-y^2}+id_{xy}$ symmetry [with extensions to spin-polarized superconducting states investigated by Koga and Matsumoto (2002a) and to $S=1$ impurities by Koga and Matsumoto (2002b)]. The quasiparticle density of states in these cases also shows a full gap, as for *s*-wave superconductors, but the sequence of transformations now results in a model with a coupling of the impurity to two angular momenta of the conduction electrons. NRG calculations for this two-channel model give a ground state which is always a spin doublet for arbitrary values of $T_K/\Delta_{sc}$, in contrast to the *s*-wave case, and no level crossing is observed. This is supported by calculations of the impurity susceptibility which show that the effective magnetic moment is always finite, although strongly reduced with increasing $T_K/\Delta_{sc}$ (Matsumoto and Koga, 2002). These authors argued that the orbital dynamics of the Cooper pairs is responsible for the ground-state spin.

This interpretation has been questioned by Fritz and Vojta (2005), where it was shown that, indeed, the local quasiparticle density of states of the superconductor is the only necessary ingredient in a number of cases, in particular for unconventional superconductors. Applied to the model studied in Matsumoto and Koga (2001), this means that the results of the NRG calculations for the effective two-channel model can also be understood from a single-band calculation, where screening is absent for a hard-gap density of states and particle-hole symmetry.

The results of Fritz and Vojta (2005) also have important consequences for the study of impurities in unconventional superconductors with $d_{x^2-y^2}$ symmetry. In this case, the mappings which have been used for the models discussed above result in an impurity model with coupling to infinitely many bands to which the NRG method clearly cannot be applied. For certain geometries, however, it is sufficient to consider only the quasiparticle density of states which, for a pointlike impurity, show a soft gap with exponent $r=1$.

This simplification was used earlier by Vojta and Bulla (2002b) (at that time it was argued to be a reasonable approximation). The results of this work are therefore valid for both the soft-gap Kondo model and impurities in *d*-wave superconductors. Vojta and Bulla (2002b) motivated their investigations with experimental results for nonmagnetic impurities in cuprate superconductors, which have been seen to generate magnetic moments. As discussed in this work, an effective model for this problem then takes the form of a Kondo model in a *d*-wave superconductor. Connections to experimental results can indeed be made within this framework. For example, the *T* matrix $T(\omega)$ displays a very narrow peak at finite frequencies with the peak energy corresponding to the energy scale which vanishes at the quantum phase transition from a screened to an unscreened moment. A very similar peak has been observed in STM experiments.

This work was later extended in Vojta, Zitzler, *et al.* (2002), where the effects of local and global magnetic fields have been investigated. For the case of a local field $h_{loc}$, the quantum phase transition for zero field persists for $h_{loc}\neq 0$, but for a global field, the quantum phase transition turns into a sharp crossover since the global field induces a finite spectral weight at the Fermi level.

The investigations described so far are mainly applicable to impurities in the bulk or on the surface of a superconducting host. A different geometry is realized in quantum dot systems (see Sec. IV.A.3). For superconducting leads, such a setup introduces a new control parameter to the problem, that is, the phase difference $\Phi=\Phi_L-\Phi_R$ between the phases of the two superconducting leads. The resulting Josephson current, in particular the transition from 0- to $\pi$-junction behavior, has been studied by Choi, Lee, *et al.* (2004) and Oguri *et al.* (2004).

Choi, Lee, *et al.* (2004) investigated various static and dynamic properties for this geometry with identical *s*-wave superconductors as the two leads. For zero phase difference, $\Phi=0$, the local pairing correlation shows a sign change at $T_K/\Delta_{sc}\approx 0.42$. Physically, this is connected to the same quantum phase transition as described above since for $\Phi=0$ and identical leads the model can be mapped onto the same model as discussed by Satori *et al.* (1992). For finite phase difference (or for nonidentical leads) the system remains a two-channel problem and the NRG analysis is more complicated. Nevertheless, detailed information on ground state properties such as the single-particle excitation spectrum has been obtained by Choi, Lee, *et al.* (2004).

Oguri *et al.* (2004) studied the Hamiltonian of an Anderson impurity coupling to two superconducting leads simplified by the limit $|\Delta_{sc,L}|\gg|\Delta_{sc,R}|$ in which the model can be mapped exactly onto a single-channel one with an extra superconducting gap on the impurity. Results for this limit show that the phase difference changes both the energy and the wave function of the bound state. In particular, the phase difference appears to work against the screening of the local moment.

### D. Orbital effects

#### 1. Multiorbital Anderson model

The physics of the Kondo effect requires the existence of local magnetic moments, as realized, for example, in systems with open *d* or *f* shells, such as transition metal or rare-earth impurities in nonmagnetic host metals. For such systems, the local Coulomb correlations and

Hund's exchange determine the electronic structure of the impurity and they usually give rise to finite spin and orbital magnetic moments. Thus a realistic description of such impurities in solids requires taking both spin and orbital magnetic moments into account. The same is true for the compounds of transition metal, rare-earth, and actinide elements, where the interplay of orbital and spin degrees of freedom gives rise to rich phase diagrams (Imada *et al.*, 1998). Among the methods to theoretically study the properties of these materials, the dynamical mean-field theory (see Sec. V) has become a standard approach. Since in this approach one ends up with an effective quantum impurity problem which retains the full local orbital and spin structure of the original lattice system, the development of a reliable method to solve quantum impurity models with orbital and spin degrees of freedom is of crucial importance.

In this section we, therefore, discuss the application of the NRG method to situations where orbital and spin degrees of freedom are both present. Some orbital effects in quantum dots have been introduced in Sec. IV.A.3 and will be discussed below. The appropriate model is again a suitable extension of the single-impurity Anderson model (2) and is given by

$$H = \sum_k \sum_{mm'\sigma} \epsilon_{k\sigma}^{mm'} c_{km\sigma}^\dagger c_{km'\sigma} + \sum_{m\sigma} \varepsilon_{m\sigma} n_{m\sigma}^f + \frac{U}{2} \sum_{m\sigma} n_{m\sigma}^f n_{m\bar{\sigma}}^f + \frac{2U' - J}{4} \sum_{m\neq m'} \sum_{\sigma\sigma'} n_{im\sigma}^f n_{im'\sigma'}^f - J \sum_{m\neq m'} \vec{S}_m^f \cdot \vec{S}_{m'}^f - \frac{J}{2} \sum_{m\neq m'} \sum_{\sigma} f_{m\sigma}^\dagger f_{m\bar{\sigma}}^\dagger f_{m'\bar{\sigma}} f_{m'\sigma} + \frac{1}{\sqrt{N}} \sum_k \sum_{mm'\sigma} (V_{k\sigma}^{mm'} c_{km\sigma}^\dagger f_{m'\sigma} + \text{H.c.}), \quad (137)$$

where $m$ labels the orbital degrees of freedom and $n_{m\sigma}^f = f_{m\sigma}^\dagger f_{m\sigma}$, with $\vec{S}_m^f = \frac{1}{2}\Sigma_{\alpha\beta} f_{m\alpha}^\dagger \vec{\sigma}_{\alpha\beta} f_{m\beta}$. In addition to the intraorbital Coulomb term $U$ also occurring in Eq. (2), the following interaction terms are present now: an interorbital Coulomb repulsion $U'$ and an exchange term $J$. We have split the exchange term in accordance with standard notation (Imada *et al.*, 1998) into a Heisenberg-like spin exchange term (Hund's coupling) and an orbital exchange term. To account for the proper combination of operators in the general exchange contribution, an additional part proportional to $J$ appears in the interorbital Coulomb term. For free atoms, rotational invariance usually imposes $U' = U - 2J$ as a constraint for the different Coulomb parameters (Imada *et al.*, 1998). Further modifications to the model (137) can be made to take into account, for example, spin-orbit and crystal-field effects.

The mapping of Eq. (137) onto a linear chain model [see Eq. (26) of Sec. II], clearly leads to $m$ semi-infinite conduction chains coupled to the local Hamiltonian, which in turn means that at each step of the iterative diagonalization, the Hilbert space increases by a factor $4^m$. For large $m$, this exponential increase in the number of states makes the NRG truncation scheme useless, because the number of states one can keep is much too small to allow for a reasonable accuracy. Thus calculations for the model (137) involving a full $d$ shell ($m=5$), or even a full $f$ shell ($m=7$), and taking into account all interactions, seem to be impossible.

In practice, however, one is typically not interested in rotationally invariant situations, as described by Eq. (137), but in situations where the impurity is embedded in the crystalline environment of a solid. The reduced point-group symmetry due to the crystalline electric field then leads to a splitting of the orbital degeneracy. The energy associated with this crystal-field splitting can be much larger than the temperatures one is interested in experiments, for example, in 3$d$ transition metals. Furthermore, the local Coulomb interaction can lead to a localization of electrons in the lower crystal-field multiplets as happens, for example, in the case of manganese in a cubic environment (Imada *et al.*, 1998). In this case, these states form a localized spin according to Hund's rules. For manganese, for example, this results in a high-spin state ($S=3/2$) of the threefold-degenerate $t_{2g}$ orbitals, which couples ferromagnetically to the twofold-degenerate $e_g$ electrons. Thus the actual number of relevant orbitals, and hence the number of semi-infinite chains coupling to the local Hamiltonian, may be considerably reduced. Similar effects can be observed in the higher rare-earth elements, for example, in gadolinium.

If the local point-group symmetry is reduced sufficiently, one may, in fact, be left with a localized spin $S$ coupled to a single spin-degenerate, correlated orbital hybridizing with conduction states. This Kondo-Anderson model is given by Eq. (2) supplemented with the ferromagnetic exchange term $-J_H \vec{S}\cdot\vec{s}_d$, with $\vec{s}_d$ the spin density of the correlated level in the Anderson model. Such a Kondo-Anderson model was studied by Sakai *et al.* (1996) and Peters and Pruschke (2006) and shown to exhibit different types of screening, ranging from conventional Kondo screening to two-stage screening and local singlet formation or the two-channel Kondo effect.

### 2. NRG calculations: An overview

A first serious attempt to study effects of true orbital degeneracy with the NRG method can be found in Sakai *et al.* (1989). However, these authors did not study the full Hamiltonian (137), but a SU($N$) version of it, using values of $N$ ranging from 2 [i.e., the standard single-impurity Anderson model (2)] to 5, representative for rare-earth ions like samarium or thulium in solids under the influence of a crystalline field (Shimizu *et al.*, 1990; Allub and Aligia, 1995). Since the SU($N$) model has a large degeneracy of the individual levels, it allows for a considerable size reduction of the individual Hilbert spaces in the diagonalization. This enabled the authors to use the NRG method to calculate physical properties, including dynamical quantities, and to study, for example, the development of the Kondo temperature or the behavior of the Abrikosov-Suhl resonance as a func-

tion of degeneracy (Sakai *et al.*, 1989; Shimizu *et al.*, 1990). Similar investigations for the model (137) with fixed orbital degeneracy $m=2$ in the presence of a magnetic field were by Zhuravlev *et al.* (2004), a comparison with STM experiments for Cr(001) surface states by Kolesnychenko *et al.* (2005), and a detailed study of the dependence of the low-energy properties of the multiorbital Anderson model for $m=2$ with $J>0$ by Pruschke and Bulla (2005). Furthermore, from the fixed-point level structure, interesting information about quantities like residual interactions in the heavy Fermi-liquid state can be extracted (Hattori *et al.*, 2005). In particular for an $f^2$ ground state—as possibly realized in uranium compounds—a subtle enhancement of interorbital interactions can be observed (Hattori *et al.*, 2005), which can lead to superconducting correlations in a triplet channel when used as the effective interaction in a model for heavy fermion superconductivity.

While these studies deal with the conventional Kondo effect in multiorbital models, it was noted (Cox and Zawadowski, 1998) that for higher rare-earth and actinide elements the orbital structure in connection with spin-orbit coupling and crystal-field effects can result in an orbital multiplet structure that leads to the two-channel Kondo effect (see Sec. IV.B). Multiorbital models of that type were studied by Sakai *et al.* (1996); Shimizu *et al.* (1998); Shimizu, Hewson, and Sakai (1999); Shimizu, Sakai, and Suzuki (1999); Koga (2000); and Hattori and Miyake (2005), covering a wide range of aspects possibly realized in actinide heavy fermion systems. The authors could identify parameter regimes where non-Fermi-liquid properties related to the two-channel Kondo effect can be observed and could, in addition, identify relevant symmetry breakings like crystal-field splittings or external fields that eventually lead to conventional Kondo physics below a temperature scale connected to the energy scale of the symmetry breaking.

As mentioned in the introductory remarks of this section, the crystal-field splitting is usually much larger than the relevant low-energy scales. However, this does not need to be true in general. Besides uranium-based compounds (Kusunose, 2005), a possible example where the crystal-field splitting can actually be of the order of the Kondo scale is $Ce_{1-x}La_xNi_9Ge_4$ (Scheidt *et al.*, 2006). For higher temperatures, the ground state seems to be a quadruplet, i.e., it can be described by a multiorbital Anderson model with $m=2$. The states building this quadruplet are obtained from spin-orbit coupled $f$ states, which results in different $g$ factors for its members. Interestingly, these different $g$ factors in connection with the small crystal-field splitting can lead to behavior where specific heat and susceptibility seem to have different low-energy scales (Scheidt *et al.*, 2006). However, this discrepancy can be resolved by observing that the difference in $g$ factors leads to a "protracted" screening behavior for the specific heat in NRG calculations, while the system as a whole has only one, but strongly reduced Kondo temperature. In addition, NRG results for the low-energy spin dynamics show an anomalous energy dependence, which is related to the difference in the $g$ factors entering the local susceptibility (Anders and Pruschke, 2006).

Conventionally, the Hund's exchange $J$ appearing in Eq. (137) is positive, i.e., mediating a ferromagnetic interaction leading to Hund's first rule. However, there may be circumstances, for example, coupling to vibrational modes, Jahn-Teller distortions, or crystal-field-induced anisotropies (De Leo and Fabrizio, 2004), which can lead to an effective $J<0$, i.e., *antiferromagnetic* exchange. In this case we encounter a situation similar to the multi-impurity problem (see Sec. IV.C.1), where the exchange was generated by the RKKY effect. Under special conditions, an antiferromagnetic exchange then could lead to a quantum phase transition between Kondo screening and nonlocal singlet formation. Consequently, one may expect a similar transition for the multiorbital model, too, when one varies $J$ from the ferromagnetic to the antiferromagnetic regime. Such a model was studied by Fabrizio *et al.* (2003) and, with an additional single-ion anisotropy, by De Leo and Fabrizio (2004) for two orbitals, i.e., $m=2$. The model indeed shows the anticipated quantum phase transition, which in this case is driven by the competition between the local antiferromagnetic exchange coupling and the hybridization to band states. Furthermore, one can study the development of the spectral function across this transition (De Leo and Fabrizio, 2004). One finds that the impurity spectral function on the Kondo screened side of this transition shows a narrow Kondo peak on top of a broader resonance. As has also been observed by Pruschke and Bulla (2005) and Peters and Pruschke (2006) this broad resonance is related to the exchange splitting $J$. The narrow peak transforms into a pseudogap on the unscreened side of the transition.

De Leo and Fabrizio (2005) have demonstrated that NRG calculations are possible even for $m=3$, using the symmetries of the model to reduce the size of the Hilbert space blocks. They studied a realistic model for a doped $C_{60}$ molecule, taking into account the orbitally threefold-degenerate $t_{2u}$ lowest unoccupied molecular orbitals. Again, coupling to vibrational modes can lead to Hund's coupling with negative sign. In this regime, one observes non-Fermi-liquid behavior for half filling $n=3$, associated with a three-channel, $S=1$ overscreened Kondo model. Interestingly, the critical susceptibilities associated with this non-Fermi-liquid appear to be a pairing in the spin and orbital singlet channels (De Leo and Fabrizio, 2005). Using conformal field theory, these authors deduced the residual entropy

$$S(T=0)=\frac{1}{2}\ln\left[\frac{\sqrt{5}+1}{\sqrt{5}-1}\right],$$

and also corresponding fractional values for the local spectral function $\rho_f(0)$ at the Fermi energy, which leads to nonunitary values in the conductance and a noninteger power law for $\rho_f(\omega)-\rho_f(0)$. Away from half filling, a quantum phase transition occurs between Kondo screening and local singlet formation as a function of

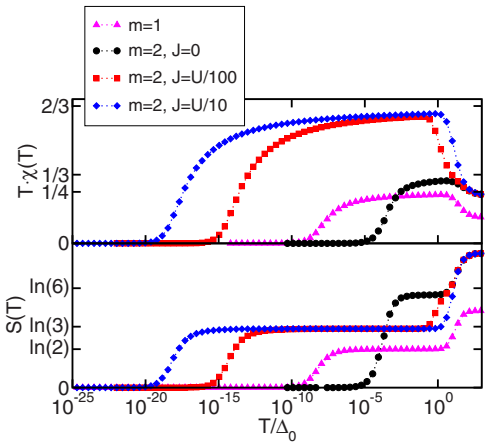


FIG. 22. (Color online) Effective local moment $T\chi(T)$ (upper panel) and entropy (lower panel) for a two-orbital impurity Anderson model. Model parameters are $U/\Delta_0=16\pi$ at particle-hole symmetry. For comparison the results for one orbital are included (triangles).

filling (De Leo and Fabrizio, 2005). Multiorbital models also arise in the context of quantum dots as described in Secs. IV.A.3 and IV.C.1.

### 3. Selected results on low-energy properties

In the following we present some selected results for the properties of the multiorbital Anderson model (137) with orbital degeneracy $m=2$.

*Effect of Hund's coupling.* As a first example we discuss the influence of Hund's exchange $J$ on the low-energy properties of the model Eq. (137). We consider only $J\geq 0$, i.e., the usual atomic ferromagnetic exchange, and in addition use the constraint $U'=U-2J$. For the conduction electrons we assume a band with a flat density of states $\rho_c^{(0)}(\epsilon)=N_F\Theta(D-|\epsilon|)$ and use $\Delta_0=\pi V^2 N_F$ as the energy scale. Results for thermodynamic quantities are shown in Fig. 22.

The calculations in Fig. 22 are for $U/\Delta_0=16\pi$ and particle-hole symmetry. NRG parameters are $\Lambda=5$ and 2500 retained states per iteration. The triangles are results from a calculation with $m=1$ for the same parameters. For $J=0$ (circles) we find the behavior expected for an SU(4) symmetry, i.e., an energy scale $T_K^m$ that is related to the Kondo scale at $m=1$, $T_K^{m=1}$, by $T_K^m=(T_K^1)^{1/m}$. However, even a small Hund coupling $J=U/100$ leads to a dramatic reduction of $T_K$, which increases with increasing $J$. We note here that for $J>0$ the effect of the orbital exchange term in Eq. (137) is negligible, i.e., the results are indistinguishable if one does the calculation with and without this contribution. Very often, the orbital exchange term is neglected in theoretical studies of transition metal compounds (Imada *et al.*, 1998), an approximation which is supported by the above result.

*Crystal-field effects.* Experiments showing unusual specific heat, magnetic susceptibility, and resistivity data for $Ce_{1-x}La_xNi_9Ge_4$ have drawn attention because this material has the "largest ever recorded value of the electronic specific heat at low temperature" (Killer *et al.*, 2004) of $\gamma(T)=\Delta C/T\approx 5\ \mathrm{J\ K^{-2}\ mol^{-1}}$. While the $\gamma$ coefficient continues to rise at the lowest experimentally accessible temperature, the magnetic susceptibility tends to saturate at low temperatures.

One possible scenario (Anders and Pruschke, 2006; Scheidt *et al.*, 2006) to account for the behavior of $Ce_{1-x}La_xNi_9Ge_4$ is a competition of Kondo and crystal-field effects which leads to a crossover regime connecting incoherent spin scattering at high temperatures and a conventional strong-coupling Fermi-liquid regime at temperatures much lower than the experimentally accessible 30 mK. The Hund's rule ground state of $Ce^{3+}$ with $j=5/2$ is split in a tetragonal symmetry (Killer *et al.*, 2004) into three Kramers doublets. If the crystalline electric field (CEF) parameters are close to those of cubic symmetry, the two low-lying doublets $\Gamma_7^{(1)}$ and $\Gamma_7^{(2)}$, originating from the splitting of the lowest $\Gamma_8$ quartet, are well-separated from the higher-lying $\Gamma_6$ doublet. Ignoring this $\Gamma_6$ doublet, we discuss two extreme limits. In a cubic environment, the CEF splitting vanishes and the low-temperature physics is determined by an SU(4) Anderson model. In a strongly tetragonally distorted crystal, on the other hand, the crystal-field splitting of the quartets is expected to be large. In this case, the low-temperature properties are determined by an SU(2) Anderson model. If, however, the material parameters lie in the crossover regime where the effective low-temperature scale $T^*$ is of the order of the crystal-field splitting $\delta_{\mathrm{CEF}}=E_{\Gamma_7^{(2)}}-E_{\Gamma_7^{(1)}}$, then the excited doublet will have significant weight in the ground state so that the total magnetic response differs from a simple SU(4) Anderson model.

Such a situation can be captured by an SU(4) Anderson model with infinite $U$ whose Hamiltonian is given by (Scheidt *et al.*, 2006)

$$H=\sum_{k\alpha}\epsilon_{k\alpha\sigma}c_{k\alpha\sigma}^\dagger c_{k\alpha\sigma}+\sum_{\alpha\sigma}E_{\alpha\sigma}|\alpha\sigma\rangle\langle\alpha\sigma| + \sum_{k\alpha\sigma}V_{\alpha\sigma}(|\alpha\sigma\rangle\langle 0|c_{k\alpha\sigma}+c_{k\alpha\sigma}^\dagger|0\rangle\langle\alpha\sigma|), \tag{138}$$

where $|\alpha\sigma\rangle$ represents the state $\Gamma_7^{(\alpha)}$ with spin $\sigma$ and energy $E_{\alpha\sigma}$ on the Ce $4f$ shell, and $c_{k\alpha\sigma}$ annihilates a corresponding conduction electron state with energy $\epsilon_{k\alpha\sigma}$. Note that locally only fluctuations between an empty and a singly occupied Ce $4f$ shell are allowed.

While the entropy and specific heat for the model (138) can be calculated in the usual way, the Ce contribution to the susceptibility requires some more thought because the spin-orbit-coupled states $\Gamma_7^{(\alpha)}$ have different $g$ factors, which we label by $g_\alpha$. Thus the total susceptibility is given by (Scheidt *et al.*, 2006)

$$\chi_{\mathrm{imp}}=\mu_B^2\sum_\alpha g_\alpha^2\chi_{\mathrm{imp}}^{(\alpha)}. \tag{139}$$

While the $g$ factors are, in principle, determined by the CEF states of the multiplets, we view them as adjustable

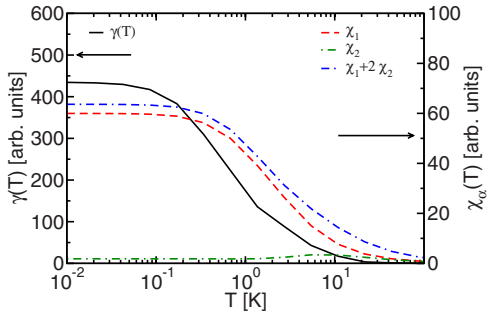


FIG. 23. (Color online) Comparison between $\gamma(T)=C(T)/T$ versus $T$ and the susceptibility contributions of the two doublets versus $T$ for $E_{\Gamma_7^{(1)}}/\Delta_0=-8.5$, $\delta_{\mathrm{CEF}}/\Delta_0=0.015$, and $g_2^2/g_1^2=2$. The contribution of the lower doublet $\chi_1$ is much larger than the one of the upper doublet $\chi_2$. NRG parameters are $\Lambda=4$ and 1500 states kept in each step.

parameters and fix them together with $E_{\Gamma_7^{(\alpha)}}$ by comparison with experiment (Scheidt *et al.*, 2006).

Comparison between the temperature dependence of $\gamma(T)$ and $\chi(T)$ is shown in Fig. 23, assuming a ratio of $g_2^2/g_1^2=2$ for a good fit to the experimental data (Scheidt *et al.*, 2006). The ground-state doublet dominates the magnetic response at low temperature and tends to saturate at temperatures higher than the $\gamma$ coefficient, consistent with the experiments (Killer *et al.*, 2004). We find this behavior only for CEF splittings $\delta_{\mathrm{CEF}}\approx T^*(\delta_{\mathrm{CEF}})$, while for much larger or much smaller values $\chi(T)$ and $\gamma(T)$ saturate simultaneously.

### E. Bosonic degrees of freedom and dissipation

In the models discussed so far, the bath consists of noninteracting fermionic degrees of freedom while the impurity is represented by either a fermion or a spin. This section deals with quantum impurity systems involving *bosonic* degrees of freedom. We distinguish between models in which only a small number of bosonic degrees of freedom couples to the impurity and models where the impurity couples to a bosonic bath (corresponding to an infinite number of bosonic degrees of freedom). As we show below, the first case can be dealt with in the usual scheme, provided the subsystem consisting of impurity and bosons can be treated as a large impurity which is then coupled to the fermions. The second class, however, requires a different setup for the NRG procedure.

We first consider the so-called Anderson-Holstein model (Hewson and Meyer, 2002) in which the impurity is linearly coupled to a single bosonic degree of freedom (typically a phonon mode):

$$H=H_{\mathrm{SIAM}}+\lambda(b^\dagger+b)\sum_\sigma f_\sigma^\dagger f_\sigma+\omega_0 b^\dagger b, \tag{140}$$

with $H_{\mathrm{SIAM}}$ the Hamiltonian of the single-impurity Anderson model as in Eq. (2). The coupling to bosonic operators ($b^\dagger$ and $b$) does not influence the mapping of the conduction electron part of the Hamiltonian to a semi-infinite chain. This means that bosons enter the iterative diagonalization only in the very first step in which the coupled impurity-boson subsystem has to be diagonalized. The fact that only a limited number of bosonic states $n_b$ can be taken into account in this diagonalization imposes some restrictions on the parameters $\lambda$ (the electron-phonon coupling strength) and $\omega_0$ (the frequency of the phonon mode). As discussed by Hewson and Meyer (2002), it should be sufficient to include a number of $n_b\approx 4\lambda^2/\omega_0^2$ bosonic states for the initial diagonalization. With an upper limit of $n_b\approx 1000$ this means that the limit $\omega_0\to 0$ (with fixed $\lambda$) cannot be treated within this setup.

Apart from this minor restriction, Hewson and Meyer (2002) showed that the NRG method (which is nonperturbative in both $\lambda$ and $U$) works well for this type of impurity model. In particular, both electron and phonon spectral functions as well as dynamic charge and spin susceptibilities can be calculated with a high accuracy.

As discussed by Jeon *et al.* (2003) and Choi, Park, and Jeon (2003), the calculation of the phonon spectral function needs some extra care and the authors introduced an improved method [as compared to Hewson and Meyer (2002)]. The proper calculation of the phonon spectral function is important to discuss the softening of the phonon mode; see also the discussion in Sec. V.C in the context of lattice models with coupling to phonons.

The low-energy features of the model Eq. (140) can be partly explained by an effective single-impurity Anderson model in which the coupling to phonons is included in an effective interaction $U_{\mathrm{eff}}$. An explicit form of this interaction can only be given in the limit $\omega_0\to\infty$: $U_{\mathrm{eff}}=U-2\lambda^2/\omega_0$. Interestingly, Hewson *et al.* (2004) have shown that an effective quasiparticle interaction can be defined for any value of $\omega_0$. This can be accomplished with the renormalized perturbation theory by fitting the lowest-lying energy levels obtained in the NRG calculations to those from a renormalized Anderson model.

These investigations represent a starting point for various applications of the NRG method to coupled electron-phonon systems. For investigation of transport properties of single-molecule devices, for which the coupling to local phonons is a natural ingredient, similar models to Eq. (140) have been investigated by Cornaglia *et al.* (2004) and Cornaglia and Grempel (2005a). Not only the coupling to the electron density as in Eq. (140), but also the change of the hybridization between molecule and leads due to phonons, has been shown to be important for the conductance properties (Cornaglia *et al.*, 2005).

Different physical phenomena can be expected in multiorbital systems when the impurity degrees of freedom couple to Jahn-Teller phonons. Such a model has been investigated by Hotta (2006) and it was argued that within this model a new mechanism of Kondo phenomena with nonmagnetic origin can be established.

Two different strategies have been developed to study impurity models with a coupling to a bosonic bath, i.e., a bosonic environment with a continuous spectral density

$J(\omega)$. We discuss these strategies in the context of the spin-boson model

$$H = -\frac{\Delta}{2}\sigma_x + \frac{\epsilon}{2}\sigma_z + \sum_i \omega_i a_i^\dagger a_i + \frac{\sigma_z}{2}\sum_i \lambda_i (a_i + a_i^\dagger). \tag{141}$$

This model naturally arises in the description of quantum dissipative systems (Leggett *et al.*, 1987). The dynamics of the two-state system, represented by the Pauli matrices $\sigma_{x,z}$, is governed by the competition between the tunneling term $\Delta$ and the friction term $\lambda_i(a_i+a_i^\dagger)$. The $a_i$ constitute a bath of harmonic oscillators responsible for the damping, characterized by the bath spectral function

$$J(\omega) = \pi \sum_i \lambda_i^2 \delta(\omega - \omega_i). \tag{142}$$

A standard parametrization of this spectral density is

$$J(\omega) = 2\pi\alpha\omega_c^{1-s}\omega^s, \quad 0 < \omega < \omega_c, \quad s > -1. \tag{143}$$

The case $s=1$, known as Ohmic dissipation, allows a mapping of the spin-boson model onto the anisotropic Kondo model [for the definition of the Hamiltonian and the relation of its parameters to those of the spin-boson model, see Costi and Kieffer (1996)]. The first strategy is then to apply the NRG method to the anisotropic Kondo model and to treat the fermionic conduction band in the usual way. Though restricted to the Ohmic case, such calculations have been shown to give accurate results for dynamic and thermodynamic quantities of the corresponding spin-boson and related models, as discussed in the following.

The focus of Costi and Kieffer (1996) has been the equilibrium dynamics of the spin-boson model, in particular the spin-spin correlation function $\chi(\omega) = \langle\langle \sigma_z; \sigma_z \rangle\rangle$ at temperature $T=0$. An interesting finding of this study is that the spin relaxation function $\chi''(\omega)/\omega$ exhibits a crossover from inelastic to quasielastic behavior as $\alpha$ exceeds the value $1/3$ signaling the onset to incoherent dynamics which occurs at $\alpha \geq 1/2$ (Leggett *et al.*, 1987). The accuracy of this approach has been shown via comparison to exactly solvable limiting cases, such as the Toulouse point $\alpha=0.5$, and via the generalized Shiba relation. The issue of scaling and universality, concepts which are quite naturally connected to renormalization group treatments of the Kondo problem, have been discussed in the context of the spin-boson model by Costi (1998). Universal scaling functions have been calculated for thermodynamic quantities (the specific heat), the static susceptibility, and the spin-relaxation function. Scaling as a function of temperature or frequency has been observed in the limit $\Delta \to 0$ for *fixed* coupling strength $\alpha$; this means that the scaling functions depend on the value of $\alpha$. This is illustrated, for example, in Fig. 2 in Costi (1998), which shows the temperature dependence of the specific heat for different $\alpha$. In particular, a signature distinguishing weakly from strongly dissipative systems is found in $\gamma(T) = C(T)/T$, which exhibits a peak for $\alpha < 1/3$ but is monotonic in temperature for $\alpha \geq 1/3$. This, together with the above-mentioned behavior in the spin-relaxation function, is reminiscent of measurements on $Ce_{1-x}La_xAl_3$ (Goremychkin *et al.*, 2002), but applicability of an anisotropic Kondo model here is controversial (Pietri *et al.*, 2001).

Specific heats have also been calculated for more complicated tunneling models, such as the ionic tunneling model with a spinless fermionic bath (Ferreira and Líbero, 2000), which shows similar behavior to the Ohmic spin-boson model for $\alpha \leq 1/4$, and to an extension of this including an assisted tunneling term (Ramos and Líbero, 2006). The spectral density of the former has also been investigated (Líbero and Oliveira, 1990b).

The mapping of a bosonic bath to a fermionic one has also been exploited for various other problems. Costi and McKenzie (2003) have used the NRG method to calculate the entropy of entanglement for the spin-boson model, a quantity that measures the entanglement between the spin and the environment. Interestingly, entanglement appears to be highest for $\alpha \to 1^-$, where the system undergoes a quantum phase transition from a delocalized to a localized phase.

The case of two bosonic baths which couple to different components of the impurity spin operator has been discussed by Castro Neto *et al.* (2003) and Novais *et al.* (2005). The bosonic baths in these models can be mapped onto two independent fermionic baths, and a generalization of the anisotropic Kondo model is obtained. These models are of interest to study the effect of quantum frustration of decoherence.

The second strategy to investigate impurity models with a coupling to a bosonic bath does not rely on a mapping to a fermionic impurity model. This approach—which has been termed bosonic NRG—was introduced by Bulla *et al.* (2003) in the context of the spin-boson model [for full details see Bulla *et al.* (2005)]. We mention briefly the main differences from the standard (fermionic) NRG: the logarithmic discretization is now directly performed for the bosonic bath [for the spin-boson model, the bath spectral function $J(\omega)$ Eq. (142) is discretized]; the subsequent mapping onto a semi-infinite chain is similar to the fermionic case but the resulting tight-binding chain is built up of bosonic sites. This gives rise to additional difficulties in setting up the iterative diagonalization scheme because only a finite number of bosonic states $N_b$ can be taken into account when adding one site to the chain. Furthermore, the set of $N_b$ states should in general be optimized to give the best description of the lowest-lying many-particle states, see the discussion by Bulla *et al.* (2005).

The first applications of the bosonic NRG method focused on the spin-boson model Eq. (141), in particular the sub-Ohmic case with exponents $0 < s < 1$, in the parametrization of the bath spectral function $J(\omega)$, Eq. (143). The sub-Ohmic case does not allow for the mapping to a fermionic impurity model, in contrast to the Ohmic case. Furthermore, the bosonic NRG method turns out to have certain advantages over other approaches usually applied to the spin-boson model (Leg-

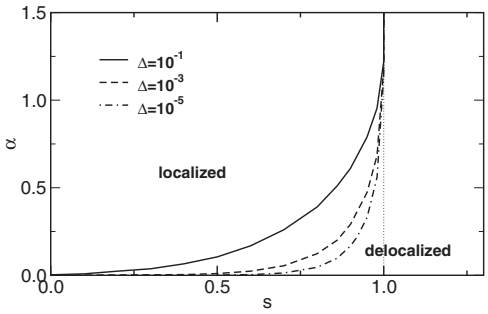


FIG. 24. Phase diagram of the spin-boson model for $T=0$ calculated with the bosonic NRG method for various values of $\Delta$. A line of quantum critical points separates the delocalized from the localized phase. Adapted from Bulla *et al.*, 2003.

gett *et al.*, 1987) as it is nonperturbative in both $\alpha$ and $\Delta$. As an example of the success of the bosonic NRG method, we show in Fig. 24 the $T=0$ phase diagram of the spin-boson model with bias $\epsilon=0$ in the $\alpha$-$s$ plane for different values of the tunneling amplitude $\Delta$. The most remarkable feature of the phase diagram is the line of quantum critical points for $0<s<1$ which terminates for $s\rightarrow 1^-$ in the Kosterlitz-Thouless transition of the Ohmic case. The critical exponents along this line have been discussed by Vojta *et al.* (2005) where it was shown that the exponents satisfy certain hyperscaling relations.

There are still quite a number of open issues and possible applications in the context of the sub-Ohmic spin-boson model which can be investigated with the bosonic NRG method [see, for example, Tong and Vojta (2006)]. In addition, the NRG method can be generalized to more complex impurity models with a coupling to a bosonic bath. Two examples are the investigations of the Bose-Fermi Kondo model (Glossop and Ingersent, 2005) and of models which are connected to electron and exciton transfer phenomena (Tornow *et al.*, 2006a, 2006b).

Technically the most challenging of the recent NRG applications is the study of impurity models which couple to both fermionic and bosonic baths. Glossop and Ingersent (2005, 2007b) presented the first treatment of such a model, the Bose-Fermi Kondo model with Ising-type coupling between spin and bosonic bath. Here the two baths are mapped on two semi-infinite chains, one for the bosonic and one for the fermionic degrees of freedom. As described above, the hopping matrix elements fall off as $\Lambda^{-n}$ for the bosonic chain, while those for the fermionic chain fall off as $\Lambda^{-n/2}$. To ensure that fermions and bosons of the same energy scale are treated at the same step, Glossop and Ingersent (2005) devised an iterative scheme that adds one site to the fermionic chain at each step, but extends the bosonic chain only at every second step. The accuracy of this approach has been tested extensively.

The physics of the Bose-Fermi Kondo model is dominated by competition between dissipation and screening, which results in a quantum phase transition from a phase with screened impurity spin to a phase with an unscreened spin. Glossop and Ingersent (2005) established that for a sub-Ohmic bath spectral function (of the bosonic bath) the two phases are separated by interacting quantum critical points, characterized by hyperscaling of the critical exponents and $\omega/T$ scaling in the local magnetic response. Furthermore, they investigated the destruction of the Kondo resonance in the Anderson version of this quantum impurity model. The Kondo resonance is visible in the screened phase of the model, and its value at $\omega=0$ remains pinned right up to the critical point, where the lowest-frequency part of the spectral function develops a non-Fermi-liquid-like power law. On the other side of the transition, the resonance turns into a dip at $\omega=0$.

The quantum phase transitions in the Bose-Fermi Kondo model turn out to be in the same universality class as the transitions in the spin-boson model. This can be understood through a mapping between the (Ising-) Bose-Fermi Kondo model and the spin-boson model where the bath spectral function has both an Ohmic and a sub-Ohmic component [the Ohmic part represents the coupling to the fermionic bath, while the sub-Ohmic part is the same as the one in the original model; see also Li *et al.* (2005)]. On the other hand, the (Ising-)Bose-Fermi Kondo model with an Ohmic bosonic bath can also be mapped onto the anisotropic Kondo model; see, for example, Borda *et al.* (2005).

## V. APPLICATION TO LATTICE MODELS WITHIN DMFT

Application of the NRG method is restricted to quantum impurity systems with the impurity degrees of freedom coupled to a *noninteracting* bath. Therefore the NRG method cannot be directly applied to lattice models of interacting particles, such as the Hubbard model [see Eq. (144) in Sec. V.A]. Early attempts to extend Wilson's concepts to such models failed (Chui and Bray, 1978; Bray and Chui, 1979; Lee, 1979). The reason for this failure was later found to be connected with boundary conditions between "system" and "environment" (White and Noack, 1992; Noack and Manmana, 2005), and led to a novel scheme nowadays known as the *density-matrix renormalization group* (Schollwöck, 2005; Hallberg, 2006), which today is a standard technique to study one-dimensional interacting quantum models.

There exists, however, an approximation for correlated lattice models, where the interacting lattice problem is mapped onto an effective quantum impurity model, for which the NRG method can be applied. Underlying this approach is the dynamical mean-field theory (DMFT). The DMFT has its origin in the investigation of correlated lattice models in the limit of infinite spatial dimensionality (Metzner and Vollhardt, 1989). A proper scaling of the hopping matrix element $t$ in models such as the Hubbard model (144) leads to a vanishing of all nonlocal self-energy skeleton diagrams. The resulting purely local self-energy $\Sigma(z)$ can be identified with the self-energy of an effective single-impurity Anderson model. In this sense we speak of a mapping of a lattice model onto an effective quantum impurity model, typically the single-impurity Anderson model as

introduced in Eq. (2), supplemented by a self-consistency condition, which determines the bath degrees of freedom of the effective quantum impurity. Since the technical details of the DMFT are not the subject of this review, we refer the reader to the review by Georges *et al.* (1996).

To investigate lattice models in the DMFT we therefore need a technique (analytical or numerical) to calculate the full frequency dependence of the self-energy for a single-impurity Anderson model defined by arbitrary input parameters [$\varepsilon_f$, $U$, $T$, and a manifestly energy-dependent hybridization function $\Delta(\omega)$]. There are many methods besides the NRG available to calculate dynamic quantities for quantum impurity models and we shall not give an overview here [for reviews see, for example, Sec. IV in Georges *et al.* (1996), Sec. III in Maier *et al.* (2005), and Bulla (2006)], but rather concentrate on the application of the NRG method to the Hubbard model (see Sec. V.A), the periodic Anderson and Kondo lattice models (see Sec. V.B), and lattice models with coupling to phonons (see Sec. V.C) within the DMFT approach.

Before we discuss the results obtained for those models, we comment on peculiarities of the NRG method when applied to DMFT calculations. The DMFT self-consistency specifies at each iteration an input hybridization function $\Delta(\omega)$, the form of which depends on the model under investigation, its parameters, and also the history of the previous DMFT iterations. The frequency dependence of $\Delta(\omega)$ has to be taken into account within the logarithmic discretization scheme, as described in Sec. II and already employed in the NRG investigations of the soft-gap Anderson model (see Sec. IV.C.2).

Concerning the output, the quantity of interest is usually the self-energy $\Sigma_{\mathrm{AM}}$ of the effective single-impurity Anderson model, although in some cases, as for the Bethe lattice, knowledge of the single-particle Green's function is sufficient for the DMFT iteration (Georges *et al.*, 1996). It has proven advantageous to calculate, within DMFT, the self-energy $\Sigma_{\mathrm{AM}}$ via the ratio of a two-particle and a one-particle Green's function [see Eq. (86)]. As discussed by Bulla *et al.* (1998) (see also Sec. III.B.2) calculation of the self-energy via Eq. (86) significantly improves the quality of the results. This approach has been used in most NRG calculations within DMFT.

### A. Hubbard model

The simplest model for correlated fermions on a lattice is the single-band Hubbard model with the Hamiltonian

$$H = -t\sum_{\langle ij\rangle\sigma}(c_{i\sigma}^{\dagger}c_{j\sigma} + c_{j\sigma}^{\dagger}c_{i\sigma}) + U\sum_{i} c_{i\uparrow}^{\dagger}c_{i\uparrow}c_{i\downarrow}^{\dagger}c_{i\downarrow}. \qquad (144)$$

Consequently, the first applications of the NRG method within DMFT focused on this model; in particular on the Mott transition, which the Hubbard model displays in the half-filled paramagnetic case. These investigations and further generalizations are described in the following sections.

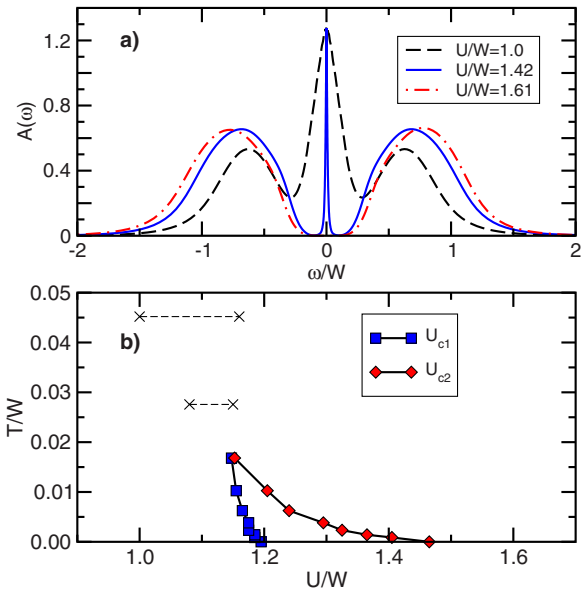


FIG. 25. (Color online) (a) Spectral functions for the half-filled Hubbard model at $T=0$ for various values of $U$ [similar data as in Fig. 2 in Bulla (1999)]. (b) Phase diagram for the Mott transition. For a comparison with other methods see the corresponding Fig. 9 in Bulla *et al.* (2001).

#### 1. Mott metal-insulator transition

Although the qualitative features of the Mott transition were correctly described very early in the development of the DMFT [see the review by Georges *et al.* (1996)], the NRG method helped to clarify a number of conflicting statements [see the discussion by Bulla (1999) and Bulla *et al.* (2001)]. The NRG method appears to be ideally suited to investigate the Mott transition because (i) the transition occurs at interaction strengths of the order of the bandwidth, which requires the use of a nonperturbative method; and (ii) at $T=0$ the Mott transition is characterized by a vanishing energy scale, $T^{*}\to 0$, when approached from the metallic side. Thus a method is needed that is able to resolve arbitrarily small energies close to the Fermi level.

The first investigation of the Mott transition with the NRG method was by Sakai and Kuramoto (1994) [see also Shimizu and Sakai (1995)]. These calculations did not use an expression of the self-energy as in Eq. (86), but nevertheless a Mott transition and a hysteresis region were observed, with critical values very close to the ones reported later by Bulla (1999).

A detailed discussion of the NRG calculations for the Hubbard model has been given by Bulla (1999) for $T=0$ and by Bulla *et al.* (2001) for finite temperatures. The main results are summarized in Fig. 25: Spectral functions calculated with the NRG method for the half-filled Hubbard model in the paramagnetic regime for different values of $U$ and $T=0$ are shown in Fig. 25(a). Upon increasing $U$ from the metallic side, the typical three-peak structure forms, with upper and lower Hubbard peaks at $\omega\approx\pm U/2$ and a central quasiparticle peak at $\omega=0$. The width of this quasiparticle peak goes to zero when the

transition is approached from below, $U \nearrow U_{c,2} \approx 1.47W$, with $W$ the bandwidth of the noninteracting model. Right at the transition, when the quasiparticle peak has disappeared, an insulating solution with a preformed gap is realized.

We remind the reader at this point that the NRG results for dynamic quantities have a certain fixed resolution on a *logarithmic* scale (cf. the discussion in Sec. III.B). This means that structures close to $\omega=0$ are much better resolved than structures at, for example, the band edges of the Hubbard bands. In contrast, the dynamical density-matrix renormalization group applied to the DMFT for the Hubbard model works with a fixed resolution on a *linear* scale; see, for example, Karski *et al.* (2005). The structures close to the inner band edges of the Hubbard bands seen in these calculations [see Fig. 2 in Karski *et al.* (2005)] cannot be resolved in present implementations of the NRG method.

Figure 25(b) shows the $T$-$U$ phase diagram for the Mott transition, considering only paramagnetic phases. As observed earlier (Georges *et al.*, 1996), there are two transition lines because the insulator-to-metal transition occurs at a lower critical value $[U_{c,1}(T)]$ than the metal-to-insulator transition $[U_{c,2}(T)]$. Within this hysteresis region, both metallic and insulating solutions can be stabilized within the DMFT self-consistency. With increasing temperature, the hysteresis region shrinks to zero at a critical $T_c$, above which there is only a crossover from metalliclike to insulatinglike solutions; this crossover region is indicated by dashed lines in Fig. 25(b). The NRG values for $U_{c,1/2}(T)$ were later verified by a number of other, nonperturbative techniques [see, for example, Tong *et al.* (2001) and Potthoff (2003)].

As discussed above, most of the NRG calculations within DMFT have been performed using Eq. (86) for the calculation of the self-energy. This quantity itself shows interesting properties [see, for example, Fig. 3 in Bulla (1999) and Fig. 5 in Bulla *et al.* (2001)], and allows calculation of the $U$ dependence of the quasiparticle weight [see Fig. 1 in Bulla (1999)].

The Mott transition can also be induced by moving away from half filling, provided the value of $U$ is larger than the $U_c$ for the half-filled case. Unfortunately, no systematic NRG calculations have been published for this filling-induced Mott transition, despite the fact that the NRG method can be easily extended to the Hubbard model away from particle-hole symmetry. Only a few results for the phase diagram (Ōno *et al.*, 2001) and spectral functions (Freericks *et al.*, 2003; Krug von Nidda *et al.*, 2003) are available.

A nice feature of the DMFT is that it also allows for the calculation of physical quantities other than the single-particle Green's function, in particular susceptibilities and also transport properties, both static and dynamic. This aspect of the DMFT was used already in the early applications [see, for example, the reviews by Pruschke *et al.* (1995) and Georges *et al.* (1996)], employing different methods to solve the effective quantum impurity problem. However, apart from discussions of the

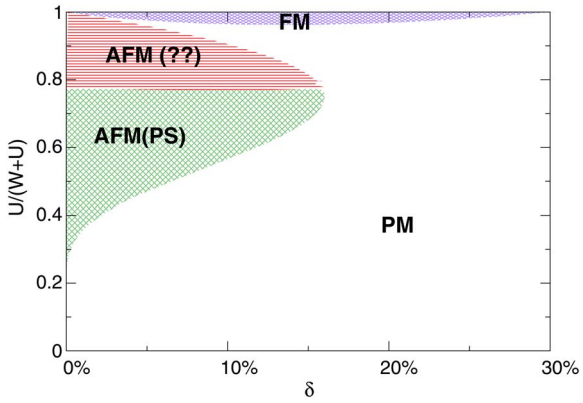


FIG. 26. (Color online) Ground-state magnetic phase diagram for the Hubbard model on a hypercubic lattice. The phases show antiferromagnetic (AFM) order, which for smaller $U$ and doping $\delta>0$ also shows phase separation (PS), and ferromagnetic order at large $U$. To display the whole interval $[0,\infty)$, the vertical axis was rescaled as $U/(W+U)$ [see also Fig. 10 in Zitzler *et al.* (2002)].

$B_{1g}$ Raman response (Freericks *et al.*, 2001, 2003) and calculations of the resistivity (Limelette *et al.*, 2003; Georges *et al.*, 2004) and the local dynamic susceptibility (Krug von Nidda *et al.*, 2003), no detailed studies of such quantities for the paramagnetic phase of the Hubbard model have been performed yet with the NRG method.

### 2. Ordering phenomena

The Mott transition from a paramagnetic metal to a paramagnetic insulator is merely one of the many features in the rich phase diagram of the Hubbard model and its generalizations. In addition, various types of ordering phenomena occur, such as charge, orbital (in case of multiorbital models), and magnetic ordering, and, possibly, superconductivity. The NRG method has been used in particular to study magnetic ordering phenomena in a wide range of parameters.

For the investigation of symmetry-broken phases within DMFT, the self-consistency equations have to be adapted appropriately (Georges *et al.*, 1996). The effective impurity models have the structure of the single-impurity Anderson model so that the application of the NRG method is straightforward [see the discussion by Zitzler *et al.* (2002)]. This work also contains a detailed study of the magnetic phases of the Hubbard model at $T=0$ both at and away from half filling. Right at half filling and for a particle-hole symmetric band structure, the ground state is always antiferromagnetically ordered. Upon doping, the situation is more complicated as shown in Fig. 26: For small values of $U$, the compressibility becomes negative, i.e., the system will undergo phase separation within the antiferromagnetic phase into a region with a half-filled antiferromagnet and a region with zero filling (van Dongen, 1996). Here the long-ranged parts of the Coulomb interaction become crucial, stabilizing charge-ordered phases like, e.g., stripes (Fleck *et al.*, 2001). For very large values of $U$,

ferromagnetic solutions can be stabilized. For intermediate $U$ and finite doping, magnetic ordering appears to exist but its type could not be determined yet.

Note that at finite $T>0$ the phase-separated state will be replaced by other phases comprising incommensurate phases also (Freericks and Jarrell, 1995b). Since we intend to provide the possibilities of the NRG method here, we do not dwell on the physics of the Hubbard model, but refer the reader to the mentioned reviews on the DMFT solutions of this model.

In contrast to this work, the NRG calculations by Zitzler *et al.* (2004) concentrated on the antiferromagnetic phase at half filling in a Hubbard model with frustration. As expected, the antiferromagnetic region in the $T$-$U$ phase diagram is suppressed upon increasing frustration. However, the resulting phase diagram turns out to be significantly different from the one proposed for the frustrated Hubbard model by Georges *et al.* (1996), where the main effect of frustration was claimed to suppress $T_N$ such that the first-order Mott transition is visible above the antiferromagnetic region. This controversial issue calls for more detailed calculations (with the NRG and other methods); after all, similarity of the phase diagram for the Hubbard model in DMFT and the experimental one for the transition metal oxide $V_2O_3$ has been claimed to be one of the early successes of DMFT (Georges *et al.*, 1996).

The optical conductivity in the antiferromagnetic phase of the Hubbard model at half filling and zero temperature has been studied by Pruschke and Zitzler (2003). For small values of $U$, the antiferromagnetic phase shows signatures of a Slater insulator, while for large $U$ a Mott-Heisenberg picture applies. There is a smooth crossover between these two limiting cases upon variation of $U$, in contrast to the Mott transition in the paramagnetic phase. Evidence from optical data has been supported by a detailed discussion of the local dynamical magnetic susceptibility, giving additional insight into the subtle changes in the physics of charge and spin degrees of freedom across the Mott metal-insulator transition (Pruschke and Zitzler, 2003; Pruschke, 2005).

When the Hubbard model Eq. (144) is supplemented by a nearest-neighbor Coulomb repulsion $V$, a transition to a charge ordered state is observed upon increasing $V$. This transition has been studied by Pietig *et al.* (1999) for the quarter-filled case. NRG calculations, together with results from the noncrossing approximation and exact diagonalization, show a phase diagram with a reentrant charge ordering transition, a feature that has also been observed in a variety of transition metal oxides. The NRG results in this work are restricted to $T=0$, where the transition is of first order. It would be interesting to extend the NRG calculations to a wider range of parameters, in particular to finite temperatures to study the change of the transition, which is continuous at higher $T$.

#### 3. Multiband Hubbard models

Application of the NRG method to the investigation of multiband Hubbard models within DMFT is still in an early stage. This is because (i) the computational effort grows considerably with the number of orbitals and (ii) the DMFT requires a very high accuracy for the calculated dynamic properties. Furthermore, self-consistent solutions of the DMFT equations have to be obtained.

The first and only DMFT results for a two-band Hubbard model using the NRG method have been presented by Pruschke and Bulla (2005). In this work, two different strategies have been used to handle the complexity of the problem. The first one is to explicitly include the orbital quantum numbers in the iterative construction of the basis states. As for the impurity models discussed in Sec. IV.D, this additional quantum number significantly reduces the typical matrix size. However, this approach fails as soon as the Hamiltonian contains terms that break the orbital symmetry.

The second strategy is an asymmetric truncation scheme: Instead of adding both orbital degrees of freedom simultaneously, the Hilbert space is truncated after adding each orbital individually, which also leads to a significant reduction of the typical matrix size. This approach works quite well for a wide range of parameters, but it appears to violate the orbital symmetry, if present. However, in the presence of a crystal-field splitting of the orbitals, such a strategy might be usable.

The focus in Pruschke and Bulla (2005) was on the role of the Hund exchange coupling $J$ in the Mott transition in the two-band Hubbard model. It was found that both the position in parameter space and the nature of the Mott transition depend on the value of $J$ and the precise form of the coupling. For example, replacement of a rotationally invariant Hund exchange by an Ising-like exchange leads to a significant change in the physics of the Mott transition. Note that such features can be partly understood on the level of the corresponding effective impurity models, which underlines the importance of thoroughly investigating the properties of the impurity models appearing in the DMFT.

#### 4. Other generalizations of the Hubbard model

We conclude this section with a brief overview of applications of the NRG method to various other generalizations of the Hubbard model. The influence of correlations in a conduction band (modeled by a Hubbard model within DMFT) on the physics of the single-impurity Anderson model has been investigated by Hofstetter *et al.* (2000). The DMFT approach allows one to map this model on an effective impurity model with two coupled correlated sites, the first one corresponding to the original impurity and the second one coming from the DMFT treatment of the Hubbard model. This two-site cluster couples to a free effective conduction band. As discussed by Hofstetter *et al.* (2000), correlations in the conduction band have a significant influence on the low-energy scale and also lead to a suppression of the Kondo resonance.

Within the so-called Anderson-Hubbard model, disorder effects can be incorporated via a random distribution of the local energies $\varepsilon_i$. This model has been studied

by Byczuk *et al.* (2004) within DMFT for binary alloy disorder. Application of the NRG method here is standard—two independent single-impurity Anderson models have to be considered at each iteration step. Nevertheless, the physics of this model is quite interesting, in particular the occurrence of a Mott transition at *noninteger* filling. The DMFT treatment in Byczuk *et al.* (2004) does not allow for true Anderson localization (as far as disorder is concerned, the DMFT is equivalent to the coherent potential approximation and the main effect of the binary disorder is to split the bands). This deficiency was cured by Byczuk *et al.* (2005) where a generalization of the DMFT approach was used, based on the geometrically averaged (typical) local density of states. This allows one to study both Mott insulating and Anderson insulating phases; see Fig. 1 of that work. The calculation has been performed using a continuous probability distribution, approximated by up to 30 different values of $\varepsilon_i$, so that in each DMFT step a corresponding number of independent single-impurity Anderson models have to be considered. All NRG calculations for the Anderson-Hubbard model have been so far restricted to $T=0$ and to phases without long-range order.

The NRG method has been used within an extension of the standard DMFT. The DMFT+$\Sigma_k$ approach as introduced by Sadovskii *et al.* (2005) and Kuchinskii *et al.* (2005) adds to the local self-energy a $k$-dependent part $\Sigma_k$. Applied to the one-band Hubbard model, the effective single-impurity Anderson model is of the same type as the one appearing in standard DMFT, the only difference is in the structure of the self-consistency equations.

For details of the NRG calculations and discussion of the physics of the Falikov-Kimball model (Anders and Czycholl, 2005) and the ionic Hubbard model (Jabben *et al.*, 2005), see the respective references. Both papers show the usefulness of the NRG approach to a wide range of correlated lattice models within DMFT, in particular for the calculation of dynamic quantities at low temperatures.

### B. Periodic Anderson and Kondo lattice models

A variety of lanthanide- and actinide-based compounds can be characterized as heavy fermion systems with a strongly enhanced effective mass of quasiparticles. These compounds contain well localized $4f$ or $5f$ orbitals coupling via a hybridization to a conduction band consisting of $s$, $p$, or $d$ orbitals. The appropriate microscopic model for these materials is the periodic Anderson model (PAM),

$$H = \varepsilon_f \sum_{i\sigma} f^\dagger_{i\sigma} f_{i\sigma} + U \sum_i f^\dagger_{i\uparrow} f_{i\uparrow} f^\dagger_{i\downarrow} f_{i\downarrow} + \sum_{k\sigma} \varepsilon_k c^\dagger_{k\sigma} c_{k\sigma} + \sum_{ij\sigma} V_{ij} (f^\dagger_{i\sigma} c_{j\sigma} + c^\dagger_{j\sigma} f_{i\sigma}). \quad (145)$$

When charge fluctuations of the $f$ orbitals are negligible, the low-energy physics of the PAM can equally be described by the Kondo lattice model

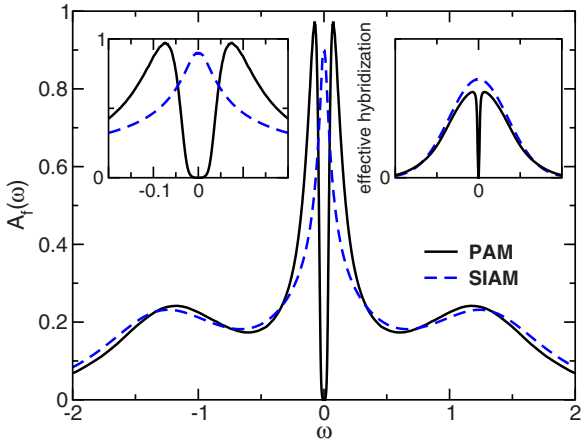


FIG. 27. (Color online) Comparison of dynamic properties for the particle-hole symmetric periodic Anderson model (solid lines) and the corresponding single-impurity Anderson model (dashed lines). Main panel, $f$-electron spectral function; left inset, enlarged view of the region around the Fermi energy; and right inset, (effective) hybridization function. Adapted from Pruschke *et al.*, 2000.

$$H = J \sum_i \vec{S}_i \cdot \vec{s}_i + \sum_{k\sigma} \varepsilon_k c^\dagger_{k\sigma} c_{k\sigma}. \quad (146)$$

In deriving the Kondo model from the PAM (145) via a Schrieffer-Wolff transformation, we approximated $V_{ij} \to V\delta_{ij}$, which is justified if one is interested only in qualitative aspects of the physics of both models.

The large effective mass in these models arises from a strongly reduced lattice coherence scale $T_0$; this is one of the reasons why the NRG method is well suited for investigation of heavy fermion behavior when the PAM or the Kondo lattice model is treated within DMFT. The main difference for the NRG treatment (as compared to the Hubbard model) lies in the DMFT self-consistency. This means that the structure of the effective impurity model is changed only via the effective hybridization $\Delta(\omega)$ (which may lead to complications as discussed later).

The PAM with on-site hybridization $V_{ij}=V\delta_{ij}$ and particle-hole symmetry on a hypercubic lattice has been discussed by Shimizu and Sakai (1995), Pruschke *et al.* (2000), and Shimizu *et al.* (2000). In this case, a hybridization gap at the Fermi level appears in the spectral functions for both conduction and $f$ electrons. This effect for the $f$ spectral function is shown in Fig. 27 by full lines in the main panel and left inset. The Kondo resonance of the corresponding single-impurity Anderson model (dashed curves in the main panel and left inset in Fig. 27), for which the hybridization function is given by the bare density of states of the lattice, is split in the periodic model. The energy scale of the gap in the PAM (proportional to the lattice coherence scale $T_0$) depends exponentially on the model parameters, like the width of the Kondo resonance in the impurity model (proportional to the Kondo temperature $T_K$). Further analysis shows that the lattice coherence scale $T_0$ is enhanced

over the impurity scale $T_K$ [for details, see Pruschke *et al.* (2000)].

The right inset to Fig. 27 shows the hybridization function of the effective impurity model after self-consistency has been reached (full line) in comparison to the same quantity entering the isolated impurity (dashed line). At first sight, the only difference seems to be the gap at the Fermi level. However, for the particle-hole symmetric case, one can show that $\Delta(\omega)$ has a pole at the Fermi level. This pole appears to be a problem for the NRG method as the logarithmic discretization explicitly excludes the point $\omega=0$, i.e., such a pole cannot be incorporated in the mapping to the semi-infinite chain. The solution is to take the pole into account exactly by choosing as "impurity" the complex consisting of $f$ and band states, i.e., including the bare hybridization explicitly, and building the DMFT around this complex (Pruschke *et al.*, 2000). Note, however, that this approach works only for a local hybridization $V_{ij}=V\delta_{ij}$.

Due to the appearance of the hybridization gap, the particle-hole symmetric PAM seems suitable to describe so-called Kondo insulators, but not the metallic heavy fermion behavior. There are various ways to drive the PAM into the metallic regime, two of which we discuss in the following. One possibility is to use asymmetric parameters for the $f$ electrons ($\varepsilon_f \neq -U/2$) and to keep the conduction band symmetric so that $n_c \approx 1$. More interesting and physically more relevant is the opposite case, namely, keeping $\varepsilon_f=-U/2$ and shifting the conduction band center of mass away from the Fermi level, so that $n_c$ is reduced from 1. This situation has been discussed in the context of Nozières' exhaustion principle (Nozières, 1998, 2005) which states that, upon decreasing $n_c$, there will not be enough conduction electrons available to screen the impurity spins. Collective screening then becomes effective only at a strongly reduced lattice coherence scale. We do not want to go into the details here and refer the reader to the discussion of the quantum Monte Carlo results in Tahvildar-Zadeh *et al.* (1997, 1999) and the discussion in Sec. 5.4 of Vidhyadhiraja and Logan (2004), which is based on results for the PAM obtained with the local-moment approach.

There is one particular feature found in the DMFT calculations which at first sight seems to support Nozières' idea, namely that, as shown in Fig. 6(b) in Pruschke *et al.* (2000), the effective hybridization function is strongly reduced in a region close to the Fermi level. Since this quantity can be interpreted as being proportional to the conduction band density of states effectively seen by the $f$ states, it seems that indeed there are fewer conduction electrons available to screen the moments of the $f$ electrons. Figure 6(a) in Pruschke *et al.* (2000) shows the corresponding $f$ spectral function, which consequently displays metallic (heavy fermion) behavior. The corresponding lattice coherence scale is reduced as compared to $T_K$; see Fig. 8 in Pruschke *et al.* (2000) where the dependence of both $T_0$ and $T_K$ on $n_c$ is plotted. However, in contrast to Nozières's original claim, i.e., $T_0 \propto (T_K)^2$, a behavior $T_0 \propto T_K$ is found, with a prefactor decreasing exponentially with decreasing $n_c$. Again, the ability of the NRG method to accurately identify exponentially small energy scales proves to be of great value here.

Another route to metallic behavior in the PAM is to incorporate a dispersion of the $f$ electrons of the form

$$t_f \sum_{\langle ij\rangle,\sigma} (f_{i\sigma}^\dagger f_{j\sigma} + f_{j\sigma}^\dagger f_{i\sigma}). \tag{147}$$

The effect of such a dispersion term—in particular the closing of the gap upon increasing $t_f$—has been studied by Shimizu *et al.* (2000) for both the particle-hole symmetric and asymmetric cases. These authors also study the relation between charge and spin gaps in the dynamical susceptibilities and the hybridization gap in the spectral function.

A metallic ground state of the particle-hole symmetric PAM can also be realized when the hybridization between $f$ electrons and $c$ electrons is only between nearest neighbors:

$$V_{ij} = \begin{cases} V, & i,j \text{ nearest neighbors}, \\ 0, & \text{otherwise}. \end{cases} \tag{148}$$

For $T=0$, the PAM with nearest-neighbor hybridization shows a notable difference to the models discussed above: the low-energy scale $T_0$ no longer depends exponentially on $U$ but vanishes at a *finite* critical $U_c$ (Held and Bulla, 2000). This behavior is reminiscent of the physics of the Mott transition in the Hubbard model. The difference, however, is that in the PAM defined by Eqs. (145) and (148) the Mott transition occurs only in the subsystem of the $f$ electrons—a gap opens in the $f$ electron spectral function while the $c$ electron part still has finite spectral weight at the Fermi level [see Fig. 3 in Held and Bulla (2000)] so that the overall system remains metallic.

The calculations described so far have been restricted to $T=0$. Finite-temperature calculations for single-particle and magnetic excitation spectra have been presented by Costi and Manini (2002) for the Kondo lattice model. As in Pruschke *et al.* (2000), one focus of these studies has been the variation of the spectra with conduction band filling $n_c$. For this case it was found that the spectra exhibit two energy scales, one being the Kondo temperature $T_K$ of the corresponding single-impurity Kondo model, the other the Fermi-liquid coherence scale $T_0$, which, for low carrier densities $n_c \ll 1$ is strongly reduced as compared to $T_K$, similarly to the observations made by Pruschke *et al.* (2000) for the PAM.

A ferromagnetic version of the Kondo lattice model with Coulomb interactions in the conduction band was studied by Liebsch and Costi (2006) in the context of the orbital-selective Mott phase of the two-band Hubbard model with inequivalent bands. The physics of this model is quite different from that of the usual Kondo lattice model. In particular, one finds, as in Biermann *et*

*al.* (2005), non-Fermi-liquid or bad metallic behavior, depending on whether the ferromagnetic exchange is isotropic or anisotropic, respectively.

All these results have been obtained for the paramagnetic phases of the PAM or Kondo lattice model. Of course, the presence of localized moments implies the possibility for magnetic ordering [for quantum Monte Carlo results within the DMFT framework, see Jarrell (1995)], which is frequently observed in heavy fermion compounds, partly in close vicinity to superconducting phases. These issues have not been addressed yet with the NRG method, but, as has been demonstrated for the Hubbard model, are of course accessible with this method, and are surely a promising project for future NRG calculations for the PAM or Kondo lattice model within the DMFT.

Magnetic quantum phase transitions in the Kondo lattice model have been the focus of calculations within the extended DMFT (Si *et al.*, 2001), for which the effective impurity model includes a coupling to both fermionic and bosonic baths. The NRG method has been generalized to such types of impurity model (see Sec. IV.E), and recent applications of the NRG method within the extended DMFT have been discussed by Glossop and Ingersent (2007a) and Zhu *et al.* (2007).

### C. Lattice models with phonons

We consider the Hubbard model Eq. (144) and supplement it by a local coupling of the electron density to the displacement of Einstein phonons with frequency $\omega_0$. This results in the Hubbard-Holstein model with the Hamiltonian

$$H = \varepsilon \sum_{i\sigma} c_{i\sigma}^\dagger c_{i\sigma} - t \sum_{\langle ij\rangle\sigma} c_{i\sigma}^\dagger c_{j\sigma} + U \sum_i c_{i\uparrow}^\dagger c_{i\uparrow} c_{i\downarrow}^\dagger c_{i\downarrow} + g \sum_{i\sigma} (b_i^\dagger + b_i) c_{i\sigma}^\dagger c_{i\sigma} + \omega_0 \sum_i b_i^\dagger b_i. \quad (149)$$

The limit $U \to 0$ of this Hamiltonian gives the Holstein model, a highly nontrivial model as discussed in the following.

Within DMFT, the model Eq. (149) maps onto the Anderson-Holstein (impurity) model, to which the NRG method was first applied by Hewson and Meyer (2002) (see Sec. IV.E). The self-consistency equations are the same for both the Hubbard-Holstein and the pure Hubbard model; the only difference lies in the calculation of the self-energy for the effective impurity model, which now contains an additional contribution from the coupling to the phonons. This contribution can also be calculated as a ratio of two correlation functions.

From a technical point of view, there is no difference in the NRG treatment of the Hubbard-Holstein model with either a finite or a zero value of $U$. Historically, the first applications of the NRG method were for the $U=0$ case [the Holstein model, see Meyer *et al.* (2002) and Meyer and Hewson (2003)] and have revealed a number of interesting results. An important point is that the NRG method (combined with DMFT) is nonperturbative in both $g$ and $U$; furthermore, it allows one to study the case of a *macroscopic* electron density (in contrast to the few-electron case). It should be mentioned that there are various other techniques which have been applied to the model Eq. (149) and many useful insights have been gained by such applications, well before the first NRG calculations for this model. As an example, see the quantum Monte Carlo calculations for the Holstein and Hubbard-Holstein models in Freericks and Jarrell (1995a) and Freericks *et al.* (1993).

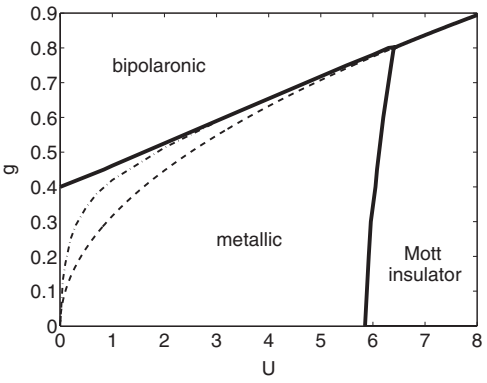


FIG. 28. Phase diagram of the half-filled Hubbard-Holstein model for $T=0$. The thick solid lines denote the phase boundaries while the dashed line corresponds to $U_{\text{eff}}=U-2g^2/\omega_0=0$. Dashed and dot-dashed lines are polaronic lines. Adapted from Koller, Meyer, and Hewson (2004).

For the half-filled case, Meyer *et al.* (2002) showed some unexpected properties for the transition from a metal to a bipolaronic insulator at a critical coupling $g_c$. In contrast to the Mott transition in the Hubbard model, no hysteresis and no preformed gap is observed here (at least for small values of $\omega_0$) which indicates that the physics of the transition to the bipolaronic insulator might be completely different (whether it is connected to locally critical behavior is an interesting subject for future research).

For large values of $\omega_0$, the physics of the transition is getting closer to that of the Hubbard model (Meyer and Hewson, 2003). This is because in the $\omega_0 \to \infty$ limit the Holstein model can be mapped onto the attractive Hubbard model, which has the same behavior as the repulsive Hubbard model when charge and spin degrees of freedom are interchanged.

The phase diagram of the Hubbard-Holstein model at half filling, $T=0$, and neglecting any long-range-ordered phases has been discussed by Jeon *et al.* (2004); Koller, Meyer, and Hewson (2004); and Koller, Meyer, *et al.* (2004). The main features are summarized in Fig. 28, which shows the position of the phase boundaries between metallic, Mott insulating, and bipolaronic insulating phases. The nature of these various transitions, together with the behavior of dynamic quantities, has been discussed by Koller, Meyer, and Hewson (2004). We point out that the behavior of the phonon spectral function shows a considerable phonon softening upon ap-

proaching the transition to the bipolaronic insulator. Such a softening is absent in the approach to the Mott insulator, for the simple reason that, close to the Mott transition, where charge fluctuations are strongly suppressed, phonons are decoupled from electrons. One of the interesting topics for future research concerns models that do show such a phonon softening even close to the Mott transition; this can possibly be accomplished by considering additional orbital degrees of freedom.

The Hubbard-Holstein model has been studied for the quarter-filled case and large values of $U$ (Koller, Hewson, and Edwards, 2005). In this situation, a strongly renormalized band of polaronic quasiparticle excitations occurs within the lower Hubbard band of the electronic spectral function.

All investigations of lattice models with electron-phonon coupling described in this section have been restricted to $T=0$ and to phases without long-range order. Generalizations to finite temperatures and ordered phases (such as superconducting and charge ordered phases) appear to be possible within the DMFT-NRG approach and will certainly give interesting results and new insights. Other possible generalizations are different types of lattice model, such as the periodic Anderson model and multiorbital models, and models with a different type of coupling between electrons and phonons.

## VI. SUMMARY

We first summarize the main scope of this review.

(i) To give a general introduction to the basic concepts of the numerical renormalization group approach (Sec. II) and to the general strategy for the calculation of physical quantities within this method (Sec. III).

(ii) To cover the whole range of applications over the last 25 years, following the seminal work of Wilson (1975a) on the Kondo problem and the work of Krishnamurthy *et al.* (1980a) on the Anderson impurity model (Secs. IV and V).

The range of applicability of the NRG method widened considerably, in particular over the last ten years. This can be easily seen in the list of references in which more than 50% of the entries are from the years starting with 2000. In physical terms, the NRG method is now being used to study different phenomena of condensed matter physics: Typical correlation phenomena such as the Mott transition and heavy fermion behavior, the physics of a two-state system in a dissipative environment, and Kondo correlations in artificial atoms such as quantum dots, to name but a few. Of course, we expect that there are many problems to which the NRG method will be applied in the future, and we hope that this review will be helpful as a starting point for such investigations.

Some of the concepts discussed in Secs. II and III are fairly recent developments. For example the generalization of the NRG to quantum impurities coupled to a bosonic environment (see also Sec. IV.E) and the calculation of time-dependent quantities (transient dynamics, see Sec. III.B.3). As only a few applications of these new concepts have been considered so far, one line of future research of the NRG method is their generalization to a broader class of impurity models.

We have discussed some open issues and ideas for further investigations in the various subsections of Secs. IV and V. We mention a few suggestions for further generalizations and applications of the NRG method:

- application of the bosonic NRG method to generalizations of the spin-boson model such as coupled spins in a dissipative environment;
- magnetic, orbital, and charge ordering in lattice models within DMFT; and
- application of multiple-shell techniques (Sec. III.B) to further improvement of the dynamics, particularly at the lowest temperatures.

What are the main open issues of the NRG approach? As discussed in Sec. IV.D, multisite and multiorbital models pose severe technical problems for the NRG method because the Hilbert space increases dramatically with the number of orbitals. This limits, in particular, the accuracy in the calculation of dynamical quantities which in turn restricts the applicability of the NRG method to multiband models within DMFT (see Sec. V.A) or its extensions. Concerning dynamical quantities, another shortcoming of the present implementations of the NRG method is the poor resolution at high frequencies, for example, features such as the band edges of upper and lower Hubbard bands in the Hubbard model or the sharply peaked and highly asymmetrical spin-resolved Kondo resonance at high magnetic fields, as shown in Fig. 7. A gradual improvement of the accuracy can, of course, be achieved by simply increasing the computational effort, but for a real breakthrough (concerning multiband models and the high-energy resolution) we probably need completely new ideas and concepts.

From a conceptual point of view it will be interesting to view the NRG method in a broader context. One step in this direction has been made by Verstraete *et al.* (2005). These authors interpreted the NRG iteration in terms of matrix product states, and established a connection to the widely used density matrix renormalization group method.

Concerning the future prospects of the numerical renormalization group, we conclude with a remark from Wilson's original paper (Wilson, 1975a, p. 777), about the prospects of the renormalization group in general:

> However, most of the unsolved problems in physics and theoretical chemistry are of the kind the renormalization group is intended to solve (other kinds of problems do not remain unsolved for long). It is likely that there will be a vast extension of the renormalization group over the next decade as the methods become more clever and powerful; there are very few areas in either elementary particle physics, solid state physics, or theoretical chemistry that are permanently immune to this infection.

**ACKNOWLEDGMENTS**

It is a pleasure to acknowledge many useful discussions on the topic of this review with present and former colleagues, including F. B. Anders, J. Bonča, L. Borda, S. Florens, J. Freericks, R. Helmes, A. C. Hewson, W. Hofstetter, K. Ingersent, S. Kehrein, J. Kroha, D. Logan, N. Manini, A. Rosch, N.-H. Tong, C. M. Varma, M. Vojta, D. Vollhardt, J. von Delft, A. Weichselbaum, P. Wölfle, G. Zaránd, A. Zawadowski, and V. Zlatić. This work was supported in part by the DFG through the collaborative research centers SFB 484 and SFB 602. We acknowledge supercomputer support by the Leibniz Computer Center, the Max-Planck Computer Center Garching under Grant No. h0301, the Gesellschaft für wissenschaftliche Datenverarbeitung Göttingen (GWDG), the Norddeutscher Verbund für Hoch- und Höchstleistungsrechnen (HLRN) under Project No. nip00015, and the John von Neumann Institute for Computing (Jülich).

**REFERENCES**

Affleck, I., and A. W. W. Ludwig, 1992, Phys. Rev. Lett. **68**, 1046.
Affleck, I., A. W. W. Ludwig, and B. A. Jones, 1995, Phys. Rev. B **52**, 9528.
Affleck, I., A. W. W. Ludwig, H.-B. Pang, and D. L. Cox, 1992, Phys. Rev. B **45**, 7918.
Alascio, B., R. Allub, and C. A. Balseiro, 1986, Phys. Rev. B **34**, 4786.
Allub, R., and A. A. Aligia, 1995, Phys. Rev. B **52**, 7987.
Alzoubi, G. M., and N. O. Birge, 2006, Phys. Rev. Lett. **97**, 226803.
Anders, F. B., 2005, Phys. Rev. B **71**, 121101.
Anders, F. B., R. Bulla, and M. Vojta, 2007, Phys. Rev. Lett. **98**, 210402.
Anders, F. B., and G. Czycholl, 2005, Phys. Rev. B **71**, 125101.
Anders, F. B., E. Lebanon, and A. Schiller, 2004, Phys. Rev. B **70**, 201306.
Anders, F. B., E. Lebanon, and A. Schiller, 2005, Physica B **359-361**, 1381.
Anders, F. B., and T. Pruschke, 2006, Phys. Rev. Lett. **96**, 086404.
Anders, F. B., and A. Schiller, 2005, Phys. Rev. Lett. **95**, 196801.
Anders, F. B., and A. Schiller, 2006, Phys. Rev. B **74**, 245113.
Anderson, P. W., 1961, Phys. Rev. **124**, 41.
Anderson, P. W., 1967, Phys. Rev. Lett. **18**, 1049.
Anderson, P. W., 1970, J. Phys. C **3**, 2436.
Balatsky, A. V., I. Vekhter, and J.-X. Zhu, 2006, Rev. Mod. Phys. **78**, 373.
Bäuerle, C., F. Mallet, F. Schopfer, D. Mailly, G. Eska, and L. Saminadayar, 2005, Phys. Rev. Lett. **95**, 266805.
Biermann, S., L. de'Medici, and A. Georges, 2005, Phys. Rev. Lett. **95**, 206401.
Boese, D., W. Hofstetter, and H. Schoeller, 2002, Phys. Rev. B **66**, 125315.
Bolech, C. J., and N. Andrei, 2002, Phys. Rev. Lett. **88**, 237206.
Borda, L., 2007, Phys. Rev. B **75**, 041307.
Borda, L., G. Zaránd, W. Hofstetter, B. I. Halperin, and J. von Delft, 2003, Phys. Rev. Lett. **90**, 026602.
Borda, L., G. Zaránd, and P. Simon, 2005, Phys. Rev. B **72**, 155311.
Bradley, S. C., R. Bulla, A. C. Hewson, and G.-M. Zhang, 1999, Eur. Phys. J. B **11**, 535.
Bray, J. W., and S. T. Chui, 1979, Phys. Rev. B **19**, 4876.
Brito, J. J. S., and H. O. Frota, 1990, Phys. Rev. B **42**, 6378.
Bulla, R., 1999, Phys. Rev. Lett. **83**, 136.
Bulla, R., 2006, Philos. Mag. **86**, 1877.
Bulla, R., T. A. Costi, and D. Vollhardt, 2001, Phys. Rev. B **64**, 045103.
Bulla, R., M. T. Glossop, D. E. Logan, and T. Pruschke, 2000, J. Phys.: Condens. Matter **12**, 4899.
Bulla, R., and A. C. Hewson, 1997, Z. Phys. B: Condens. Matter **104**, 333.
Bulla, R., A. C. Hewson, and T. Pruschke, 1998, J. Phys.: Condens. Matter **10**, 8365.
Bulla, R., A. C. Hewson, and G.-M. Zhang, 1997, Phys. Rev. B **56**, 11721.
Bulla, R., H.-J. Lee, N.-H. Tong, and M. Vojta, 2005, Phys. Rev. B **71**, 045122.
Bulla, R., T. Pruschke, and A. C. Hewson, 1997, J. Phys.: Condens. Matter **9**, 10463.
Bulla, R., N.-H. Tong, and M. Vojta, 2003, Phys. Rev. Lett. **91**, 170601.
Bulla, R., and M. Vojta, 2003, in *Concepts in Electron Correlations*, edited by A. C. Hewson and V. Zlatić (Kluwer Academic, Dordrecht), p. 209.
Byczuk, K., W. Hofstetter, and D. Vollhardt, 2004, Phys. Rev. B **69**, 045112.
Byczuk, K., W. Hofstetter, and D. Vollhardt, 2005, Phys. Rev. Lett. **94**, 056404.
Campo, V. L., Jr., and L. N. Oliveira, 2003, Phys. Rev. B **68**, 035337.
Campo, V. L., Jr., and L. N. Oliveira, 2004, Phys. Rev. B **70**, 153401.
Campo, V. L., Jr., and L. N. Oliveira, 2005, Phys. Rev. B **72**, 104432.
Castro Neto, A. H., E. Novais, L. Borda, G. Zaránd, and I. Affleck, 2003, Phys. Rev. Lett. **91**, 096401.
Chen, K., and C. Jayaprakash, 1995a, J. Phys.: Condens. Matter **7**, L491.
Chen, K., and C. Jayaprakash, 1995b, Phys. Rev. B **52**, 14436.
Chen, K., and C. Jayaprakash, 1998, Phys. Rev. B **57**, 5225.
Chen, K., C. Jayaprakash, and H. R. Krishnamurthy, 1987, Phys. Rev. Lett. **58**, 929.
Chen, K., C. Jayaprakash, and H. R. Krishnamurthy, 1992, Phys. Rev. B **45**, 5368.
Chen, K., C. Jayaprakash, and H. R. Krishnamurthy, 1995, Phys. Rev. Lett. **58**, 929.
Choi, M.-S., N. Y. Hwang, and S.-R. E. Yang, 2003, Phys. Rev. B **67**, 245323.
Choi, M.-S., M. Lee, K. Kang, and W. Belzig, 2004, Phys. Rev. B **70**, 020502.
Choi, H.-Y., T.-H. Park, and G. S. Jeon, 2003, Int. J. Mod. Phys. B **17**, 3381.
Choi, M.-S., D. Sánchez, and R. López, 2004, Phys. Rev. Lett. **92**, 056601.
Chui, S.-T., and J. W. Bray, 1978, Phys. Rev. B **18**, 2426.
Coleman, P., 1984, Phys. Rev. B **29**, 3035.
Coleman, P., L. B. Ioffe, and A. M. Tsvelik, 1995, Phys. Rev. B **52**, 6611.
Coleman, P., and A. J. Schofield, 1995, Phys. Rev. Lett. **75**, 2184.

Cornaglia, P. S., and C. A. Balseiro, 2003, Phys. Rev. B **67**, 205420.
Cornaglia, P. S., and A. Georges, 2007, Phys. Rev. B **75**, 115112.
Cornaglia, P. S., and D. R. Grempel, 2005a, Phys. Rev. B **71**, 245326.
Cornaglia, P. S., and D. R. Grempel, 2005b, Phys. Rev. B **71**, 075305.
Cornaglia, P. S., D. R. Grempel, and H. Ness, 2005, Phys. Rev. B **71**, 075320.
Cornaglia, P. S., H. Ness, and D. R. Grempel, 2004, Phys. Rev. Lett. **93**, 147201.
Costa, S. C., C. A. Paula, V. L. Líbero, and L. N. Oliveira, 1997, Phys. Rev. B **55**, 30.
Costi, T. A., 1997a, Phys. Rev. B **55**, 3003.
Costi, T. A., 1997b, Phys. Rev. B **55**, 6670.
Costi, T. A., 1998, Phys. Rev. Lett. **80**, 1038.
Costi, T. A., 1999, in *Density-Matrix Renormalization—A New Numerical Method in Physics*, edited by I. Peschel, X. Wang, M. Kaulke, and K. Hallberg (Springer, New York), p. 3.
Costi, T. A., 2000, Phys. Rev. Lett. **85**, 1504.
Costi, T. A., 2001, Phys. Rev. B **64**, 241310.
Costi, T. A., 2003, in *Concepts in Electron Correlations*, edited by A. C. Hewson and V. Zlatić (Kluwer Academic, Dordrecht), p. 247.
Costi, T. A., and A. C. Hewson, 1990, Physica B **163**, 179.
Costi, T. A., and A. C. Hewson, 1991, Physica C **185-189**, 2649.
Costi, T. A., and A. C. Hewson, 1992a, J. Magn. Magn. Mater. **108**, 129.
Costi, T. A., and A. C. Hewson, 1992b, Philos. Mag. B **65**, 1165.
Costi, T. A., and A. C. Hewson, 1993, J. Phys.: Condens. Matter **5**, L361.
Costi, T. A., A. C. Hewson, and V. Zlatić, 1994a, J. Phys.: Condens. Matter **6**, 2519.
Costi, T. A., and C. Kieffer, 1996, Phys. Rev. Lett. **76**, 1683.
Costi, T. A., J. Kroha, and P. Wölfle, 1996, Phys. Rev. B **53**, 1850.
Costi, T. A., and N. Manini, 2002, J. Low Temp. Phys. **126**, 835.
Costi, T. A., and R. H. McKenzie, 2003, Phys. Rev. A **68**, 034301.
Costi, T. A., P. Schmitteckert, J. Kroha, and P. Wölfle, 1994b, Phys. Rev. Lett. **73**, 1275.
Cox, D. L., H. O. Frota, L. N. Oliveira, and J. W. Wilkins, 1985, Phys. Rev. B **32**, 555.
Cox, D. L., and A. Zawadowski, 1998, Adv. Phys. **47**, 599.
Cragg, D. M., and P. Lloyd, 1979, J. Phys. C **12**, L215.
Cragg, D. M., P. Lloyd, and P. Nozières, 1980, J. Phys. C **13**, 803.
Cronenwett, S. M., T. H. Oosterkamp, and L. P. Kouwenhoven, 1998, Science **281**, 540.
De Leo, L., and M. Fabrizio, 2004, Phys. Rev. B **69**, 245114.
De Leo, L., and M. Fabrizio, 2005, Phys. Rev. Lett. **94**, 236401.
Dias da Silva, L. G. G. V., N. P. Sandler, K. Ingersent, and S. E. Ulloa, 2006, Phys. Rev. Lett. **97**, 096603.
Doniach, S., 1977, Physica B & C **91**, 231.
Doniach, S., and M. Šunjić, 1970, J. Phys. C **3**, 285.
Evangelou, S. N., and A. C. Hewson, 1982, J. Phys. C **15**, 7073.
Fabrizio, M., A. F. Ho, L. De Leo, and G. E. Santoro, 2003, Phys. Rev. Lett. **91**, 246402.
Ferreira, J. V. B., and V. L. Líbero, 2000, Phys. Rev. B **61**, 10615.
Fleck, M., A. I. Lichtenstein, and A. M. Oleś, 2001, Phys. Rev. B **64**, 134528.
Freericks, J. K., T. P. Devereaux, and R. Bulla, 2001, Phys. Rev. B **64**, 233114.
Freericks, J. K., T. P. Devereaux, R. Bulla, and T. Pruschke, 2003, Phys. Rev. B **67**, 155102.
Freericks, J. K., and M. Jarrell, 1995a, Phys. Rev. Lett. **75**, 2570.
Freericks, J. K., and M. Jarrell, 1995b, Phys. Rev. Lett. **74**, 186.
Freericks, J. K., M. Jarrell, and D. J. Scalapino, 1993, Phys. Rev. B **48**, 6302.
Freericks, J. K., and V. Zlatić, 2003, Rev. Mod. Phys. **75**, 1333.
Fritz, L., and M. Vojta, 2005, Phys. Rev. B **72**, 212510.
Frota, H. O., 2004, e-print arXiv:cond-mat/0401005.
Frota, H. O., and K. Flensberg, 1992, Phys. Rev. B **46**, 15207.
Frota, H. O., and L. N. Oliveira, 1986, Phys. Rev. B **33**, 7871.
Galpin, M. R., D. E. Logan, and H. R. Krishnamurthy, 2006a, J. Phys.: Condens. Matter **18**, 6571.
Galpin, M. R., D. E. Logan, and H. R. Krishnamurthy, 2006b, J. Phys.: Condens. Matter **18**, 6545.
Gan, J., 1995, Phys. Rev. B **51**, 8287.
Garst, M., S. Kehrein, T. Pruschke, A. Rosch, and M. Vojta, 2004, Phys. Rev. B **69**, 214413.
Georges, A., S. Florens, and T. A. Costi, 2004, J. Phys. IV **114**, 165.
Georges, A., G. Kotliar, W. Krauth, and M. J. Rozenberg, 1996, Rev. Mod. Phys. **68**, 13.
Gerland, U., J. von Delft, T. A. Costi, and Y. Oreg, 2000, Phys. Rev. Lett. **84**, 3710.
Glazman, L. I., and M. E. Raikh, 1988, JETP Lett. **47**, 452.
Glossop, M. T., and K. Ingersent, 2005, Phys. Rev. Lett. **95**, 067202.
Glossop, M. T., and K. Ingersent, 2007a, Phys. Rev. Lett. **99**, 227203.
Glossop, M. T., and K. Ingersent, 2007b, Phys. Rev. B **75**, 104410.
Goldenfeld, N., 1992, *Lectures on Phase Transitions and the Renormalization Group* (Addison Wesley, Reading, MA).
Goldhaber-Gordon, D., J. Gores, M. A. Kastner, H. Shtrikman, D. Mahalu, and U. Meirav, 1998, Phys. Rev. Lett. **81**, 5225.
Gonzalez-Buxton, C., and K. Ingersent, 1998, Phys. Rev. B **57**, 14254.
Goremychkin, E. A., R. Osborn, B. D. Rainford, T. A. Costi, A. P. Murani, and C. A. Scott, 2002, Phys. Rev. Lett. **89**, 147201.
Hallberg, K. A., 2006, Adv. Phys. **55**, 477.
Hattori, K., 2005, J. Phys. Soc. Jpn. **74**, 3135.
Hattori, K., and K. Miyake, 2005, J. Phys. Soc. Jpn. **74**, 2193.
Hattori, K., S. Yotsuhashi, and K. Miyake, 2005, J. Phys. Soc. Jpn. **74**, 839.
Held, K., and R. Bulla, 2000, Eur. Phys. J. B **17**, 7.
Helmes, R. W., M. Sindel, L. Borda, and J. von Delft, 2005, Phys. Rev. B **72**, 125301.
Hewson, A. C., 1993a, *The Kondo Problem to Heavy Fermions* (Cambridge University Press, Cambridge, England).
Hewson, A. C., 1993b, Phys. Rev. Lett. **70**, 4007.
Hewson, A. C., 2005, J. Phys. Soc. Jpn. **74**, 8.
Hewson, A. C., 2006, J. Phys.: Condens. Matter **18**, 1815.
Hewson, A. C., J. Bauer, and W. Koller, 2006, Phys. Rev. B **73**, 045117.
Hewson, A. C., J. Bauer, and A. Oguri, 2005, J. Phys.: Condens. Matter **17**, 5413.
Hewson, A. C., and D. Meyer, 2002, J. Phys.: Condens. Matter **14**, 427.

Hewson, A. C., A. Oguri, and D. Meyer, 2004, Eur. Phys. J. B **40**, 177.
Hofstetter, W., 2000, Phys. Rev. Lett. **85**, 1508.
Hofstetter, W., R. Bulla, and D. Vollhardt, 2000, Phys. Rev. Lett. **84**, 4417.
Hofstetter, W., J. König, and H. Schoeller, 2001, Phys. Rev. Lett. **87**, 156803.
Hofstetter, W., and H. Schoeller, 2002, Phys. Rev. Lett. **88**, 016803.
Hofstetter, W., and G. Zaránd, 2004, Phys. Rev. B **69**, 235301.
Hotta, T., 2006, Phys. Rev. Lett. **96**, 197201.
Imada, M., A. Fujimori, and Y. Tokura, 1998, Rev. Mod. Phys. **70**, 1039.
Ingersent, K., 1996, Phys. Rev. B **54**, 11936.
Ingersent, K., B. A. Jones, and J. W. Wilkins, 1992, Phys. Rev. Lett. **69**, 2594.
Ingersent, K., A. W. W. Ludwig, and I. Affleck, 2005, Phys. Rev. Lett. **95**, 257204.
Ingersent, K., and Q. M. Si, 2002, Phys. Rev. Lett. **89**, 076403.
Izumida, W., O. Sakai, and Y. Shimizu, 1997, J. Phys. Soc. Jpn. **66**, 717.
Izumida, W., O. Sakai, and Y. Shimizu, 1998, J. Phys. Soc. Jpn. **67**, 2444.
Izumida, W., O. Sakai, and S. Suzuki, 2001, J. Phys. Soc. Jpn. **70**, 1045.
Izumida, W., O. Sakai, and S. Tarucha, 2001, Phys. Rev. Lett. **87**, 216803.
Jabben, T., N. Grewe, and F. Anders, 2005, Eur. Phys. J. B **44**, 47.
Jarrell, M., 1995, Phys. Rev. B **51**, 7429.
Jayaprakash, C., H. R. Krishna-murthy, and J. W. Wilkins, 1981, Phys. Rev. Lett. **47**, 737.
Jeon, G. S., T.-H. Park, and H.-Y. Choi, 2003, Phys. Rev. B **68**, 045106.
Jeon, G. S., T.-H. Park, J. H. Han, H. C. Lee, and H.-Y. Choi, 2004, Phys. Rev. B **70**, 125114.
Jones, B., 1990, in *Field Theories in Condensed Matter Physics*, edited by Z. Tesanović (Addison-Wesley, Redwood City), p. 87.
Jones, B. A., and C. M. Varma, 1987, Phys. Rev. Lett. **58**, 843.
Jones, B. A., C. M. Varma, and J. W. Wilkins, 1988, Phys. Rev. Lett. **61**, 125.
Kang, K., M.-S. Choi, and S. Lee, 2005, Phys. Rev. B **71**, 045330.
Karski, M., C. Raas, and G. S. Uhrig, 2005, Phys. Rev. B **72**, 113110.
Killer, U., E.-W. Scheidt, G. Eickerling, H. Michor, J. Sereni, T. Pruschke, and S. Kehrein, 2004, Phys. Rev. Lett. **93**, 216404.
Kim, T.-S., L. N. Oliveira, and D. L. Cox, 1997, Phys. Rev. B **55**, 12460.
Koga, M., 2000, Phys. Rev. B **61**, 395.
Koga, M., and D. L. Cox, 1999, Phys. Rev. Lett. **82**, 2575.
Koga, M., and M. Matsumoto, 2002a, J. Phys. Soc. Jpn. **71**, 943.
Koga, M., and M. Matsumoto, 2002b, Phys. Rev. B **65**, 094434.
Koga, M., and H. Shiba, 1995, J. Phys. Soc. Jpn. **64**, 4345.
Koga, M., and H. Shiba, 1996, J. Phys. Soc. Jpn. **65**, 3007.
Kolesnychenko, O. Y., G. M. M. Heijnen, A. K. Zhuravlev, R. de Kort, M. I. Katsnelson, A. I. Lichtenstein, and H. van Kempen, 2005, Phys. Rev. B **72**, 085456.
Kolf, C., and J. Kroha, 2007, Phys. Rev. B **75**, 045129.
Koller, W., A. C. Hewson, and D. M. Edwards, 2005, Phys. Rev. Lett. **95**, 256401.
Koller, W., A. C. Hewson, and D. Meyer, 2005, Phys. Rev. B **72**, 045117.
Koller, W., D. Meyer, and A. C. Hewson, 2004, Phys. Rev. B **70**, 155103.
Koller, W., D. Meyer, Y. Ōno, and A. C. Hewson, 2004, Europhys. Lett. **66**, 559.
Krishna-murthy, H. R., J. W. Wilkins, and K. G. Wilson, 1980a, Phys. Rev. B **21**, 1003.
Krishna-murthy, H. R., J. W. Wilkins, and K. G. Wilson, 1980b, Phys. Rev. B **21**, 1044.
Krug von Nidda, H.-A., R. Bulla, N. Büttgen, M. Heinrich, and A. Loidl, 2003, Eur. Phys. J. B **34**, 399.
Kuchinskii, E. Z., I. A. Nekrasov, and M. V. Sadovskii, 2005, JETP Lett. **82**, 198.
Kusunose, H., 2005, J. Phys. Soc. Jpn. **74**, 2157.
Kusunose, H., and Y. Kuramoto, 1999, J. Phys. Soc. Jpn. **68**, 3960.
Kusunose, H., K. Miyake, Y. Shimizu, and O. Sakai, 1996, Phys. Rev. Lett. **76**, 271.
Lebanon, E., A. Schiller, and F. B. Anders, 2003a, Phys. Rev. B **68**, 041311.
Lebanon, E., A. Schiller, and F. B. Anders, 2003b, Phys. Rev. B **68**, 155301.
Lee, H.-J., R. Bulla, and M. Vojta, 2005, J. Phys.: Condens. Matter **17**, 6935.
Lee, P. A., 1979, Phys. Rev. Lett. **42**, 1492.
Leggett, A. J., S. Chakravarty, A. T. Dorsey, M. P. A. Fisher, A. Garg, and W. Zwerger, 1987, Rev. Mod. Phys. **59**, 1.
Li, M.-R., K. Le Hur, and W. Hofstetter, 2005, Phys. Rev. Lett. **95**, 086406.
Líbero, V. L., and L. N. Oliveira, 1990a, Phys. Rev. B **42**, 3167.
Líbero, V. L., and L. N. Oliveira, 1990b, Phys. Rev. Lett. **65**, 2042.
Liebsch, A., and T. A. Costi, 2006, Eur. Phys. J. B **51**, 523.
Limelette, P., P. Wzietek, S. Florens, A. Georges, T. A. Costi, C. Pasquier, D. Jérome, C. Mézière, and P. Batail, 2003, Phys. Rev. Lett. **91**, 016401.
Logan, D. E., and M. T. Glossop, 2000, J. Phys.: Condens. Matter **12**, 985.
Ma, S.-K., 1976, *Modern Theory of Critical Phenomena* (Addison-Wesley, Reading, MA).
Mahan, G. D., 1967, Phys. Rev. **163**, 612.
Mahan, G. D., 1974, in *Solid State Physics*, edited by H. Ehrenreich, F. Seitz, and D. Turnbull (Academic, New York), Vol. 29, p. 75.
Maier, T., M. Jarrell, T. Pruschke, and M. H. Hettler, 2005, Rev. Mod. Phys. **77**, 1027.
Mallet, F., J. Ericsson, D. Mailly, S. Ünlübayir, D. Reuter, A. Melnikov, A. D. Wieck, T. Micklitz, A. Rosch, T. A. Costi, L. Saminadayar, and C. Bäuerle, 2006, Phys. Rev. Lett. **97**, 226804.
Martinek, J., M. Sindel, L. Borda, J. Barnaś, J. König, G. Schön, and J. von Delft, 2003, Phys. Rev. Lett. **91**, 247202.
Matsumoto, M., and M. Koga, 2001, J. Phys. Soc. Jpn. **70**, 2860.
Matsumoto, M., and M. Koga, 2002, Phys. Rev. B **65**, 024508.
Mehta, P., N. Andrei, P. Coleman, L. Borda, and G. Zaránd, 2005, Phys. Rev. B **72**, 014430.
Metzner, W., and D. Vollhardt, 1989, Phys. Rev. Lett. **62**, 324.
Meyer, D., and A. C. Hewson, 2003, Acta Phys. Pol. B **34**, 769.
Meyer, D., A. C. Hewson, and R. Bulla, 2002, Phys. Rev. Lett. **89**, 196401.
Micklitz, T., A. Altland, T. A. Costi, and A. Rosch, 2006, Phys. Rev. Lett. **96**, 226601.
Micklitz, T., T. A. Costi, and A. Rosch, 2007, Phys. Rev. B **75**,

054406.
Millis, A. J., B. G. Kotliar, and B. Jones, 1990, in *Field Theories in Condensed Matter Physics*, edited by Z. Tesanović (Addison-Wesley, Redwood City), p. 159.
Mohanty, P., E. M. Jariwala, and R. A. Webb, 1997, Phys. Rev. Lett. **78**, 3366.
Müller-Hartmann, E., 1984, Z. Phys. B: Condens. Matter **57**, 281.
Ng, T. K., and P. A. Lee, 1988, Phys. Rev. Lett. **61**, 1768.
Nishimoto, S., and E. Jeckelmann, 2004, J. Phys.: Condens. Matter **16**, 613.
Noack, R. M., and S. R. Manmana, 2005, AIP Conf. Proc. **789**, 93.
Novais, E., A. H. Castro Neto, L. Borda, I. Affleck, and G. Zaránd, 2005, Phys. Rev. B **72**, 014417.
Nozières, P., 1974, J. Low Temp. Phys. **17**, 31.
Nozières, P., 1998, Eur. Phys. J. B **6**, 447.
Nozières, P., 2005, J. Phys. Soc. Jpn. **74**, 4.
Nozières, P., and A. Blandin, 1980, J. Phys. (France) **41**, 193.
Nozières, P., and C. T. De Dominicis, 1969, Phys. Rev. **178**, 1097.
Oguri, A., Y. Tanaka, and A. C. Hewson, 2004, J. Phys. Soc. Jpn. **73**, 2494.
Oliveira, W. C., and L. N. Oliveira, 1994, Phys. Rev. B **49**, 11986.
Oliveira, L. N., and J. W. Wilkins, 1981, Phys. Rev. B **24**, 4863.
Oliveira, L. N., and J. W. Wilkins, 1985, Phys. Rev. B **32**, 696.
Ōno, Y., R. Bulla, A. C. Hewson, and M. Potthoff, 2001, Eur. Phys. J. B **22**, 283.
Pang, H.-B., 1994, Phys. Rev. Lett. **73**, 2736.
Pang, H.-B., and D. L. Cox, 1991, Phys. Rev. B **44**, 9454.
Paul, B. C., and K. Ingersent, 1996, arXiv:cond-mat/9607190.
Paula, C. A., M. F. Silva, and L. N. Oliveira, 1999, Phys. Rev. B **59**, 85.
Perakis, I. E., and C. M. Varma, 1994, Phys. Rev. B **49**, 9041.
Perakis, I. E., C. M. Varma, and A. E. Ruckenstein, 1993, Phys. Rev. Lett. **70**, 3467.
Peters, R., and T. Pruschke, 2006, New J. Phys. **8**, 127.
Peters, R., T. Pruschke, and F. B. Anders, 2006, Phys. Rev. B **74**, 245114.
Pierre, F., A. B. Gougam, A. Anthore, H. Pothier, D. Esteve, and N. O. Birge, 2003, Phys. Rev. B **68**, 085413.
Pietig, R., R. Bulla, and S. Blawid, 1999, Phys. Rev. Lett. **82**, 4046.
Pietri, R., K. Ingersent, and B. Andraka, 2001, Phys. Rev. Lett. **86**, 1090.
Potthoff, M., 2003, Eur. Phys. J. B **36**, 335.
Pruschke, T., 2005, Prog. Theor. Phys. Suppl. **160**, 274.
Pruschke, T., and R. Bulla, 2005, Eur. Phys. J. B **44**, 217.
Pruschke, T., R. Bulla, and M. Jarrell, 2000, Phys. Rev. B **61**, 12799.
Pruschke, T., M. Jarrell, and J. K. Freericks, 1995, Adv. Phys. **44**, 187.
Pruschke, T., and R. Zitzler, 2003, J. Phys.: Condens. Matter **15**, 7867.
Pustilnik, M., and L. I. Glazman, 2001, Phys. Rev. B **64**, 045328.
Ramos, L. R., and V. L. Líbero, 2006, Phys. Rev. B **73**, 073101.
Ramos, L. R., W. C. Oliveira, and V. L. Líbero, 2003, Phys. Rev. B **67**, 085104.
Romeike, C., M. R. Wegewijs, W. Hofstetter, and H. Schoeller, 2006a, Phys. Rev. Lett. **97**, 206601.
Romeike, C., M. R. Wegewijs, W. Hofstetter, and H. Schoeller, 2006b, Phys. Rev. Lett. **96**, 196601.
Rosch, A., T. A. Costi, J. Paaske, and P. Wölfle, 2003, Phys. Rev. B **68**, 014430.
Sadovskii, M. V., I. A. Nekrasov, E. Z. Kuchinskii, T. Pruschke, and V. I. Anisimov, 2005, Phys. Rev. B **72**, 155105.
Sakai, O., and W. Izumida, 2003, Physica B **328**, 125.
Sakai, O., and Y. Kuramoto, 1994, Solid State Commun. **89**, 307.
Sakai, O., and Y. Shimizu, 1992a, J. Phys. Soc. Jpn. **61**, 2333.
Sakai, O., and Y. Shimizu, 1992b, J. Phys. Soc. Jpn. **61**, 2348.
Sakai, O., Y. Shimizu, and N. Kaneko, 1993, Physica B **186-188**, 323.
Sakai, O., Y. Shimizu, and T. Kasuya, 1989, J. Phys. Soc. Jpn. **58**, 3666.
Sakai, O., Y. Shimizu, and T. Kasuya, 1990, Solid State Commun. **75**, 81.
Sakai, O., Y. Shimizu, H. Shiba, and K. Satori, 1993, J. Phys. Soc. Jpn. **62**, 3181.
Sakai, O., S. Suzuki, and Y. Shimizu, 1997, Solid State Commun. **101**, 791.
Sakai, O., S. Suzuki, Y. Shimizu, H. Kusunose, and K. Miyake, 1996, Solid State Commun. **99**, 461.
Salmhofer, M., 1999, *Renormalization* (Springer-Verlag, Berlin).
Sasaki, S., S. De Francheschi, J. M. Elzermann, W. G. van der Wiel, M. Eto, S. Tarucha, and L. P. Kouwenhoven, 2000, Nature (London) **405**, 764.
Satori, K., H. Shiba, O. Sakai, and Y. Shimizu, 1992, J. Phys. Soc. Jpn. **61**, 3239.
Scheidt, E.-W., F. Mayr, U. Killer, W. Scherer, H. Michor, E. Bauer, S. Kehrein, T. Pruschke, and F. Anders, 2006, Physica B **378-380**, 154.
Schoeller, H., and J. König, 2000, Phys. Rev. Lett. **84**, 3686.
Schollwöck, U., 2005, Rev. Mod. Phys. **77**, 259.
Schopfer, F., C. Bäuerle, W. Rabaud, and L. Saminadayar, 2003, Phys. Rev. Lett. **90**, 056801.
Schrieffer, R., and P. A. Wolff, 1966, Phys. Rev. **149**, 491.
Shimizu, Y., A. C. Hewson, and O. Sakai, 1999, J. Phys. Soc. Jpn. **68**, 2994.
Shimizu, Y., and O. Sakai, 1995, in *Computational Physics as a New Frontier in Condensed Matter Research* (The Physical Society of Japan, Tokyo), p. 42.
Shimizu, Y., O. Sakai, and A. C. Hewson, 2000, J. Phys. Soc. Jpn. **69**, 1777.
Shimizu, Y., O. Sakai, and T. Kasuya, 1990, Physica B **163**, 401.
Shimizu, Y., O. Sakai, and S. Suzuki, 1998, J. Phys. Soc. Jpn. **67**, 2395.
Shimizu, Y., O. Sakai, and S. Suzuki, 1999, Physica B **261**, 366.
Si, Q., S. Rabello, K. Ingersent, and J. L. Smith, 2001, Nature (London) **413**, 804.
Si, Q., J. L. Smith, and K. Ingersent, 1999, Int. J. Mod. Phys. B **13**, 2331.
Silva, J. B., W. L. C. Lima, W. C. Oliveira, J. L. N. Mello, L. N. Oliveira, and J. W. Wilkins, 1996, Phys. Rev. Lett. **76**, 275.
Simon, P., P. S. Cornaglia, D. Feinberg, and C. A. Balseiro, 2007, Phys. Rev. B **75**, 045310.
Sindel, M., W. Hofstetter, J. von Delft, and M. Kindermann, 2005, Phys. Rev. Lett. **94**, 196602.
Suzuki, S., O. Sakai, and Y. Shimizu, 1996, J. Phys. Soc. Jpn. **65**, 4034.
Tahvildar-Zadeh, A. N., M. Jarrell, and J. K. Freericks, 1997, Phys. Rev. B **55**, R3332.
Tahvildar-Zadeh, A. N., M. Jarrell, T. Pruschke, and J. K. Fre-

ericks, 1999, Phys. Rev. B **60**, 10782.
Takayama, R., and O. Sakai, 1993, Physica B **188**, 915.
Takayama, R., and O. Sakai, 1997, J. Phys. Soc. Jpn. **66**, 1512.
Takegahara, K., Y. Shimizu, N. Goto, and O. Sakai, 1993, Physica B **186-188**, 381.
Takegahara, K., Y. Shimizu, and O. Sakai, 1992, J. Phys. Soc. Jpn. **61**, 3443.
Tong, N.-H., S.-Q. Shen, and F.-C. Pu, 2001, Phys. Rev. B **64**, 235109.
Tong, N.-H., and M. Vojta, 2006, Phys. Rev. Lett. **97**, 016802.
Tornow, S., N.-H. Tong, and R. Bulla, 2006a, J. Phys.: Condens. Matter **18**, 5985.
Tornow, S., N.-H. Tong, and R. Bulla, 2006b, Europhys. Lett. **73**, 913.
v. Löhneysen, H., A. Rosch, M. Vojta, and P. Wölfle, 2007, Rev. Mod. Phys. **79**, 1015.
van der Wiel, W. G., S. De Franceschi, J. M. Elzerman, S. Tarucha, and L. P. Kouwenhoven, 2002, Phys. Rev. Lett. **88**, 126803.
van der Wiel, W. G., S. De Franceschi, T. Fujisawa, J. M. Elzerman, S. Tarucha, and L. P. Kouwenhoven, 2000, Science **289**, 2105.
van Dongen, P. G. J., 1996, Phys. Rev. B **54**, 1584.
Vavilov, M. G., and L. I. Glazman, 2003, Phys. Rev. B **67**, 115310.
Verstraete, F., A. Weichselbaum, U. Schollwöck, J. I. Cirac, and J. von Delft, 2005, e-print arXiv:cond-mat/0504305.
Vidhyadhiraja, N. S., and D. E. Logan, 2004, Eur. Phys. J. B **39**, 313.
Vojta, M., 2006, Philos. Mag. **86**, 1807.
Vojta, M., and R. Bulla, 2002a, Eur. Phys. J. B **28**, 283.
Vojta, M., and R. Bulla, 2002b, Phys. Rev. B **65**, 014511.
Vojta, M., R. Bulla, and W. Hofstetter, 2002, Phys. Rev. B **65**, 140405.
Vojta, M., N.-H. Tong, and R. Bulla, 2005, Phys. Rev. Lett. **94**, 070604.
Vojta, M., R. Zitzler, R. Bulla, and T. Pruschke, 2002, Phys. Rev. B **66**, 134527.
Weichselbaum, A., and J. von Delft, 2007, Phys. Rev. Lett. **99**, 076402.
White, S. R., 1991, Phys. Rev. B **44**, 4670.
White, S. R., and R. M. Noack, 1992, Phys. Rev. Lett. **68**, 3487.
Wilson, K. G., 1975a, Rev. Mod. Phys. **47**, 773.
Wilson, K. G., 1975b, Adv. Math. **16**, 170.
Wilson, K. G., and J. Kogut, 1974, Phys. Rep. **12**, 75.
Withoff, D., and E. Fradkin, 1990, Phys. Rev. Lett. **64**, 1835.
Yanson, I. K., V. V. Fisun, R. Hesper, A. V. Khotkevich, J. M. Krans, J. A. Mydosh, and J. M. van Ruitenbeek, 1995, Phys. Rev. Lett. **74**, 302.
Yoshioka, T., and Y. Ohashi, 1998, J. Phys. Soc. Jpn. **67**, 1332.
Yoshioka, T., and Y. Ohashi, 2000, J. Phys. Soc. Jpn. **69**, 1812.
Yoshida, M., M. A. Whitaker, and L. N. Oliveira, 1990, Phys. Rev. B **41**, 9403.
Yotsuhashi, S., and H. Maebashi, 2002, J. Phys. Soc. Jpn. **71**, 1705.
Zaránd, G., L. Borda, J. von Delft, and N. Andrei, 2004, Phys. Rev. Lett. **93**, 107204.
Zaránd, G., C.-H. Chung, P. Simon, and M. Vojta, 2006, Phys. Rev. Lett. **97**, 166802.
Zhu, J.-X., S. Kirchner, R. Bulla, and Q. Si, 2007, Phys. Rev. Lett. **99**, 227204.
Zhu, L., and C. M. Varma, 2006, e-print arXiv:cond-mat/0607426.
Zhuravlev, A. K., V. Y. Irkhin, and M. I. Katsnelson, 2007, Eur. Phys. J. B **55**, 377.
Zhuravlev, A. K., V. Y. Irkhin, M. I. Katsnelson, and A. I. Lichtenstein, 2004, Phys. Rev. Lett. **93**, 236403.
Žitko, R., and J. Bonča, 2006, Phys. Rev. B **74**, 045312.
Žitko, R., and J. Bonča, 2007, Phys. Rev. Lett. **98**, 047203.
Zitzler, R., T. Pruschke, and R. Bulla, 2002, Eur. Phys. J. B **27**, 473.
Zitzler, R., N.-H. Tong, T. Pruschke, and R. Bulla, 2004, Phys. Rev. Lett. **93**, 016406.
Zlatić, V., T. A. Costi, A. C. Hewson, and B. R. Coles, 1993, Phys. Rev. B **48**, 16152.